Coordination Chemistry Reviews 492 (2023) 215225

Contents lists available at ScienceDirect

Coordination Chemistry Reviews

journal homepage: www.elsevier.com/locate/ccr

Review

Metal-based gels: Synthesis, properties, and applications

Giacomo Picci [a], Claudia Caltagirone [a,*], Alessandra Garau [a], Vito Lippolis [a], Jessica Milia [a], Jonathan W. Steed [b,*]

[a] Dipartimento di Scienze Chimiche e Geologiche, Università degli Studi di Cagliari, S.S. 554 Bivio per Sestu, 09042 Monserrato, CA, Italy
[b] Department of Chemistry, Durham University, South Road, Durham DH1 3LE, UK

ARTICLE INFO

Keywords:
Supramolecular gels
Supramolecular metallogels
Self-assembly
Metal ions

ABSTRACT

This review covers various aspects of recent developments on the design, the synthesis, the characterization of gels that: (i) are formed in the presence of metal ions (metallogels); (ii) are based on coordination complexes as gelators. Particular attention is devoted to systems that show recognition and sensing properties towards different analytes.

1. Introduction

Gels are ubiquitous soft materials widely used in everyday life. Probably, gelatin which is a natural product made of hydrolysed collagen that forms a transparent, elastic thermoreversible gel when cooled below about 35 °C, represents the most familiar gel in Nature. Fundamentally, we can define a gel when in a system characterized by the presence of two (or more) components, a fibrous or colloidal solid-like phase is able to immobilize a large fluid volume, causing the formation of a continuous structure of macroscopic dimension [1]. A gel is commonly (although not always reliably) identified by performing the inversion tube test, that assess whether or not the material resists to gravitational force when the tube is flipped upside down. However, it is the rheological behaviour that defines the solid-like properties of the material. The protein scientist Dorothy Jordan Lloyd was particularly interested in the properties of gels, and she described them as materials that are "easier to recognize than to define" [2]. Gelatin in particular involves a physically entangled network structure with disordered regions and crystalline triple helical cross-links [3,4]. Generally, it is by means of a sol–gel transition process that an artificial gel is obtained. Indeed, in the case of metal oxide polymeric materials (maybe the most well-known artificial gels), a mixture of colloidal particles dispersed in a solvent (a sol), due to the hydrolysis and the polycondensation of monomeric metal salts, swells up, giving a continuous inorganic network containing the liquid phase (gel) [3]. Materials obtained *via* sol–gel processes find application in a wide range of fields, such as optics [5], energy space [6], sensing and biosensing [7–9], controlled drug delivery and release [10], and chromatography [11,12].

Amongst the strategies for the preparation of gel phase materials, the supramolecular bottom-up approach can be used to form highly ordered nanostructures from small molecules, namely Low Molecular Weight Gelators, through non-covalent interactions, such as hydrophobic interactions, hydrogen bonds (HBs) and π-π interactions. Low Molecular Weight Gels (LMWGs), or supramolecular gels, represent a class of emerging materials based on the fibrous self-assembly of small molecules, such as bis-ureas [13,14], amides [15,16], nucleobase derivatives [17–19], fatty acids, steroids [20], amino acids derivatives [15], dendrites [21,22], and porphyrins [23], into long, anisotropic structures, most commonly fibres [24]. At a specific concentration termed the critical gelation concentration (CGC), these fibres entangle or otherwise form cross-links, leading to a network capable of immobilizing the solvent through surface tension or capillary forces. These gels differ from the cross-linked polymer gels based on covalent interactions since the presence of non-covalent interactions, as well as their balance in the

* Corresponding authors.
E-mail addresses: ccaltagirone@unica.it (C. Caltagirone), jon.steed@durham.ac.uk (J.W. Steed).

https://doi.org/10.1016/j.ccr.2023.215225
Received 17 March 2023; Accepted 4 May 2023
Available online 7 June 2023

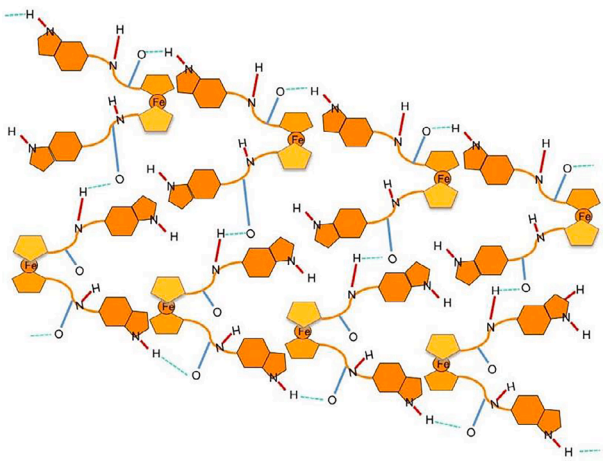

Fig. 1. Simplified scheme of the supramolecular assembly of **1** via the formation of HB between the indole and amide NHs and the C═O. Copyright Wiley 2017. Reproduced with permission from ref. [61].

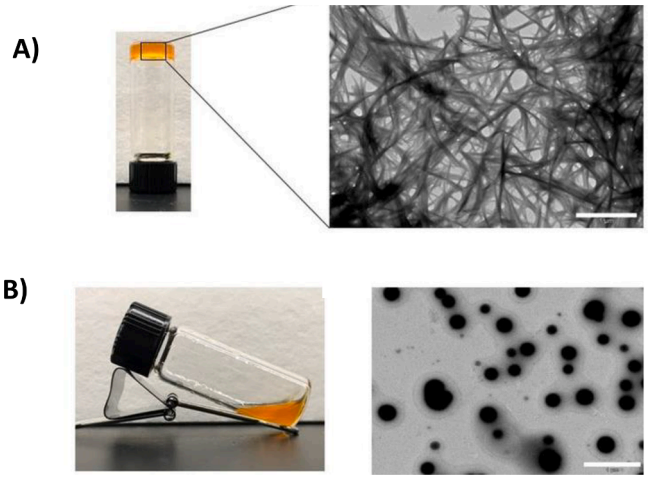

Fig. 2. A) TEM image recorded at room temperature of the gel of **1** obtained in dichlorobenzene (2.7% w/v, scale bar = 1 μm; B) gel at minimum gelation concentration turning into a solution after treatment with iron(III) perchlorate and formation of spheres as measured by TEM (scale bar = 1 μm). Copyright Wiley 2017. Reproduced with permission from ref. [61].

formation of the nanostructure, allows the control of important features, such as morphologies and the mechanical/rheological properties, of the materials. Particularly, these properties can be reversed by the application of an external stimulus, such as an input of energy, or a chemical input. LMWGs can be identified by their melting point (T_{gel}), a temperature above which the gel phase turns to a sol phase. Hence, supramolecular gels are typically/usually prepared by dissolving the gelator in a warm solution, and allowing it to cool below the T_{gel} [3]. There are also sonogels formed by sonication [25,26] and light-responsive gels which can change their morphology upon irradiation with a light of specific wavelength [27–29]. When the solvent in which the gel fibres grow is water, the gel is a hydrogel, whereas in a typical organogel the liquid component is an organic solvent. Over the last two decades, the scientific community has constantly increased its interest in the development of new synthetic gel systems, such as ionogels [30–33] and eutectogels [34–36], which are formed in non-conventional solvents, such as ionic liquids and deep eutectic solvents, respectively. When a metal, in the form of a coordination compound or as metal nanoparticle is part of the gel network [37], the gel is called metallogel and the first example of this type of material was reported in 1841 as a lithium urate hydrogel [38]. Metallogels can find applications in different fields such as catalysis [39], nanoparticle templating, magnetism, proton conduction, and sensing [40,41] and for this reason they have been widely studied [42].

When a metallogel is formed by a discrete coordination complex, it can be considered a supramolecular gel as the gel network can be formed through supramolecular interactions such as ligand/co-ligand, metal/solvent, metal/counteranion, bulk solvent interactions [37]. The functionalization of the gelator could have a crucial role in the control of the metal/gelator intermolecular interactions to form the metallogel. Metallogels [43] of this type are particularly interesting because, by changing the nature of the metal centre, the coordination geometry, and the ligands, it is possible to impart different and intriguing spectroscopic, catalytic and redox properties to the materials that cannot be achieved in metal-free gels [44–47]. Compel demonstrated how the variation of poly-ethylene glycol dimethoxy ethers (glyme) chain length and water content can affect the extent of polymer interaction and the mechanical and optical properties of the metallogel [48]. Although the design of new synthetic systems able to gel remains challenging, there have been some attempts to adopt rational approaches towards designing metallogelators [49]. For example, an improvement of the stability of supramolecular gels can be achieved by the presence of metal ions, and the change of the nature of metal ions allows for a wide control over the mechanical strength of gel [50–52] as a consequence of nanoparticles formation [53]. Furthermore, metallogels could also be used to form a porous imprint on organic polymers [54]. In this review article, the highlights of the recent research on supramolecular metallogels will

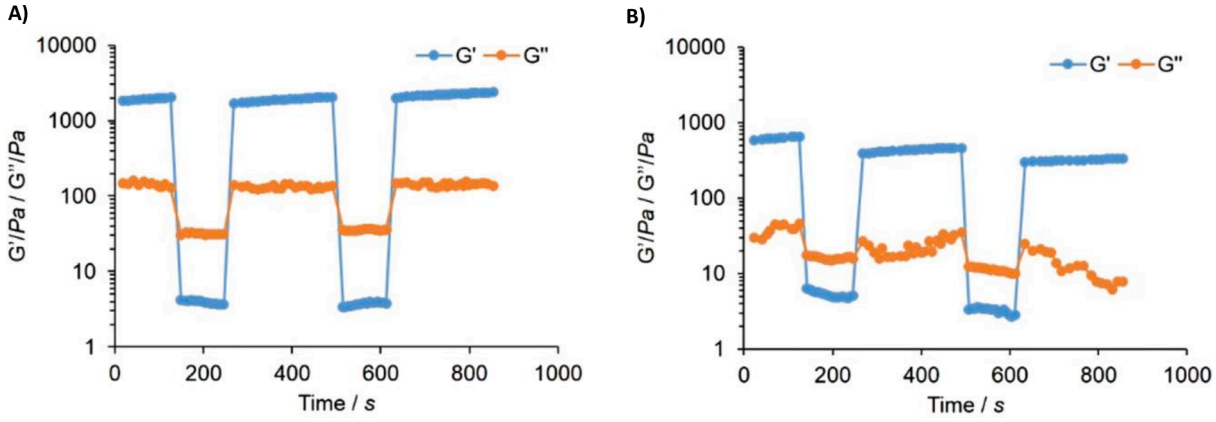

Fig. 3. Alternating strain rheology for: A) the organogel of **2**; B) the organogel of **2** in the presence of $[Fe(\mu\text{-}S)_2Cl_4]^{2-}$ in MeCN/toluene (1:2 v/v). Copyright Springer 2019. Reproduced with permission from ref. [62].

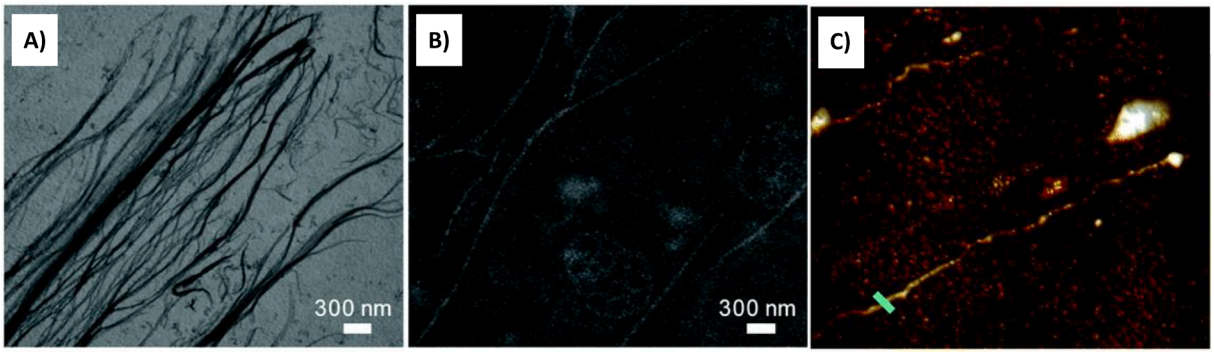

Fig. 4. A) TEM; B) SEM and C) AFM images of **3** (7 mM) in water at room temperature. Copyright RSC 2017. Reproduced with permission form ref. [63].

be reported, focusing on their applications in catalysis, pollutant remediation, gas absorption, and molecular sensing. Although this topic will not be covered in this review, it is interesting to note that various supramolecular polymers containing metal ions, based on hierarchical self-assembly (HSA) have been recently reported [11–13].

2. Organometallic gels

In the quest for stimuli responsive materials and in particular supramolecular-polymers and gels, the use of an organometallic scaffold has also been considered. In particular, ferrocene(Fc)-containing amino acids and peptides can easily self-assemble and gelate due to the formation of non-covalent interactions such as HBs, forming a wide range of nanostructures including nanofibres, nanotubes and nanovesicles [55–60]. Indeed, amino acids are well known for their ability to form HBs and binds metal ions. On the other hand, the distance of the two cyclopentadiene rings, ideal for the formation of HBs between attached functionalities such as amino acids/peptide strands, makes ferrocene useful for the design of LMWGs. Moreover, Fc redox responsiveness can be transferred to supramolecular self-assembled gels.

Given that among the 20 common amino acids, tryptophan (TrP) has the largest nonpolar surface, the greatest electrostatic potential for cation-π interactions and the indole NH group is capable of hydrogen-bonding donation, Kraatz and co-workers have recently considered the Fc bio-conjugate **1** as possible gelator, featuring two Trp-Trp dipeptides linked to the organometallic Fc scaffold [61].

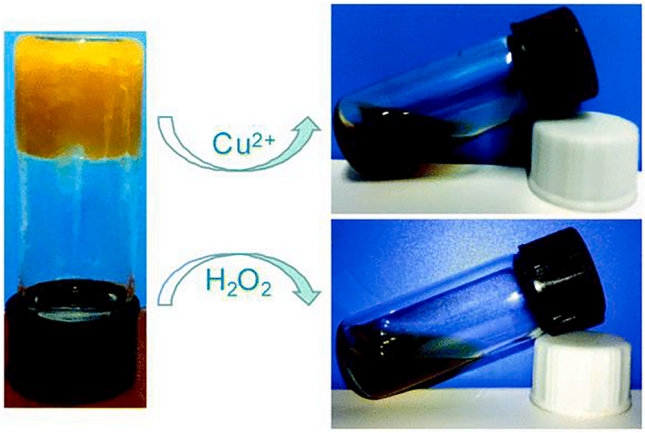

Fig. 6. Stimuli-responsiveness images of the gel formed by **3**. Copyright RSC 2017. Reproduced with permission from ref. [63].

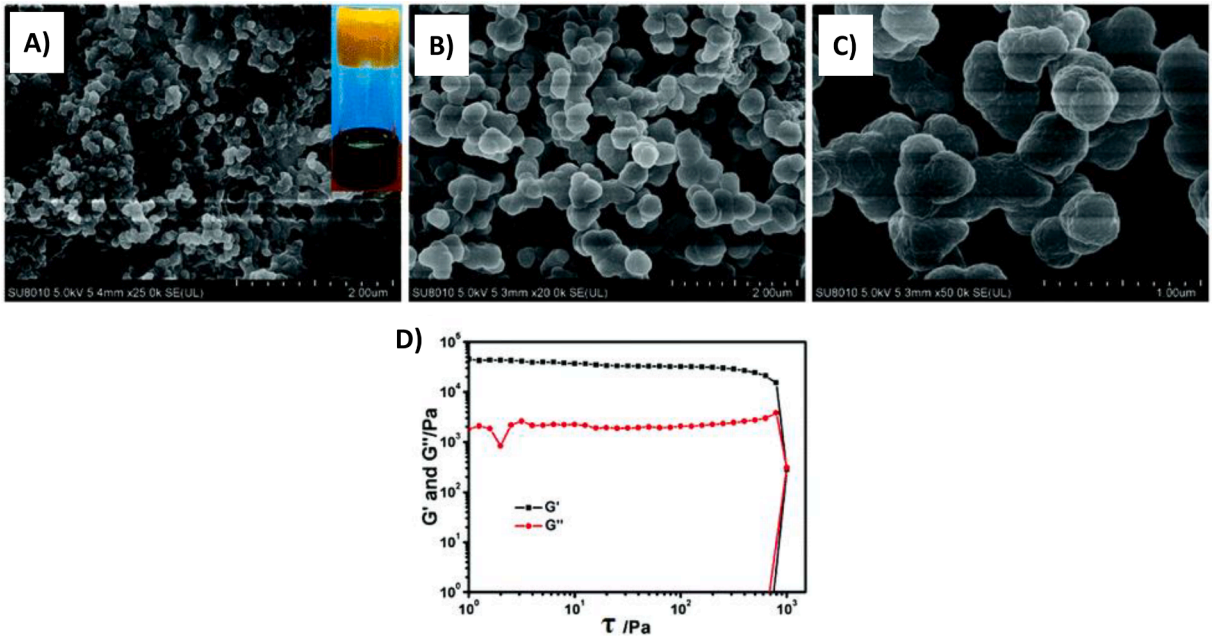

Fig. 5. (A–C) SEM images at increasing magnification levels of the gel of **3** at room temperature; D) dynamic oscillatory stress sweep of the gel. Copyright RSC 2017. Reproduced with permission form ref. [63].

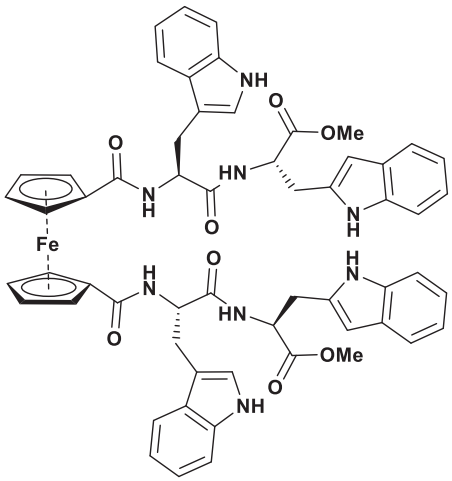

1

The X-ray crystal structure of **1** shows that both proximal and one distal (with respect to the Fc moiety) NH indolic functions are involved in the HB formation with solvent molecules, either Et_2O or THF. On the other hand, the HB interactions between the remaining distal NH function and a carbonyl group of a neighboring molecule of **1**, forms a linear ordering of discrete molecules in the crystal. Furthermore, also the amide NH, located between two Trp side chains, and the other carbonyl group adjacent the Fc moiety on a neighboring Fc bio-conjugate molecule, as well as the amide NH closest to the Fc moiety on one dipeptide chain and the central carbonyl group on the second dipeptide unit (and *vice versa),* are involved in the formation of additional HB to thickens the supramolecular architecture. A simplified scheme of the intermolecular HBs between neighboring units of **1**, which is responsible for the formation of a nanofibrillar network structure, is shown in Fig. 1.

Compound **1** forms a gel in nitrobenzene (after sonication) and dichlorobenzene (on cooling a hot solution) at 3.4% and 2.7% w/v, respectively, with melting points at these concentrations of 54 and 56 °C, respectively. Frequency sweep rheology evidenced the soft nature of the material (G′ was found to be higher than G\prime\prime , with a G′/G\prime\prime ratio of 0.279 as index of its elasticity). Interestingly, self-healing experiments evidenced the capability of the gel of **1** to spontaneously self-heal after being broken and to recover the mechanical properties over cycles of strain addition and lifting, not observed/noticed for the Fc-dicarboxylic acid derivative of the single amino acid Trp [55].

TEM images of a dried gel solution of **1** show the presence of nanofibres as the main morphology (Fig. 2A). However, the addition of iron (III) perchlorate to the gel of **1** cause a gel-sol transition. This was confirmed by the TEM image reported in Fig. 2B, in which it is possible to notice/observe the disappearance of the entangle fibres and the formation of nanospheres. In dichlorobenzene the gel of **1** expressed supramolecular chirality, as demonstrated by concentration-dependent circular dichroism (CD), with a strong positive Cotton effect at around 500 nm. This signal disappeared upon the addition of a oxidizing agent, due to the disruption of the supramolecular helicity.

Intra- and intermolecular weak interactions in Fc-peptide conjugates can be tuned passing from systems featuring two adjacent peptide chains linked to the Fc organometallic core, to systems featuring only one pedant peptide chain with dramatic consequence on the gelation behaviour [59].

In particular, the bio-conjugate **2** was studied by Kraatz and co-workers for supramolecular gelation and stimuli responsive behaviour [62]. Gelator **2** was dissolved in hot toluene and chlorobenzene, forming an organogel when cooled at 25 °C (minimum gelation concentration (MGC) 6 mM and 8 mM for the two solvents, respectively). Interestingly, reversible sol–gel transformations were obtain over several cycles of heat-cool processes ($T_{gel} = 45$ °C and 55 °C for toluene and chlorobenzene, respectively). The obtained gel is opaque and metastable as a precipitate is formed after 1–2 h after gelation. However, a transparent organogel as nanofibres of 28 (±7) nm (from TEM measurements) can be obtained from MeCN/toluene (1:2 v/v) which is stable for several months in ambient conditions (MGC 8 mM, T_{gel} 52 °C at MGC). Despite the presence of the imidazole moiety in **2**, no gel was formed in the mixed solvent system MeCN/toluene (1:2 v/v) in the presence of Co^{2+}, Ni^{2+}, Cu^{2+} and Zn^{2+}. However, the presence of the binuclear cluster $[Fe(\mu\text{-}S)_2Cl_4]^{2-}$ favored gelation with nanotubular morphology (average diameter of nanotubes 24 (±6) nm from TEM measurements), thus representing the first example of prebiotic self-assembly.

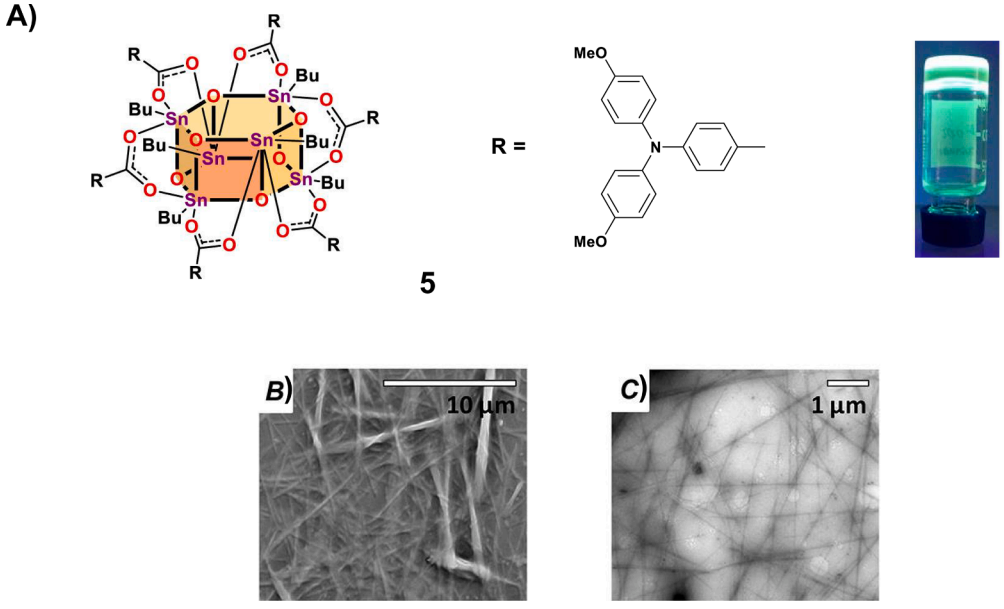

Fig. 7. A) Chemical structure of gelator **5** and inversion tube test of the organogel of **5** in benzene under the UV light; B) and C) SEM and TEM images, respectively, of the xerogel of **5** obtained in benzene. Copyright ACS 2022. Reproduced with permission from ref. [64].

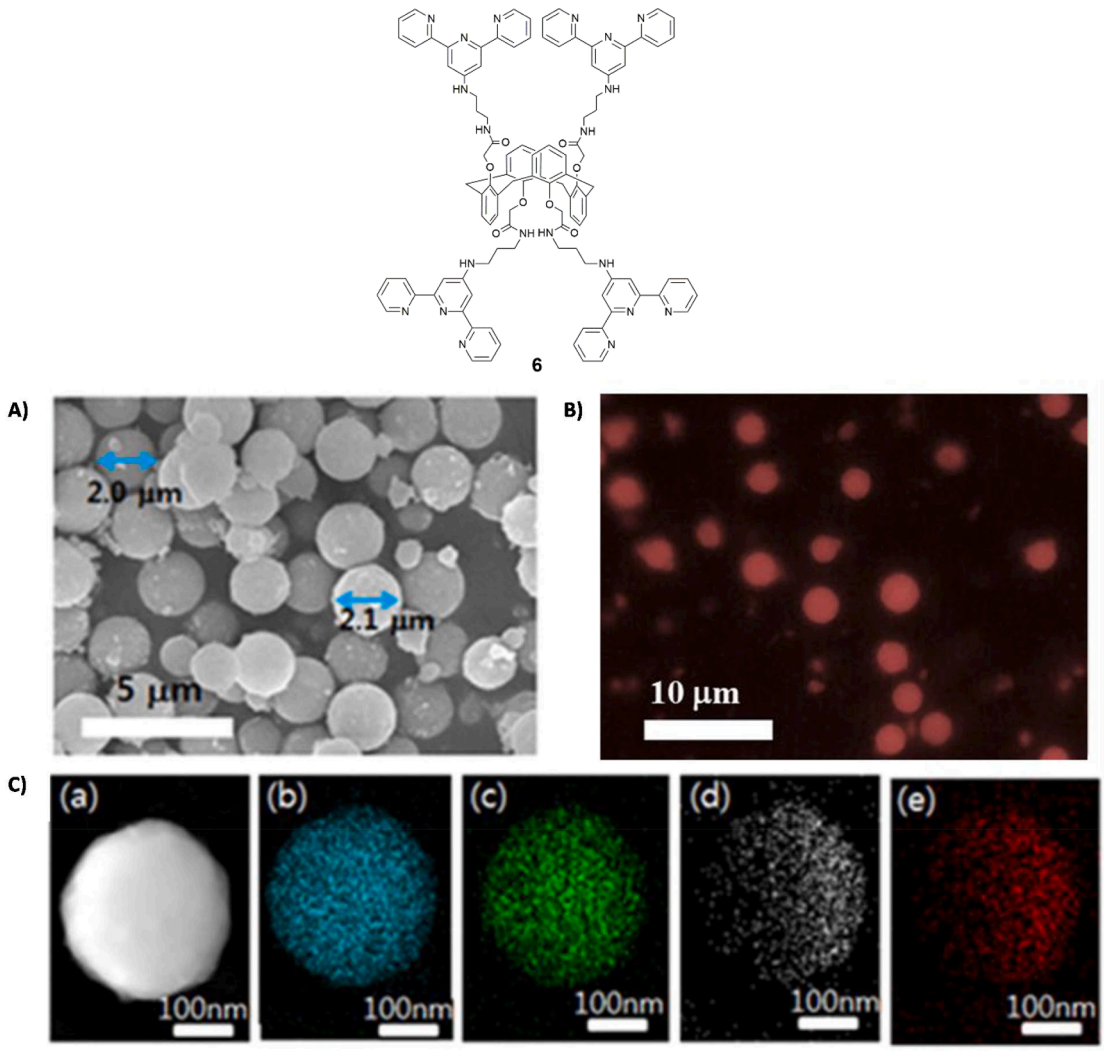

Fig. 8. A) SEM and B) fluorescence microscopy images of Pt^{2+}-**6** metallogel (1.0 wt%) in DMSO/H_2O (3:7 v/v); C) energy Dispersive Spectroscopy (EDX) mapping of the Pt^{2+}-**6** metallogel, (a) bright-field image, (b) platinum, (c) carbon, (d) oxygen, and (e) nitrogen components. Copyright ACS 2014. Reproduced with permission from ref. [65].

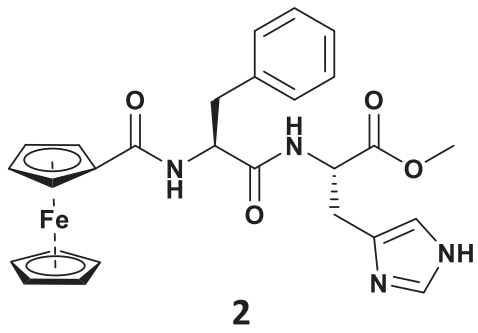

Sweep frequency rheology (from 0.1 to 100 rad s^{-1}) evidenced a significant dependence of the ratio between G′ and G\prime\prime from the medium. Indeed, an increase of G′/G\prime\prime was observed on passing from the organogel prepared from toluene to the organogels prepared in MeCN/toluene (1:2 v/v) both in the absence and in the presence of the binuclear cluster $[Fe(\mu\text{-}S)_2Cl_4]^{2-}$, thus supporting the high elastic character of gels obtained from the mixed solvent system. Furthermore, the organogels obtained from **2** in MeCN/toluene (1:2 v/v) showed a thixotropic behaviour.

Indeed, as shown in Fig. 3A, the organogel of **2** immediately recovered its initial mechanical properties after removal of the high strain. However, the presence of $[Fe(\mu\text{-}S)_2Cl_4]^{2-}$ caused an uncomplete recover of the G′ modulus after removal of the high strain in each cycle (Fig. 3B). Interestingly, the addition of equimolar $Fe(ClO_4)_3$ to the organogel obtained from **2** in MeCN/toluene (1:2 v/v) caused a gel-sol transition accompanied by a colour change of the solution from yellow to deep blue, suggesting the oxidation of the Fc moiety. However, the solution turned back to yellow upon the addition of ascorbic acid, with the reformation of the original organogel after the neutralization of the solution with ammonia. These findings suggested that the organogel formation depends on the protonation state of the imidazole ring of the histidine residue in **2**.

Fc has been used to modify β-Cyclodextrins (CDs) by Aiyou Hao and co-workers [63]. They studied two new CD derivatives, **3** (BA-Fc-CD) and **4** (HA-Fc-CD) linked with ferrocene, as supramolecular gelators.

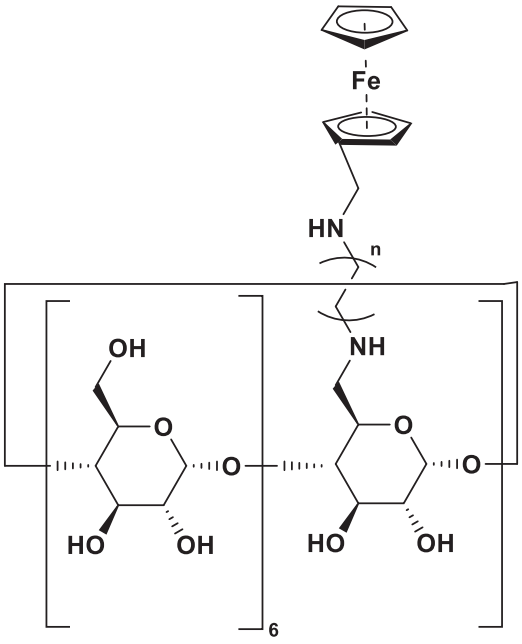

n = 2; BA - Fc - CD (3)
n = 3; HA - Fc - CD (4)

Gelator **3** aggregates at a concentration of 7.0 mM in water in the form of micron-scale flexible fibres, as demonstrated by the transmission electron spectroscopy (TEM), scanning electron spectroscopy (SEM) and atomic force microscopy (AFM) images reported in Fig. 4A-C, respectively. It has been observed that also **4** aggregates in a similar fashion.

When **3** was mixed with N-methyl pyrrolidone (NMP) and acetone a new organogel formed. The SEM images reported in Fig. 5A–C evidence a three-dimensional network structures of spherical aggregates. The material expressed a solid-like behaviour, with a G′/G\prime\prime >10 and a crossover point close to 10^3 Pa (Fig. 5D for the dynamic oscillatory sweep stress rheology).

Interestingly, upon the addition of oxidant species, such as H_2O_2 or copper(II) ions, a gel sol transition was observed, accompanied by a dramatic colour change from yellow to deep blue (Fig. 6), demonstrating the stimuli-responsive behaviour of this gel.

Collavini, Sánchez, Delgado and co-workers reported the gelation behaviour of a new organostanoxane drum **5** [64]. Gelator **5** formed fluorescent stable organogels in aromatic solvents, such as benzene and toluene (Fig. 7).

The formation of the gel was found to be extremely concentration dependent. SEM and TEM analysis demonstrated that the morphology of the material is characterized by a thick fibrous network. The authors suggested that the gel formation is triggered by C—H···π interactions, as supported by the ^{1}H NMR experiments conducted at variable temperature.

3. Luminescent metallogels

By combining metal centers and different ligands *via* coordination interactions, supramolecular gels with fascinating properties such as photoluminescence, can be obtained. Jung and co-workers reported a calix[4]arene derivative containing terpyridine (**6**) able to form metallogel in DMSO/H_2O (3:7 v/v) in the presence of Pt^{2+} (added as its chloride salt) [65]. The SEM, image of the Pt^{2+}-**6** metallogel obtained displayed spherical structures with diameters of 1.8–2.1 μm (Fig. 8A).

The Pt^{2+}-**6** metallogel showed a strong red colour emission upon excitation at 420 nm (Fig. 9A). The intensity and the wavelength emission depends on the DMSO/H_2O ratio in the solvent mixture, which affects the formation of Pt-Pt and π-π stacking interactions.

Although the presence of the Pt^{2+}, along with a different DMSO/H_2O ratio, influenced the optical properties of the Pt^{2+}-**6** metallogel, the concentration of the metal ion did not affect the rheological properties of the material. Indeed, the Pt^{2+}-**6** metallogel formed upon the addition of 4 equivs. of Pt^{2+}, remains stable for further addition of platinum salt.

M. Haukka and co-workers described the self-healing properties of luminescent metallogels formed by platinum(II) complexes of terpyridine based gelators **7** and **8** bearing perfluoroalkyl and alkyl side chains [66].

The rapid gelation of the complex {[Pt(**7**)Cl]Cl}, that occurred both in DMSO and in DMF, is due to the simultaneous presence of Pt-Pt and F-F interactions (Fig. 10), which are also responsible for the construction of hierarchical superstructures. These interactions are also responsible for the self-assembly-induced luminescence with an emission band at about 650 nm (Fig. 11B), and self-healing. As show in Fig. 11B the fluorescence intensity emission decreases as the temperature increases and a blue shift, from 640 nm to 600 nm, occurs by varying the temperature from 25 °C to 80 °C. Temperature sweep rheology experiments revealed that the gel formed by {[Pt(**7**)Cl]Cl} did not change its rheological properties in this range of temperature.

K.C. Chang and co-workers reported the study of a series of platinum (II) complexes with the gelator **9** [67].

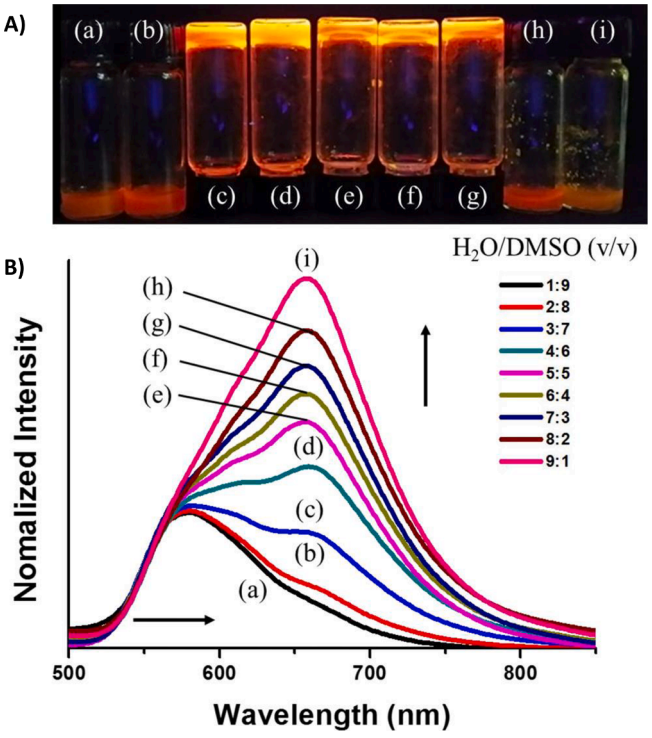

Fig. 9. A) Photograph of the Pt^{2+}-**6** metallogel at 1.0 wt% under UV light at various H_2O/DMSO volume ratios (from 1:9 to 9:1 v/v); B) emission spectra of the Pt^{2+}-**6** metallogel at 1.0 wt% under UV light at various H_2O/DMSO volume ratios (from 1:9 to 9:1 v/v) at 25 °C. Copyright ACS 2014. Reproduced with permission from ref. [65].

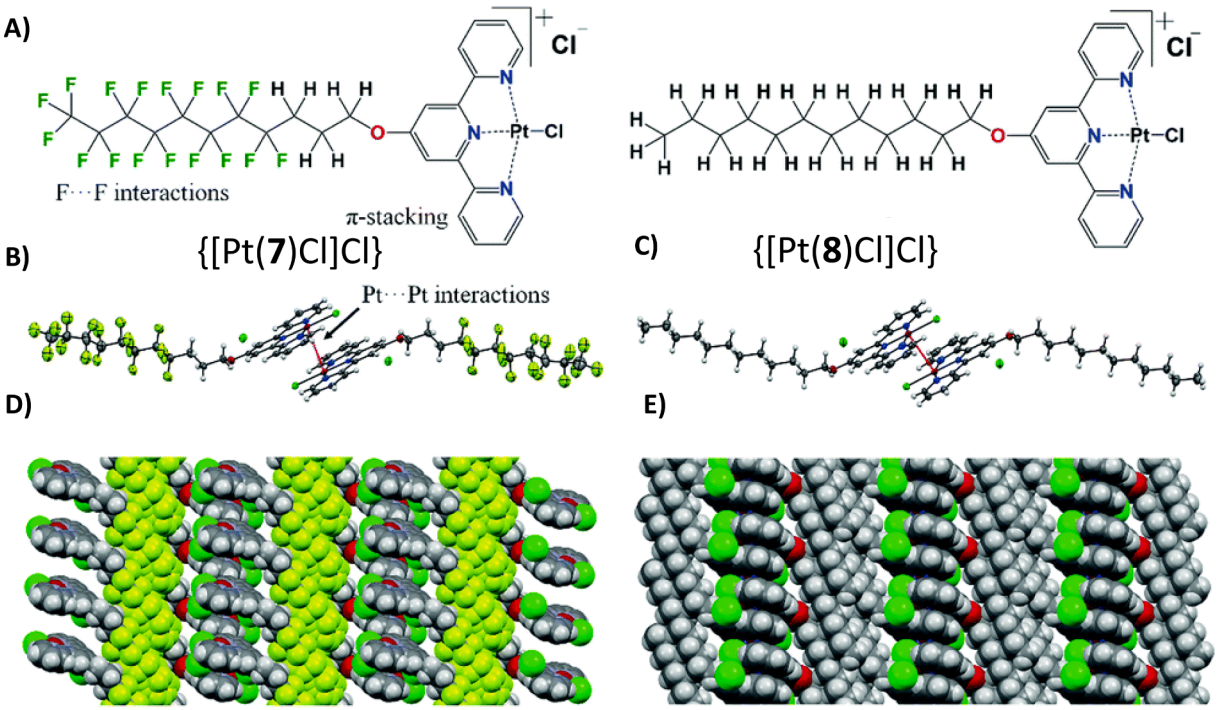

Fig. 10. A) {[Pt(**7**)Cl]Cl} and {[Pt(**8**)Cl]Cl} complexes; B) and C) SCXRD of {[Pt(**7**)Cl]Cl} and {[Pt(**8**)Cl]Cl} respectively, with Pt···Pt interaction; D) and E) crystal packing of {[Pt(**7**)Cl]Cl} and {[Pt(**8**)Cl]Cl}, respectively. Copyright RSC 2020. Reproduced with permission from ref. [66].

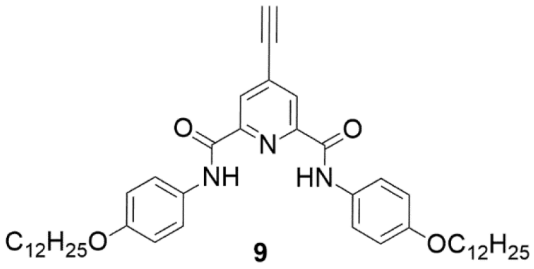

9

In the formation of these complexes several type of non-covalent interactions, such as HB, π-π, and Van der Waals, are combined to form an entangle network able to entrap organic solvents and to form the luminescent metallogel Pt^{2+}-**9**. The increase of the temperature caused the gel-sol transition of Pt^{2+}-**9**, with an enhancement of the emission of Pt^{2+}-**9**, due to the formation of the low-energy excimer assemblies in the excited state. Indeed, as shown in Fig. 12A, Pt^{2+}-**9** exploited the higher degree of freedom at the molecular level as a consequence of the increase of the temperature and the break of the metallogel, to self-assemble/rearrange in molecular aggregates and to form the excimer.

Yam and co-workers report a luminescent gold(III) complexes obtained with a chlorogold(III) precursor and gelator **10** [68].

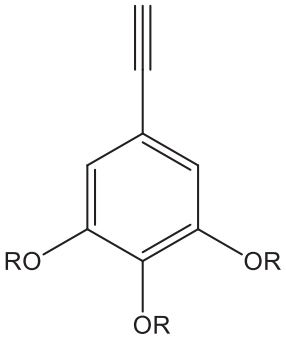

10

R = OCH_3 **10a**
$OC_{12}H_{25}$ **10b**
$OC_{16}H_{33}$ **10c**
$OC_{18}H_{37}$ **10d**

These bis-cyclometalated alkynylgold(III) complexes exhibit gelation properties due to hydrophobic-hydrophobic interactions and π–π stacking. In particular, metallogel of **10d** is highly stable and show an appreciable change in absorption and emission spectra during the sol–gel transition observable upon an increase of the temperature from 10 to 40 °C (Fig. 13). This system can be used as a probe to detect microenvironmental changes.

Lanthanide ions, especially Tb^{3+} and Eu^{3+}, have interesting photoluminescence properties including their high quantum yield, narrow band emission, high photochemical stability, long luminescence lifetime (μs–ms range), and low long-term toxicity and have recently been used to synthesize metallogels with interesting properties [69–71]. In this context, the pyridine-2,6-dicarboxylic acid derivative **11**, was found to form 3D self-assembly units when reacting in different stoichiometry ratios (1:2 and 1:3 Ln^{3+}/**11**) with Tb^{3+} and Eu^{3+} as their trifluoromethanesulfonate salts (Fig. 14) [72]. Supramolecular polymers formed under microwave conditions in 1:3 stoichiometry, when further treated with acetate salts of Eu^{3+} or Tb^{3+} in methanol, formed luminescent gels emitting with a characteristic red (Tb^{3+}) or green (Eu^{3+}) lanthanide based emission (Fig. 15).

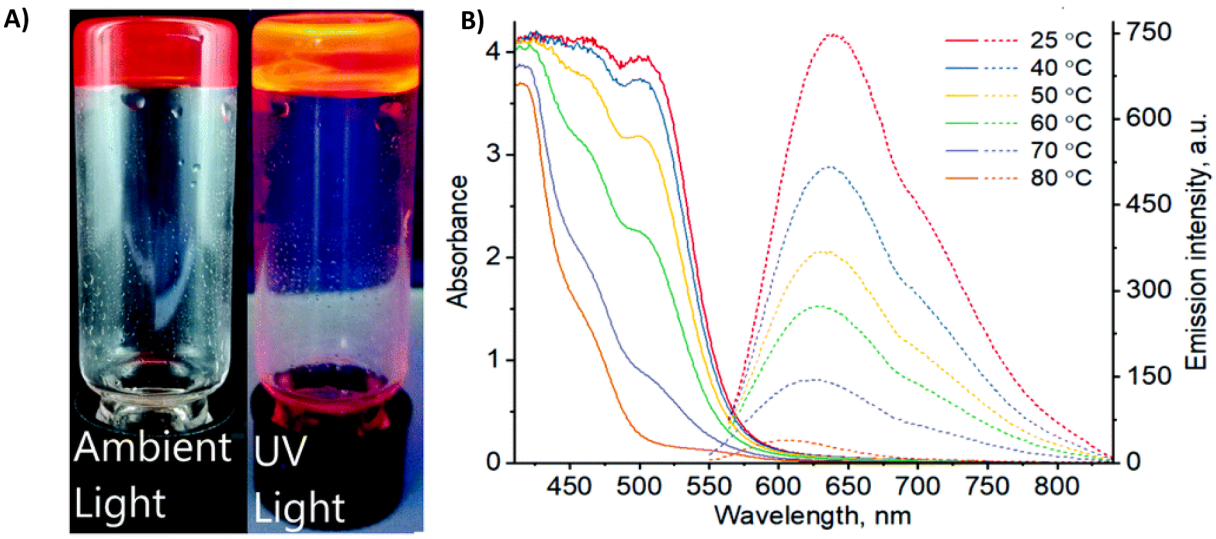

Fig. 11. A) Pictures of the gel formed by {[Pt(**7**)Cl]Cl} in DMSO in the presence and in the absence of UV-light radiation; B) UV–Vis (solid lines) and fluorescence (dashed lines) spectra of the gel formed by {[Pt(**7**)Cl]Cl} (0.6%) in DMSO at different temperatures ($\lambda_{ex} = 550$ and 530 nm for $T = 25$–60 °C and $T = 70$–80 °C, respectively). Copyright RSC 2020. Reproduced with permission from ref. [66].

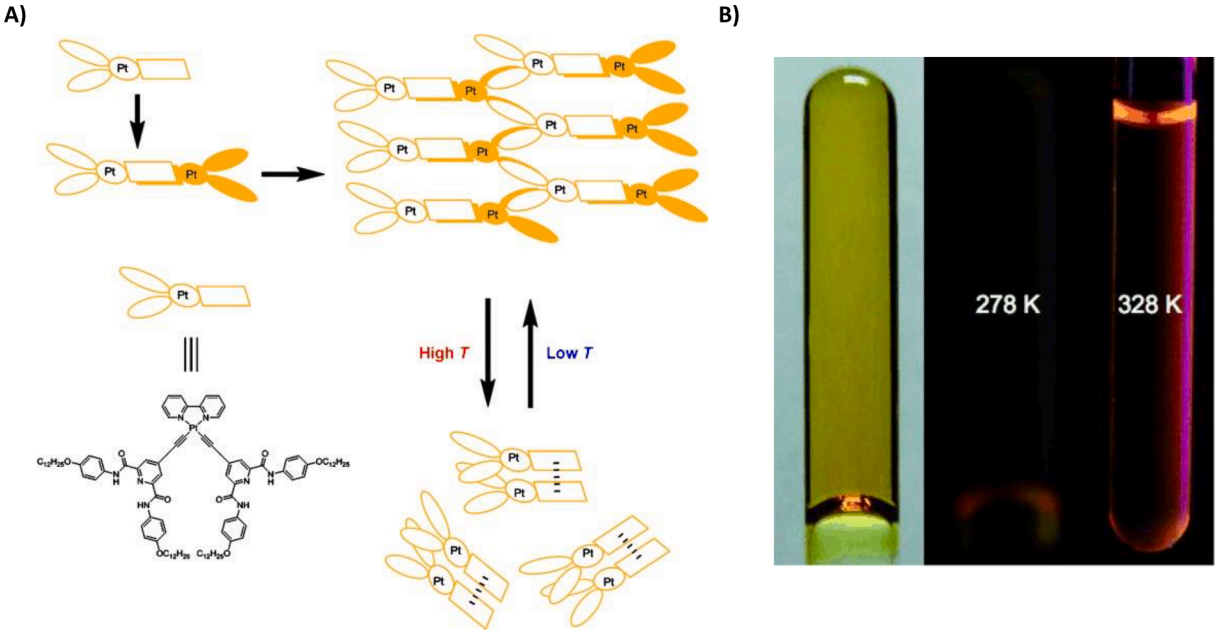

Fig. 12. A) Scheme of excimer formation in the excited state at high temperatures for Pt^{2+}-**9**; B) Pt^{2+}-**9** in toluene in the viscous form at 328 K (right), in the gel form at 278 K (middle), and at 298 K under the UV–Vis lamp ($\lambda_{ex} = 365$ nm). Copyright Wiley 2012. Reproduced with permission from ref. [67].

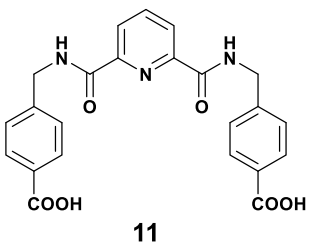

11

The authors prepared a new gel by adding various stoichiometry ratios of Ln^{3+} as their acetate salts, to a solution of the Ln^{3+} complex of **11** ($Ln(\mathbf{11})_3$) in MeOH, with Ln = Tb, Eu. The most stable soft gel was obtained as a opaque gel with a $Ln(\mathbf{11})_3/Ln(CH_3COO)_3$ molar ratio of 1:0.5. The Eu^{3+} and Tb^{3+} gels exhibited self-healing properties as show in Fig. 15F–I. Indeed, the reassemble of the gel spontaneously by self-healing process was noticed after cutting the gel in two.

To take advantage of the optical properties of the two gels obtained with each rare earth, a new soft material was obtained by mixing equal volumes of the two lanthanide gels previously described. A new luminescent gel was obtained featuring characteristic emission bands attributable to the Tb^{3+} emission at 545 nm, and to the Eu^{3+} emission at 616 nm (Fig. 15E).

More recently, H. Niu and co-workers described another example of gelator capable to form luminescent lanthanide-based metallogels. Gelator **12** formed a gel in the presence of Eu^{3+} (Eu^{3+}-**12**), Tb^{3+} (Tb^{3+}-**12**), and both Eu^{3+} and Tb^{3+} (Eu^{3+}/Tb^{3+}-**12**) (Fig. 16) [73]. Among them, Eu^{3+}/Tb^{3+}-**12** xerogel was found to selectively recognize methanol over a variety of solvents (Fig. 16A). For this reason, Eu^{3+}/Tb^{3+}-**12**

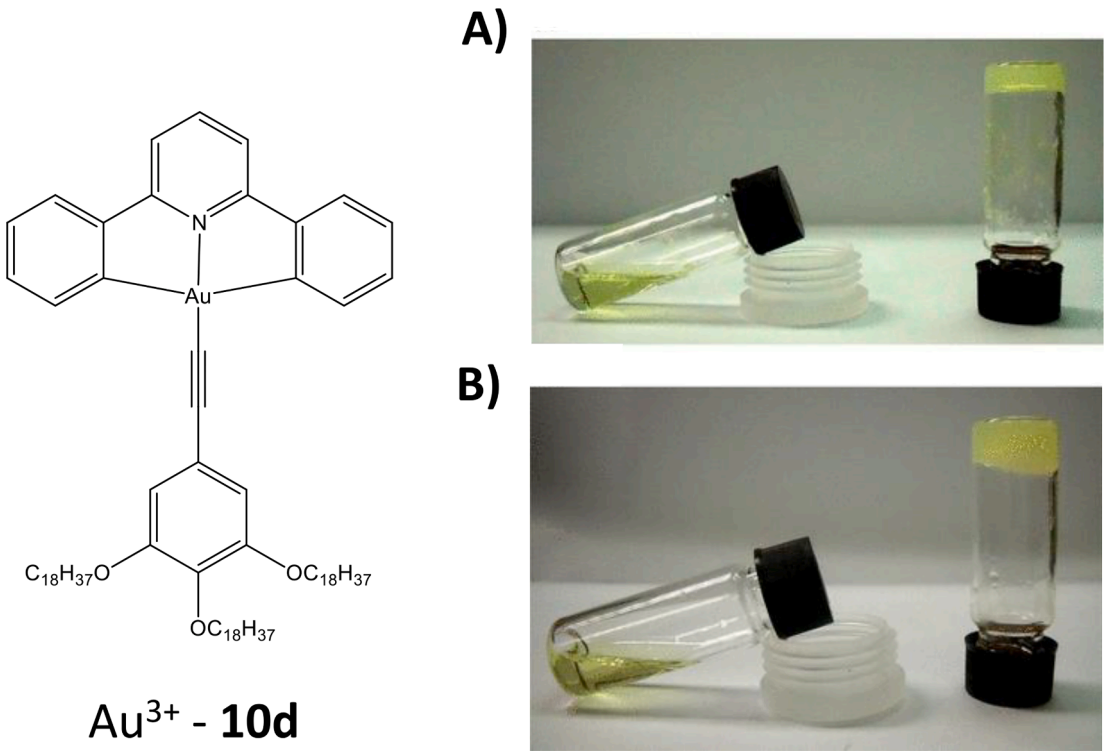

Fig. 13. Gel of **10d** obtained in A) hexane; and B) cyclohexane; on the left the sol obtained at elevated temperature ([Au] = 4.6 mg/mL). Copyright ACS 2013. Reproduced with permission from ref. [68].

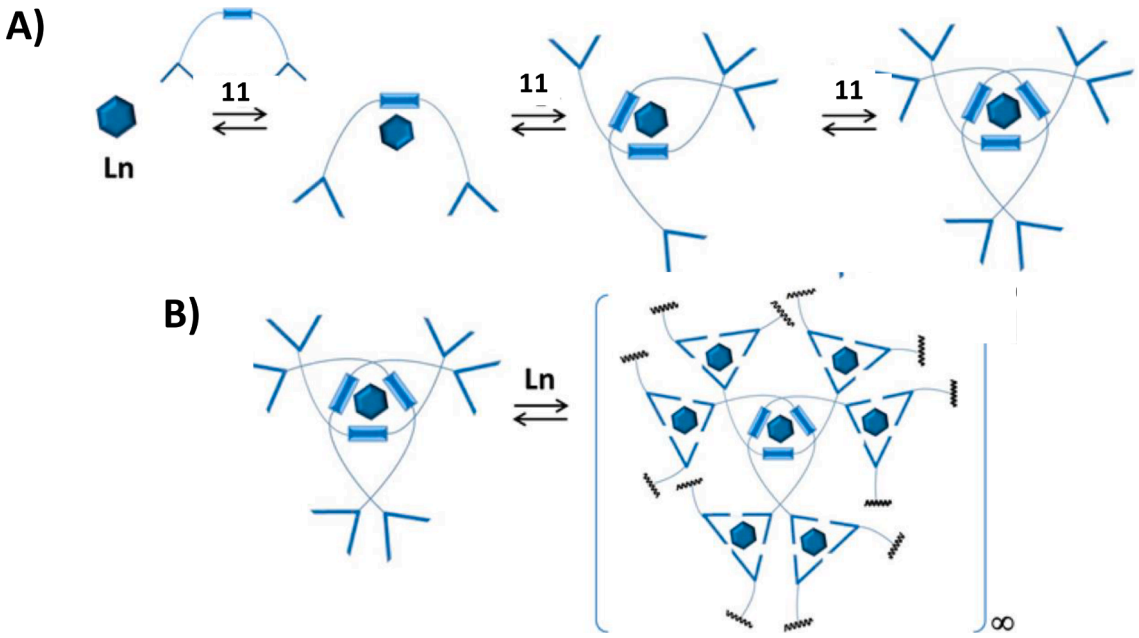

Fig. 14. A) Self-Assembly formation of Ln^{3+}-**11**; B) the metallo-supramolecular polymers obtained. Copyright ACS 2015. Reproduced with permission from ref. [72].

xerogel was used to prepare a self-calibrated fluorescent sensor for the recognition of methanol with excellent detection reproducibility and fast response. The sensor was prepared by using a cellulose filter paper soaked into an ethanol suspension of Eu^{3+}/Tb^{3+}-**12** xerogel, and after drying in air, it was exposed to methanol vapour. Furthermore, the prepared Eu^{3+}/Tb^{3+}-**12** paper-based sensor has demonstrated good response and recyclability to methanol vapour when placed in a nitrogen atmosphere.

Holten-Andersen and co-workers reported a luminescent metallogels obtained with lanthanide (Eu^{3+}, Tb^{3+}) and a terpyridyl-end-capped four arm poly(ethylene glycol) gelator **13** (Fig. 17) [74].

In particular, by adding increasing amount of Tb^{3+} (as its perchlorate salt) to a solution of **13** in DMF/MeCN (1:1 v/v) up to a gelator/lanthanide stoichiometry ratio of 2:1, a green emissive gel Tb^{3+}-**13** was obtained. The same procedure by using the perchlorate salt of Eu^{3+} allowed to obtain a red emissive gel Eu^{3+}-**13**. Curiously, with the aim to

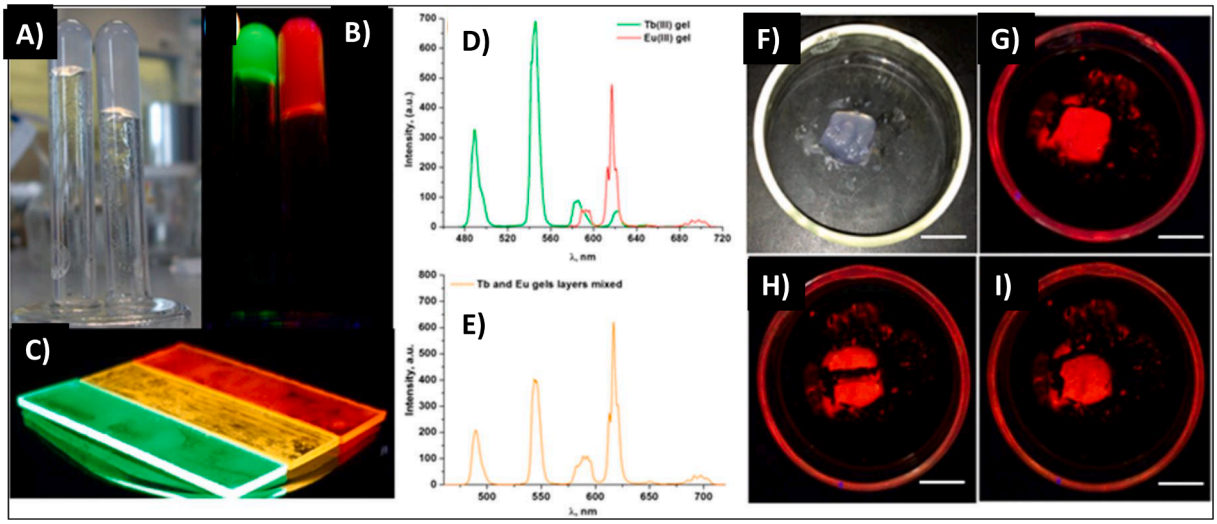

Fig. 15. Eu^{3+} and Tb^{3+} gels of **11** A) in day light; and B) under UV light; C) luminescence of Eu^{3+}, Tb^{3+}, and Eu^{3+}/Tb^{3+} gels of gelator **11** on quartz plates; D) Eu^{3+}, Tb^{3+}; and E) Eu^{3+}/Tb^{3+}-**11** mixed gel luminescence spectra at 25 °C ($\lambda_{ex} = 275$ nm); F – I) healing experiment of Eu^{3+}-**11** gel with F) Eu^{3+} gel under day light, G) under UV light, H) gel after being cut in half, and I) self-healing properties of the gel (scale bars, 1 cm). Copyright ACS 2015. Reproduced with permission from ref. [72].

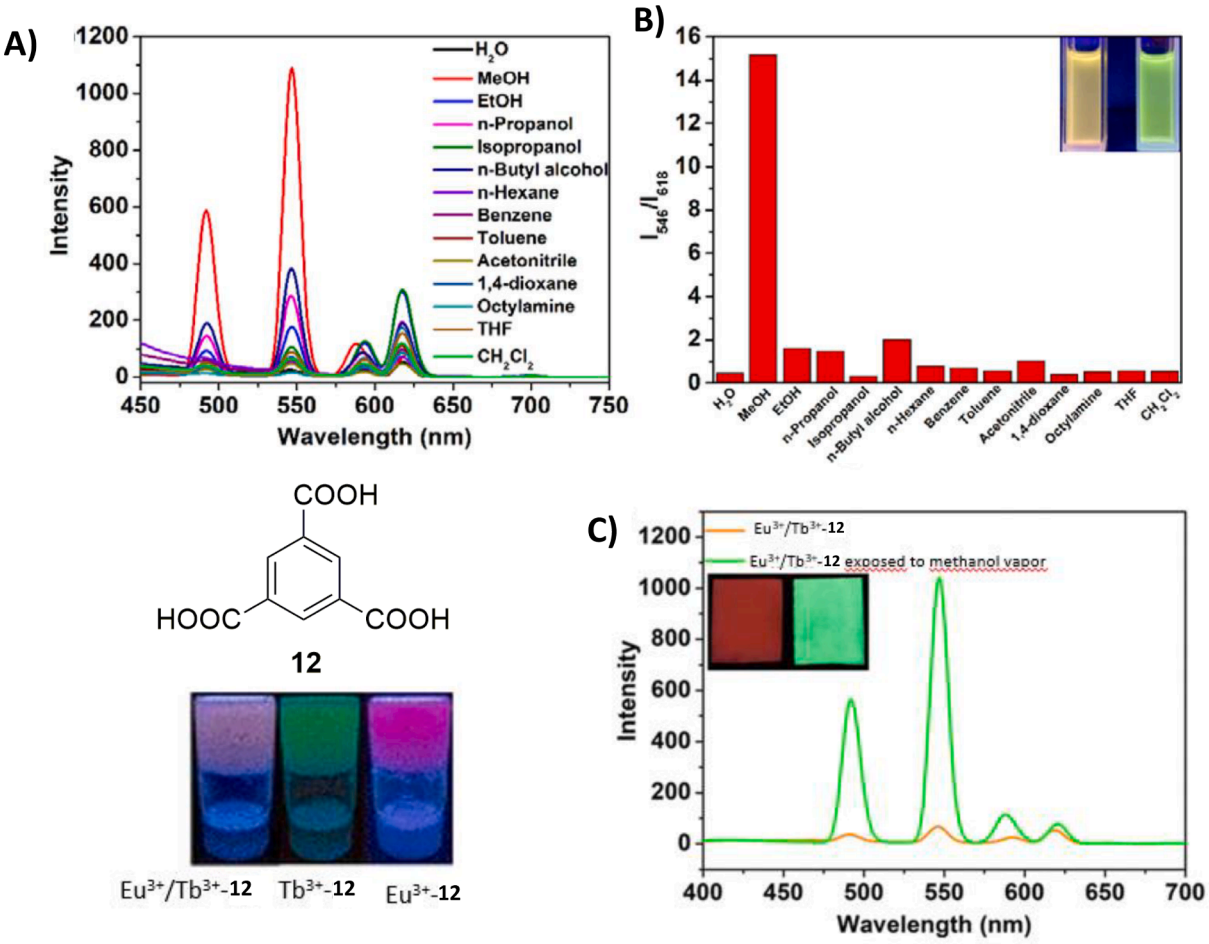

Fig. 16. Molecular structure of **12** and representation of its gels (Eu^{3+}-**12**), (Tb^{3+}-**12**), and (Eu^{3+}/Tb^{3+}-**12**) under the UV lamp at 302 nm. A) Luminescence spectra of the Eu^{3+}/Tb^{3+}-**12** xerogel dispersed in different solvents; B) Histogram of the intensity ratios of Tb^{3+} (546 nm) to Eu^{3+} (618 nm), inset: different emission visible by naked eye of a dispersed solution in MeOH (right) and EtOH (left) of Eu^{3+}/Tb^{3+}-**12**; C) fluorescence spectra of the Eu^{3+}/Tb^{3+}-**12** paper-based sensor before and after exposing to MeOH vapour, inset: effect of the exposition of the Eu^{3+}/Tb^{3+}-**12** paper-based sensor to MeOH vapour (right). Copyright ACS 2021. Reproduced with permission from ref. [73].

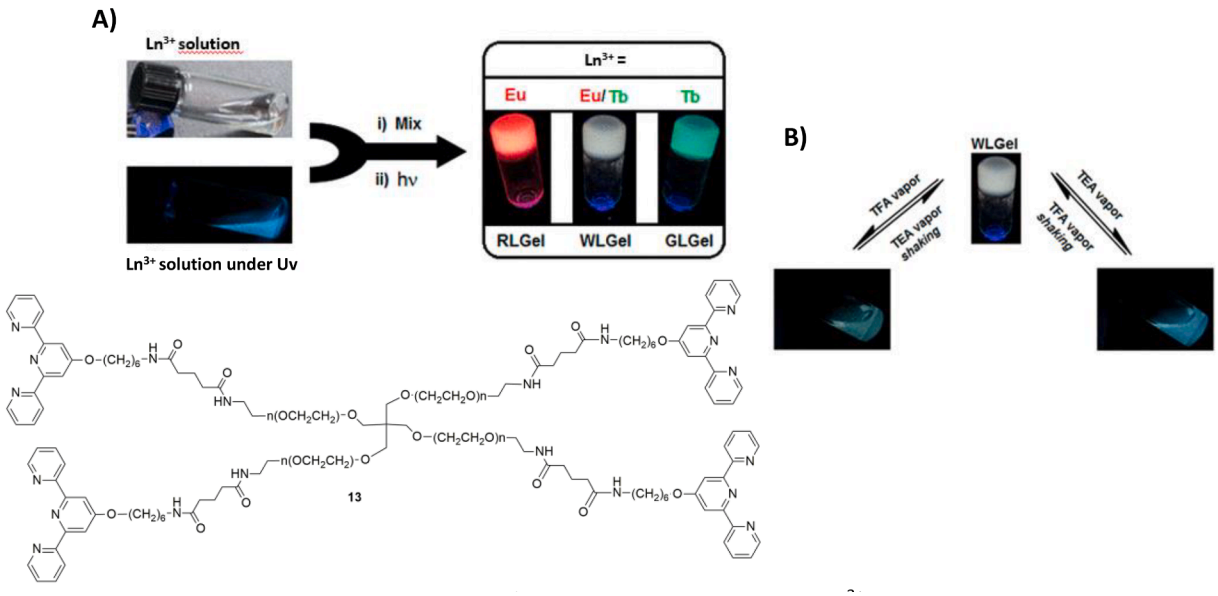

Fig. 17. Chemical structure of gelator **13**. A) Schematic preparation of Ln^{3+} coordination-based luminescent metallogels under UV light ($\lambda_{ex} = 365$ nm, 3.5 wt% gelator **13**, DMF/MeCN 1:1 v/v); B) stimuli-responsive emission colour changes and phase transitions of white-light metallogel (WLGel): pH-triggered vapochromism. Copyright ACS 2015. Reproduced with permission from ref. [74].

modulate the emission of the material obtained, the authors reported the emission spectra of the red emissive gel upon the addition of increasing amount of the green emissive gel. As a result, a white light gel was obtained with a ratio between Eu^{3+} and Tb^{3+} of 4:96 (Fig. 17A). These findings offered an enormous potential regarding the possibility to exploit these stimuli-responsive properties. Indeed, a reversible gel-sol transition accompanied with a significant change of the emission spectrum was observed by treating the white light emitting Eu^{3+}/Tb^{3+}-**13** gel with vapours of trifluoroacetic acid and triethylamine (Fig. 17B).

Das and co-workers developed a novel family of gel containing lanthanides (Eu^{3+}, Tb^{3+}, and mixed Eu^{3+}/Tb^{3+} or Eu^{3+}/Ir^{3+}) using the terpyridine derivative **14**-X (X = F, Cl) (Fig. 18) [75].

The Eu^{3+}-**14**-X and Tb^{3+}-**14**-X metallogels expressed an intense red and greed emission, respectively, under the UV light at 365 nm. Interestingly, also in this case a white light emitting gel Eu^{3+}-**14**-F/Tb^{3+}-**14**-F was obtained by mixing the Eu^{3+} and Tb^{3+} perchlorate salts with **14**-F in a 1:1:1 molar ratio in DMF. Furthermore, the luminescence of the material could be modified/modulated by changing the ratio of the three components of the system (See Fig. 18).

These metallogels can be used to fabricate a luminescent agarose gel by a simple drop casting procedure and also transparent luminescent poly(methyl methacrylate) (PMMA) films by embedding the gel into a PMMA polymer matrix without affecting the optical properties of the metallogels.

Another example of lanthanide based metallogels were reported by H. Wang and co-workers [76]. Indeed, gelator **15** was found to be able to form the Tb^{3+}-**15** metallogel through HB and π-π stacking interactions (Fig. 19).

Tb^{3+}-**15** was characterised by a stable luminescent behaviour, attributable to the thermal stability of the gels. In addition, under alkaline and acidic conditions, Tb^{3+}-**15** exhibited an "on–off" luminescence behaviour, which depends upon the external acidic/alkaline stimuli (Fig. 20).

M. Xue and co-workers obtained photoluminescent lanthanide metallogels by mixing the aromatic carboxylic ligands **16a–c** with Tb^{3+} or Eu^{3+} nitrate salts [77]. As shown in Fig. 21, the metallogels expressed an intense green and red luminescence, due to the presence of the Tb^{3+} and Eu^{3+} respectively, under the UV lamp at 365 nm.

Tb^{3+}-**16c** metallogel obtained in a mixture of DMF/H_2O (1:1 v/v) was found to be the most stable of the series, as indicated by the sweep stress rheology measurements. Furthermore, Tb^{3+}-**16c** exhibited remarkable self-healing, self-supporting, and film-forming properties (Fig. 22).

Wang and co-workers reported another example of lanthanide based metallogel by using the triazine derivative **17** [78]. Upon heating, **17** was able to gelate in the presence of Tb^{3+}(as its chloride hydrate salt). The Tb^{3+}-**17** metallogel obtained exhibited an excellent mechanical stability, as well as a retained luminescence, over a wide range of temperature (0–100 °C). Furthermore, Tb^{3+}-**17** xerogel expressed an intense green luminescence when dispersed in aqueous solution (Fig. 23), conferring it a great potential as biomolecules sensor.

Dubey and co-workers obtained a fluorescence metallogel by mixing two non-fluorescent components, the phenyl-succinic acid derived ligand **18** and LiOH in DMF [79]. In this gel, Li^+ ion plays a crucial role in the gelation process because it causes the aggregation of single ligand molecules and also contributes to generate a fluorescent emission by imposing a restriction on intra-molecular proton transfer to the excited state (ESIPT), thus causing the chelation-enhanced fluorescence (CHEF) phenomenon (Fig. 24).

Liu and co-workers prepared a quinolinol-functionalized L-glutamide fluorescent gelator **19** able to form chiral metallogels in the presence of Li^+, Zn^{2+}, and Al^{3+} (Fig. 25A) [80]. Among them the Zn^{2+}-**19** metallogel was able to recognize the (*R,R*)- and (*S,S*)-1,2-diaminocyclohexane enantiomers, with fluorescence emission changes appreciable by naked eye under a UV lamp. Indeed, when Zn^{2+}-**19** metallogel interacted with the (*S,S*) enantiomer, the emission of the metallogel under irradiation at 365 nm turned from cyan to yellow. On the other hand, the addition of the (*R,R*) enantiomer caused a gel-sol transition of the Zn^{2+}-**19** metallogel, with no significant changes in the fluorescence emission (Fig. 25B).

4. Metallogels for sensing

The development of metallogels as smart materials for sensing applications is a hot topic within supramolecular chemistry. It is possible to design different gelators able to form metallogels behaving like sensors

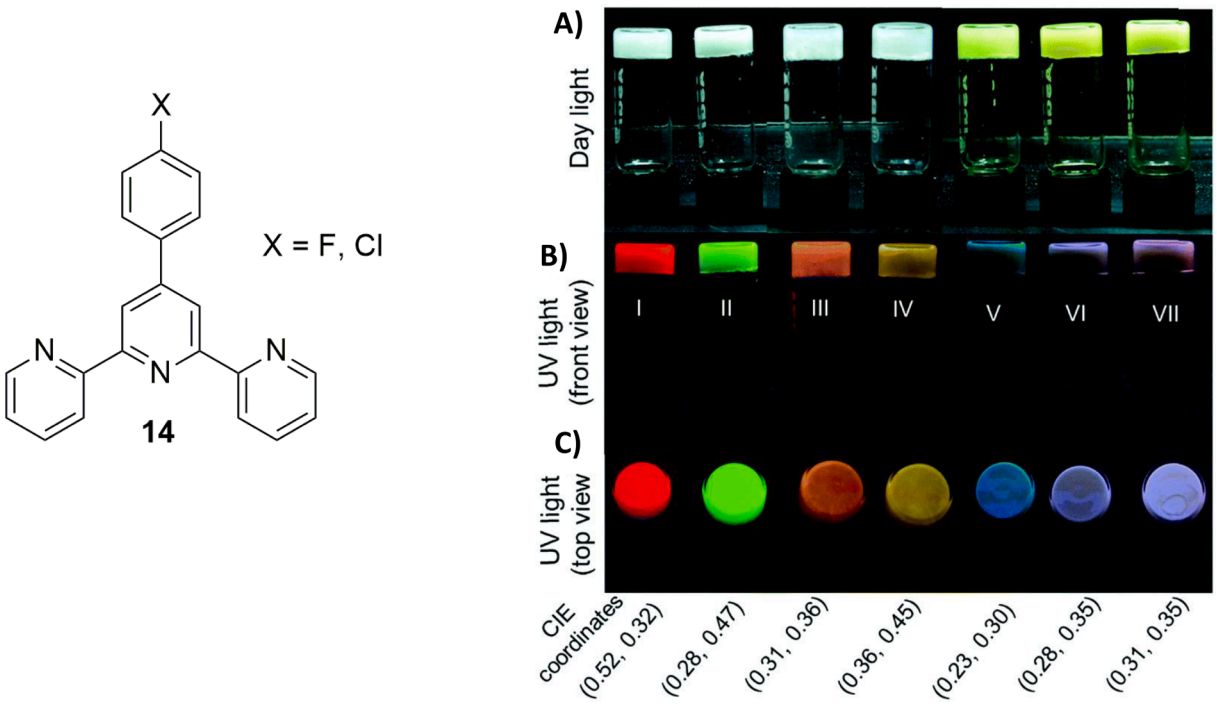

Fig. 18. Molecular structure of **14**-X (X = F and Cl); Inversion tube test of metallogels A) under ambient light; and B) and C) under UV lamp (λ_{ex} = 365 nm). I: Eu^{3+}-**14**-F, II: Tb^{3+}-**14**-F, III: Eu^{3+}-**14**-F/Tb^{3+}-**14**-F, IV: Eu^{3+}-**14**-F/2(Tb^{3+}-**14**-F), V: Ir^{3+}-**14**-F, VI: Eu^{3+}-**14**-F-Ir^{3+}, and VII: Eu^{3+}-**14**-Cl-Ir^{3+}. Copyright RSC 2018. Reproduced with permission from ref. [75].

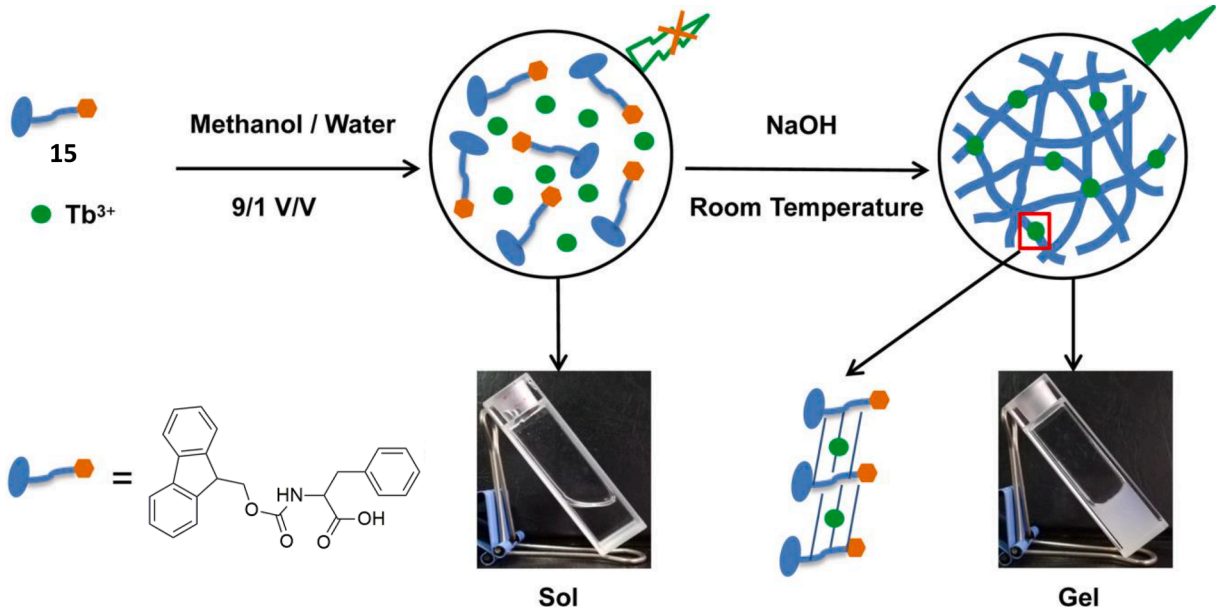

Fig. 19. Scheme of the Tb^{3+}-**15** gel formation. Copyright Elsevier 2019. Reproduced with permission from ref. [76].

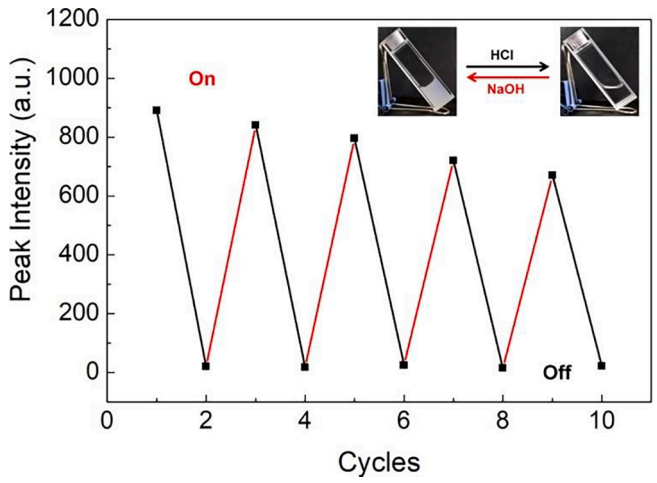

Fig. 20. Luminescence response of Tb^{3+}-**15** upon the addition of HCl (black line) and NaOH (red line). Copyright Elsevier 2019. Reproduced with permission from ref. [76].

for small neutral molecules and for charged species such as anions and cations. Anion sensing is one of the most studied applications for metallogels. Weitao Gong, Guiling Ning and collaborators reported an amide-based metallogel for fluoride sensing based on gelator **20** [81]. When **20** dissolves in DMF it self-assemble forming a strong organogel at 0.5% w/v with a T_{gel} of 58 °C. Gelator **20** emits fluorescence in the blue region both in solution and in the gel phase due to its twisted and rigid molecular structure.

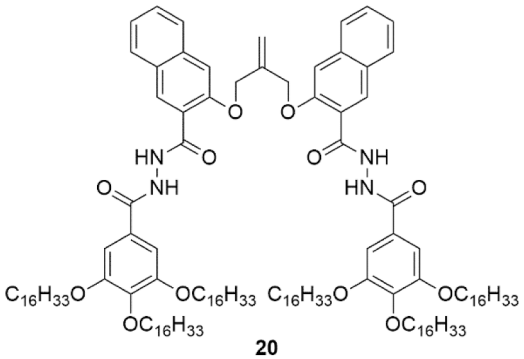

20

Authors evaluated the effect of the diffusion of various transition metal ions such as Cu^{2+}, Zn^{2+}, Hg^{2+} Cd^{2+}, Pb^{2+} Cr^{3+}, Ni^{2+}, Fe^{3+} Co^{2+}, Ag^{+}, lanthanide ion Ce^{2+}, and alkaline earth metal ions such as Mg^{2+} and Ca^{2+} into the supramolecular organic gel of **20**. Interestingly, the presence of Zn^{2+} caused a gel-gel transition with a change in the fluorescence emission from blue to light blue with a bathochromic shift of 20 nm and a partial quenching of the fluorescence. The supramolecular organogel formed by **20** emitted a blue fluorescence while the supramolecular metallogel Zn^{2+}-**20** emitted a light blue fluorescence with a quenching effect under the UV lamp at 365 nm and a red shift of the emission wavelength of 20 nm. Fig. 26A shows the effect on the emission properties of the organogel of **20** upon the addition of the metal ions investigated.

The anion recognition properties of the organogel formed by **20** and the metallogel Zn^{2+}-**20** have been investigated by adding stoichiometric amounts of a series of anions such as AcO^{-}, NO_3^{-}, $H_2PO_4^{-}$, F^{-}, Br^{-}, I^{-}, CN^{-}, and OH^{-} (in the form of tetrabutylammonium salts). When F^{-} diffused into the metallogel Zn^{2+}-**20** at room temperature, an intense blue-green emission was observed under the UV lamp as shown in Fig. 26 D. This change in the fluorescence emission was attributed to the formation of the new metallogel Zn^{2+}-**20**-F. As reported in Fig. 26 C upon addition F^{-} into the metallogel solution in DMF an increase of the intensity of the emission band at 465 nm was observed accompanied by a bathochromic shift of 35 nm.

Sebastian and Prasad reported about the ability of gelator **21** to form a cyanide-selective metallogel with Cu^{2+} [82]. The molecular skeleton of gelator **21** contains a terpyridine moiety that can facilitate the formation of the metallogel due to its chelating properties, and an acyl hydrazone linkage that can promote the gelation process *via* the formation of HBs. Gelator **21** formed organogels in various solvents and solvent mixtures like DMSO/H_2O, DMF/H_2O, dioxane/H_2O, and MeCN/H_2O (all in ratio 1:1 v/v) with a critical gelation concentration (CGC) value of 1 mg/mL. The organogel formed in DMSO/H_2O (1:1 v/v) was used for further studies and showed a strong emission probably due to an aggregation induced emission (AIE) process.

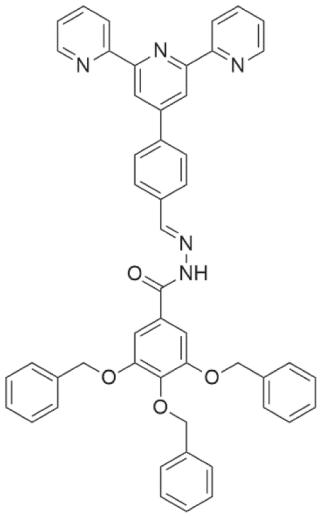

21

Upon the addition and diffusion of Cu^{2+} ions into the organogel of gelator **21** a green nonluminescent copper metallogel was obtained. Gelation studies proved that gelation is hampered when the concentration of metal was more than 0.8 equivs. [further studies have been carried out with 0.5 equivs. of copper(II)]. SEM has been used to analyze the gel morphology, Fig. 27A reports the SEM image of the Cu^{2+}-**21** metallogel that shows a fibrous nature, common in supramolecular gels. Rheological studies were performed to investigate the mechanical properties of the gel (Fig. 27B). The values of G′ and G\prime\prime are higher for the organogel than the metallogel and this is probably because the coordination of the metal ion causes a conformational change of the gelator with the terpyridine rings becoming planar and weakening the self-assembling process and hence the resulting gel.

The CN^{-} responsive behaviour of metallogel Cu^{2+}-**21** has been investigated. Upon addition of various anions to the metallogel a selective enhancement of the fluorescent emission was detected only upon addition of CN^{-}, due to the well-known affinity of Cu^{2+} for this anion. With all the other anion tested (F^{-}, Cl^{-}, Br^{-}, I^{-}, AcO^{-}, $H_2PO_4^{-}$, N_3^{-}, SCN^{-}, S^{2-}, ClO_4^{-}) no relevant changes were observed. Sensing studies were carried out by adding 100 μL (1 M) solutions of various anions to the metallogel. In Fig. 28 it is possible to observe the differences in the fluoresce emission of the free gelator, the metallogel Cu^{2+}-**21**, and the metallogel Cu^{2+}-**21** in the presence of cyanide. The observed behaviour was explained considering a decomplexation of Cu^{2+} from gelator **21** with the formation of stable $[Cu(CN)_x]^{2-x}$ species as confirmed by UV–Vis absorption spectroscopy and PXRD.

Another example of metallogel for cyanide sensing was reported by Ghosh, Deepa and Damodaran [83]. The two gelators mono-N-oxide pyridyl amides **22** and **23** were synthetized and the possible formation of metallogels was investigated.

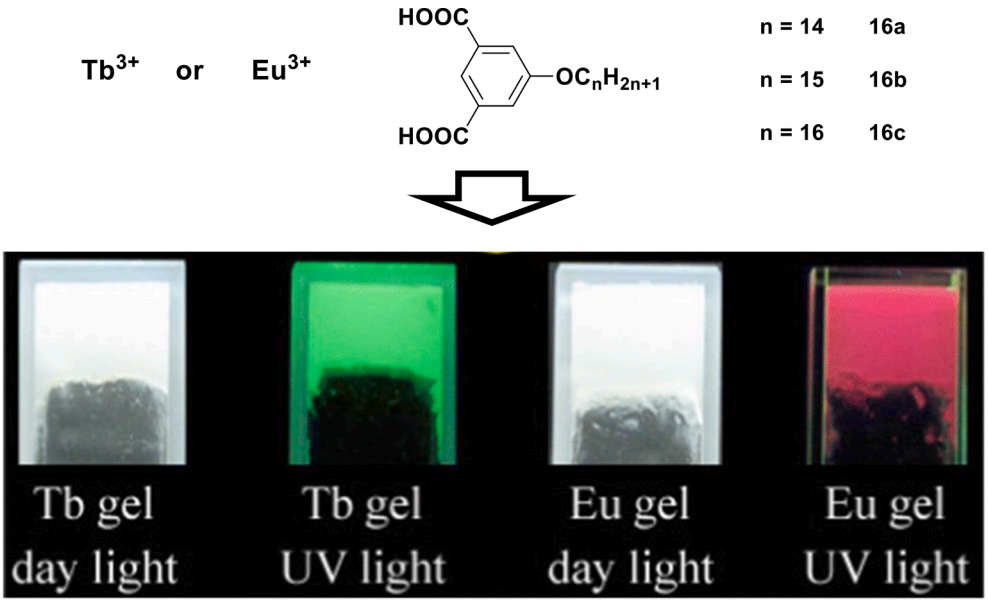

Fig. 21. Molecular structures of **16a–c**; Tb^{3+}-**16c** and Eu^{3+}-**16c** metallogels under day and UV light. Copyright Springer 2020. Reproduced with permission from ref. [77].

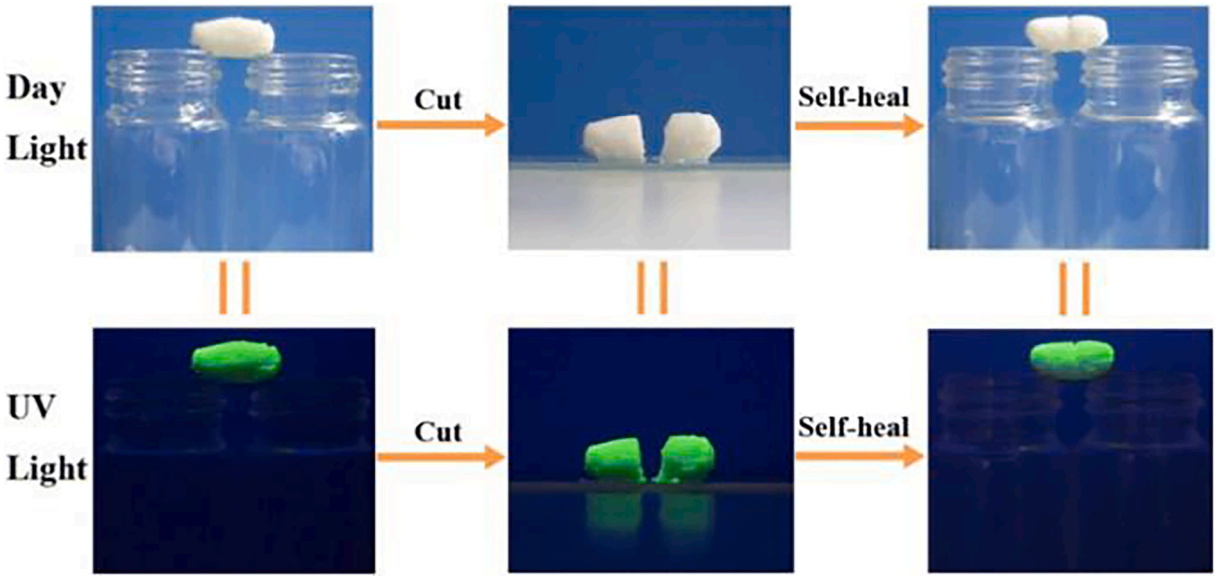

Fig. 22. Self-supporting and self-healing behaviour of Tb^{3+}-**16c** metallogel in DMF/H_2O (1:1 v/v) under day UV light. Copyright Springer 2020. Reproduced with permission from ref. [77].

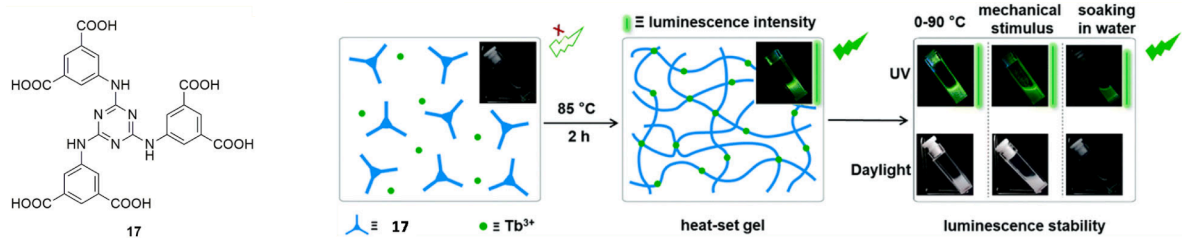

Fig. 23. Chemical structure of **17**; cartoon describing the preparation of Tb^{3+}-**17** metallogel. Copyright RSC 2020. Reproduced with permission from ref. [78].

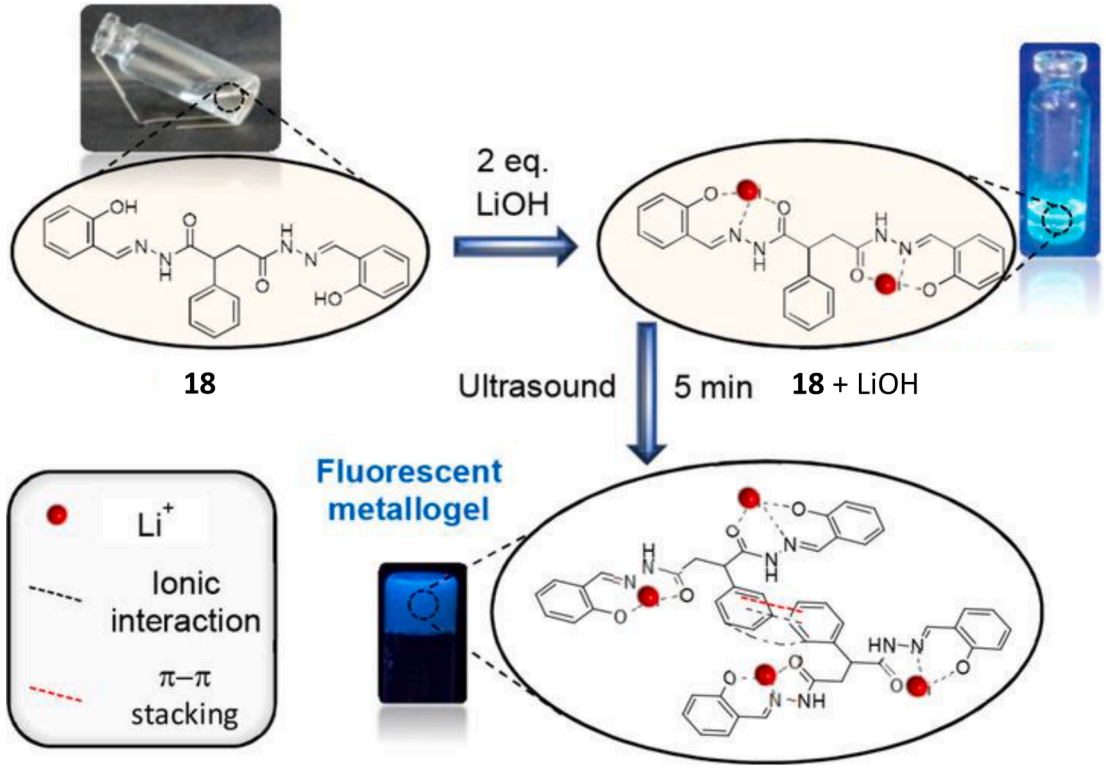

Fig. 24. Schematic pathway for the formation of the Li^{+}-**18** metallogel with the associate emission changes. Copyright Wiley 2020. Reproduced with permission from ref. [79].

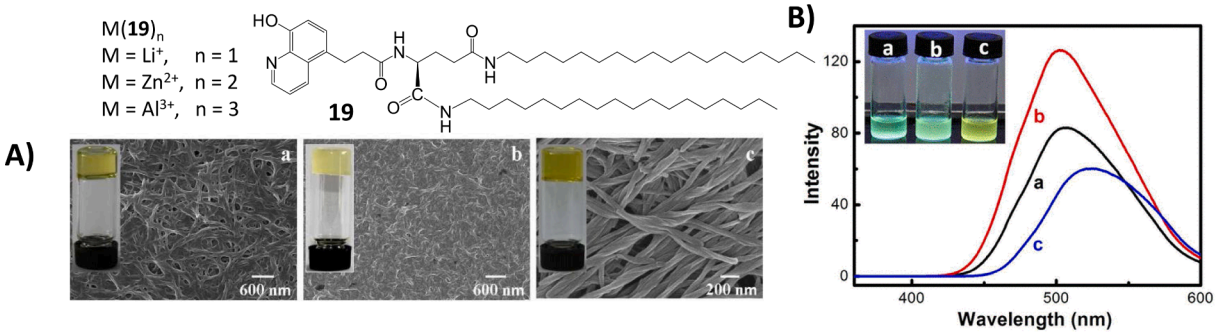

Fig. 25. Structure of gelator **19**; A) SEM images of (a) Li^{+}-**19**, (b) Zn^{2+}-**19** and (c) Al^{3+}-**19** xerogels obtained by the corresponding metallogels obtained in THF; B) fluorescence spectra of (a) the Zn^{2+}-**19** metallogel and (b) upon the addition of 1 equiv. of (b) (*R,R*)- and (c) (*S,S*)-1,2-diaminocyclohexane in THF ($\lambda_{exc} = 340$ nm). Copyright ACS 2013. Reproduced with permission from ref. [80].

The gel formation was analysed by adding Zn^{2+} and Cd^{2+} salts dissolved in H_2O to a solution containing **22** and **23** in H_2O or DMF. Metal-induced gelation process and the gel formation was observed in water for zinc(II) chloride and cadmium(II) chloride complexes, while in presence of acetate and nitrate salts, metallogels were not obtained. The complex Zn^{2+}–**23** formed weaker metallogel than Zn^{2+}–**22**. In Fig. 29A and 29B SEM images on the Cd^{2+}-**22** and Zn^{2+}-**22** xerogels, respectively, are reported showing fibrous needle/block type networks, typical of supramolecular gels. The anion responsive behaviour of the metallogels was studied. Anions such as CN^{-}, F^{-}, and I^{-} caused a collapse of the 3D networks of metallogels Zn^{2+}–**22** and Zn^{2+}–**23**, while Cl^{-} and Br^{-} did not have any effect on the materials. As per Cd^{2+}–**22** and Cd^{2+}–**23**, the disruption of the gels was caused only by the addition of CN^{-}, while the presence of halides did not cause any changes. These findings suggest that the gel-sol transition of metallogels Cd^{2+}–**22** and Cd^{2+}–**23** could be exploit to sense cyanide in aqueous solution.

Qi Lin, You-Ming Zhang and co-workers described the anion sensing ability of metallogels based on gelator **24** (Fig. 30). The mechanism of sensing is based on a novel approach named "competitive coordination control AIE mode" whose action is schematically shown in Fig. 30 [40].

Gelator **24** formed a stable supramolecular organogel in DMF that showed a strong fluorescent blue AIE. The formation of metalloges obtained by adding or diffusing different metal ions as their perchlorate salts in the organogel of **24** in DMF was investigated. Certain metals such as Cu^{2+}, Hg^{2+}, Fe^{3+} or Cr^{3+} formed non-emitting metallogels (Cu^{2+}-**24**, Hg^{2+}-**24**, Fe^{3+}-**24**, and Cr^{3+}-**24**). Interestingly, a strong yellow fluorescence was observed during the formation of metallogel Zn^{2+}-**24** (the fluorescence emission of the metallogel was bathocromically shifted of

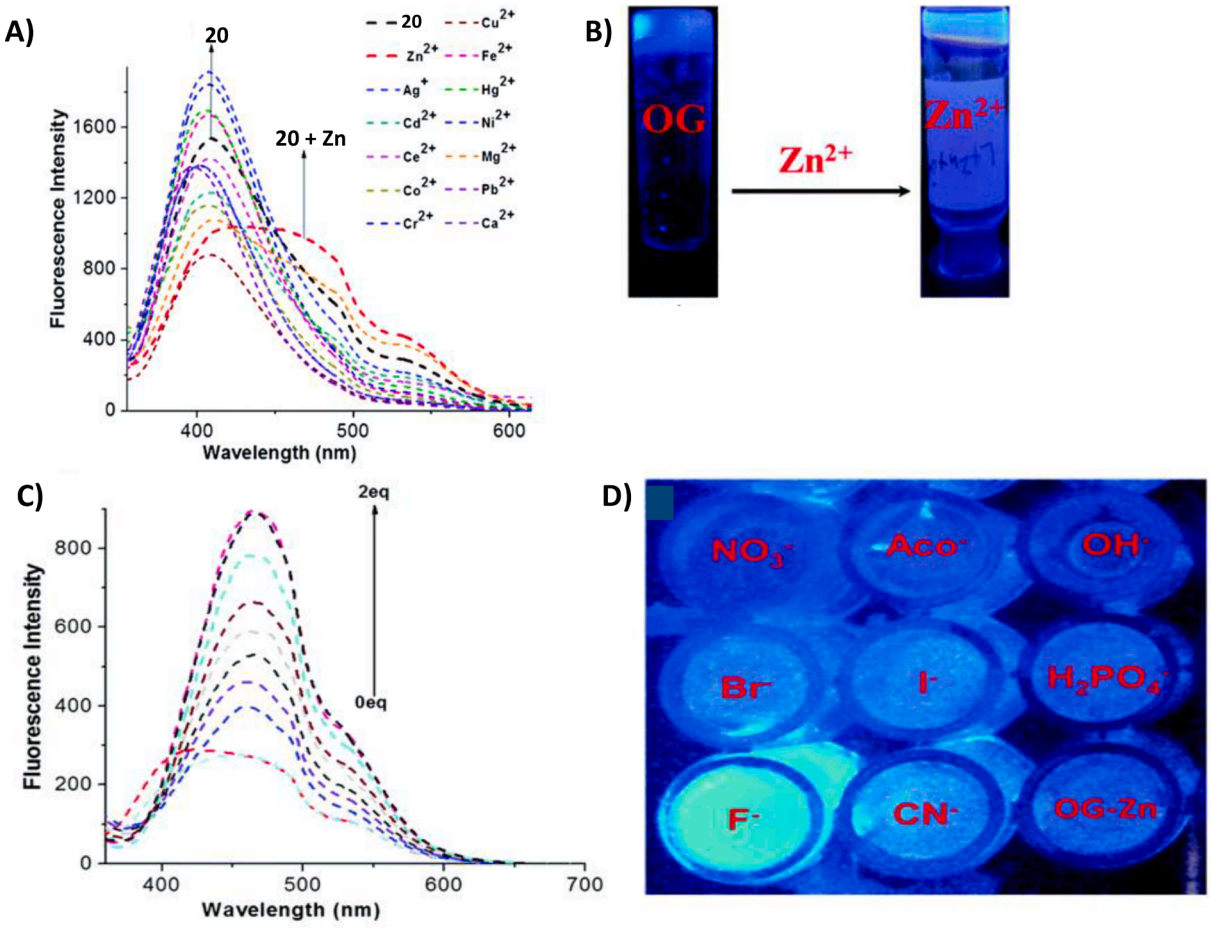

Fig. 26. A) Effect on the fluorescence emission of the organogel of **20** upon the addition of 1 equiv. of the metal ions considered; B) pictures showing the fluorescence of the organogel of **20** and of the metallogel Zn^{2+}-**20**; C) fluorescence titration of the metallogel Zn^{2+}-**20** with F^- in DMF; D) picture of the metallogel Zn^{2+}-**20** (in DMF) in the presence of various anions under a UV lamp at at 365 nm. Copyright RSC 2016. Reproduced with permission from ref. [81].

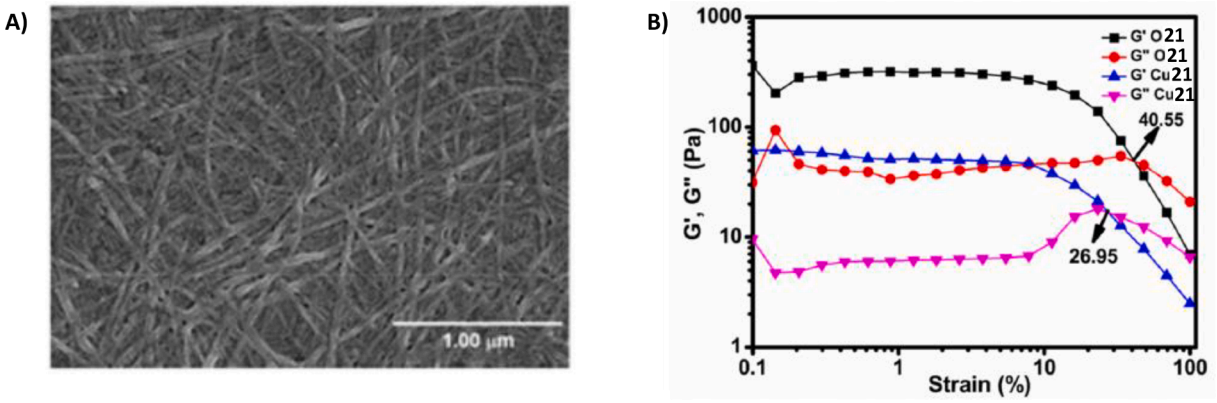

Fig. 27. A) SEM image of the metallogel Cu^{2+}-**21**; B) dynamic strain sweep rheology measurements. Copyright ACS 2020. Reproduced with permission from ref. [82].

ca. 40 nm with respect to the organogel). Upon the addition of various anions (CN^-, ClO_4^-, N_3^-, S^{2-}, SCN^-, AcO^-, $H_2PO_4^-$, and halides F^-, Cl^-, Br^-, I^-) to the metallogels different responses were obtained. Predictably, in DMF various changes in the metallogels fluorescence were obtained in line with the stimuli of the different anions: in particular, a "turn-on" fluorescence was observed for the metallogels Fe^{3+}-**24** and Cu^{2+}-**24** in presence of CN^-. A similar response was observed for the metallogels Hg^{2+}-**24** and Cr^{3+}-**24** in the presence of SCN^- and S^{2-}. Metallogel Zn^{2+}-**24** was able to sense I^- selectively by a "turn-off" fluorescence change. A metallogel-based sensor array was also prepared to understand the response of the system when various analytes were present simultaneously. Distinctively, all metallogels could selectively sense CN^-, SCN^-, S^{2-} and I^- in water when implemented in an array.

Mukhopadhyay and co-workers developed organogelators **25** and **26** containing a carboxamide group, which expressed the tendency to form gels in DMSO and DMF in the presence of little H_2O quantities [84].

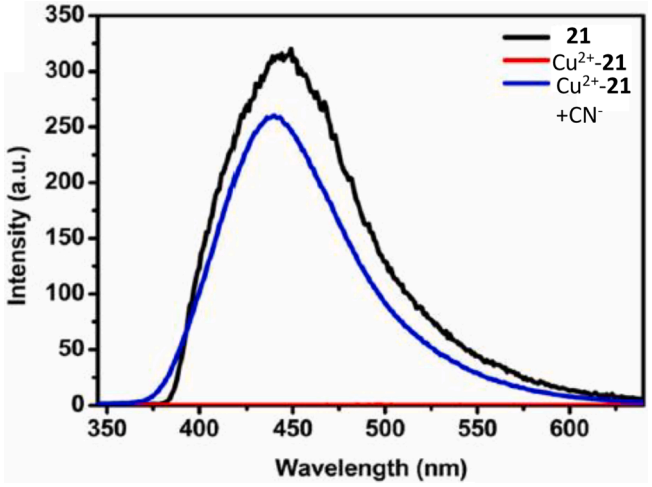

Fig. 28. Comparison of emission spectra of metallogel Cu^{2+}-**21** + CN^- with those of metallogel Cu^{2+}-**21** and the organogel of **21**. Copyright ACS 2020. Reproduced with permission from ref. [82].

Also in this case, the gel formation, and thus the self-assemby process, causes aggregation-induced emission enhancement (AIEE) phenomena for both gelators **25** and **26**. The possibility to form metallogels upon the addition to various metal ions such as Ag^+, Cd^{2+}, Co^{2+}, Cu^{2+}, Fe^{2+}, Fe^{3+}, Ni^{2+}, and Zn^{2+} (as their perchlorate salts) was investigated. The gelator **25** formed supramolecular metallogels in the DMF/H_2O mixture upon the addition of metal ion in a 2:1 molar ratio with respect to the gelator. Metal ions Ag^+, Fe^{2+}, and Fe^{3+}, caused a complete "turn-off" of the fluorescence, while with the other metal ions only a partial switching off of the emission was observed. The gelator **26**, on the other hand, did not show the tendency to form metallogels in a 2:1 molar ratio, and only turbid solutions were obtained. In the presence of Zn^{2+} and Cd^{2+} a switching on of the fluorescence was observed in solution, with a maximum in the emission at around 440 nm. Metallogels formation was only observed when the gelator **26** and the metal ions were in 2:0.5 gelator/metal molar ratio. All metallogels showed a quenching of the emission, but only for the Fe^{2+}-**26** metallogel the fluorescence was completely switched off. The effect of the presence of a series of anion guests (CN^-, SCN^-, Br^-, Cl^-, I^-, N_3^-, AcO^-, ClO_4^-, and S^{2-}) to the metallogels was investigated using fluorescence spectroscopy. In particular, metallogels Ni^{2+}-**25** and Co^{2+}-**25** could selectively sense sulfide ion,

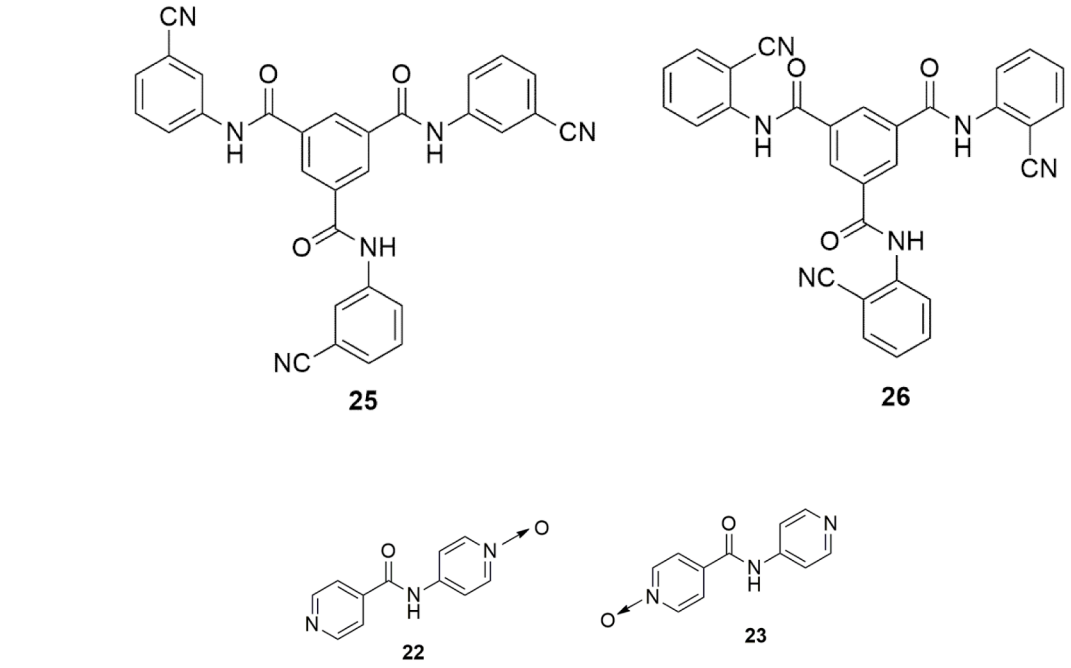

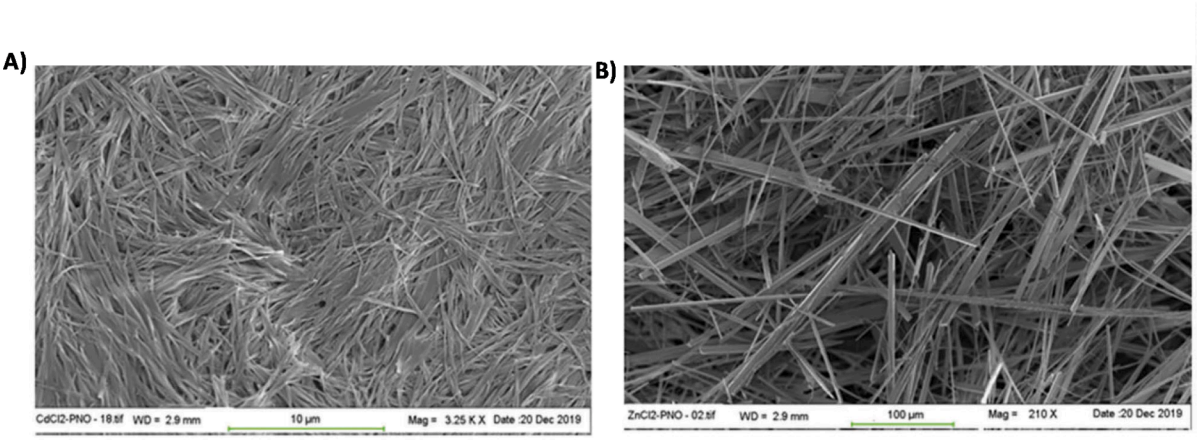

Fig. 29. SEM images of A) xerogels of Cd^{2+}-**22** in H_2O at 3.7 wt%; and B) xerogels of Zn^{2+}-**22** in DMF/H_2O (1:1 v/v) at 2.8 wt%. Copyright Taylor and Francis 2020. Reproduced with permission from ref [83].

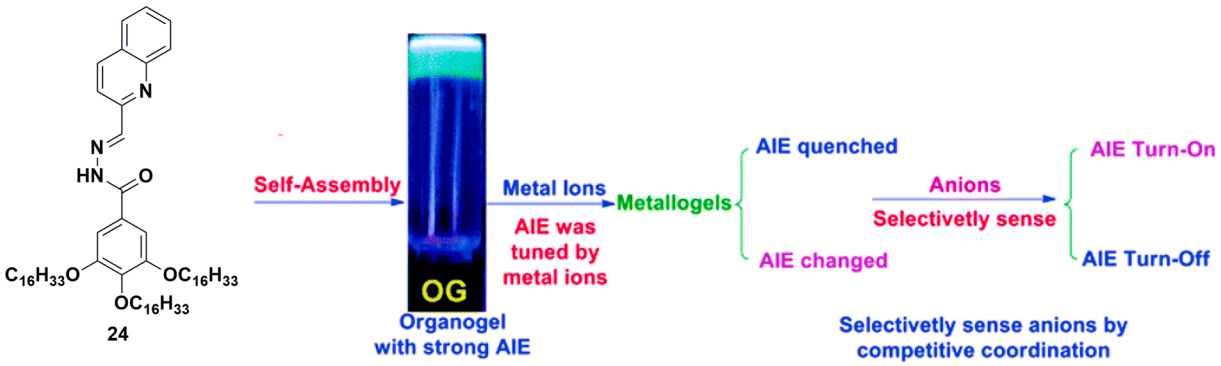

Fig. 30. Gelator **24** and its mechanism of action. Copyright RSC 2015. Adapted from ref. [40].

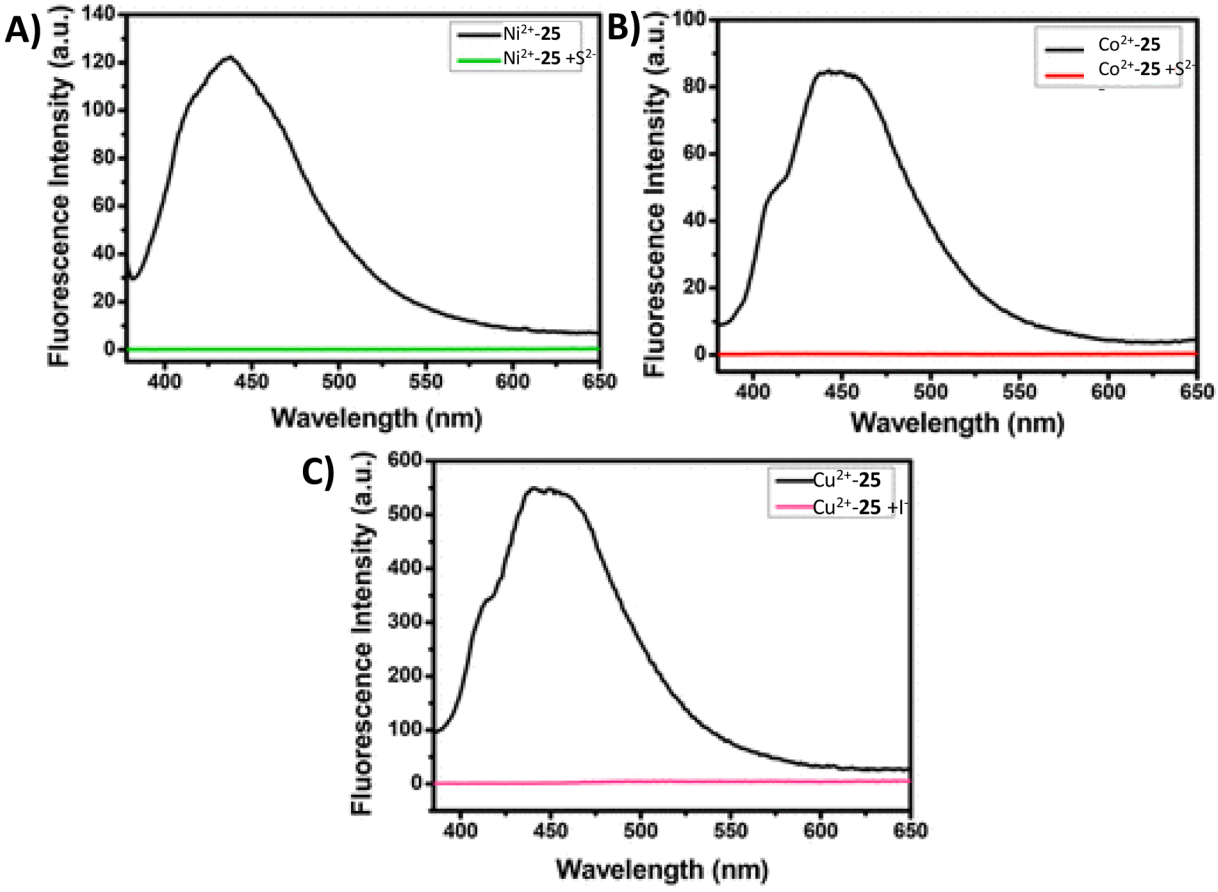

Fig. 31. Fluorescence spectra of metallogels of **25** in DMF with different anions ($\lambda_{exc} = 355$ nm). A) Ni^{2+}-**25** and Ni^{2+}-**25** in the presence of S^{2-}; B) Co^{2+}-**25** and Co^{2+}-**25** in the presence of S^{2-}; C) Cu^{2+}-**25** and Cu^{2+}-**25** in the presence of I^{-}. Copyright ACS 2018. Adapted with permission form ref [84].

while Cu^{2+}-**25** could sense iodide. Fig. 31 shows the fluorescence spectra of metallogels treated with anions. In all cases a "turn-off" fluorescence was observed.

Interestingly, the Cu^{2+}-**25** gel showed also catalytic activity in the oxidation reaction of catechol to quinone in aerobic conditions.

Chen, Yin and co-workers studied the anion sensing properties of a new gelator (**27**) derived from glutamic acid that contains o-hydroxynaphthaldehyde as a coordinating and fluorogenic moiety [85]. The formation of organogels with gelator **27** was hampered by the presence of intramolecular HB interactions; however, in the presence of one or two metal ions in a solution of **27** in DMSO (or DMF), the formation *via in situ* coordination of stable metallogels was observed. Interestingly, the metallogels formed in DMSO were more stable than those formed in DMF.

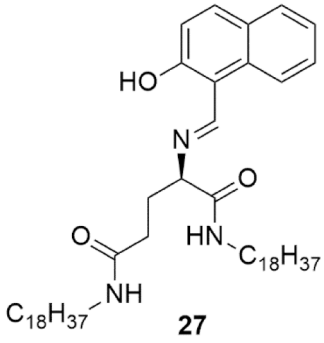

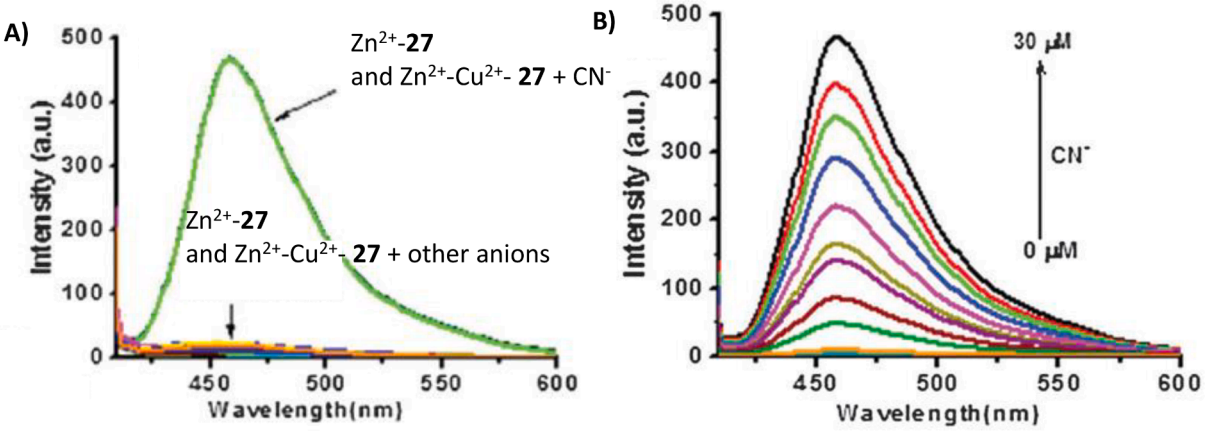

Fig. 32. A) Fluorescence spectra of Zn^{2+}-**27**, Cu^{2+}-**27** and Zn^{2+}/Cu^{2+}-**27** in the presence of various anions (0.1 M in DMSO); B) fluorescence titrations of Zn^{2+}/Cu^{2+}-**27** with CN^- (0–30 mM). Copyright RSC 2016. Reproduced with permission form ref [85].

The gelation process was favoured by the addition of 1 equiv. of sodium acetate into the solution of **27** in the presence of Fe^{3+}, Fe^{2+}, Zn^{2+}, Hg^{2+}, Cu^{2+}, Ni^{2+}, Ag^{+}, and Al^{3+}, while K^{+}, Ba^{2+}, Cd^{2+}, Co^{2+}, and Pb^{2+}, were not able to form metallogels suggesting the cation dependence in the gelation process. Upon the addition of 2 equivs. of various anions [NO_2^-, F^-, Cl^-, Br^-, I^-, CN^-, HSO_4^-, $H_2PO_4^-$, SO_4^{2-}, SO_3^{2-}, HSO_3^-, S^{2-}, and Cys (cysteine)] to the metallogels, it was found that a selective enhancement of the fluorescence emission of gel Zn^{2+}/Cu^{2+}-**27** occurred with a specific selectivity over S^{2-} and Cys. (Fig. 32).

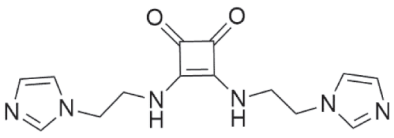

30

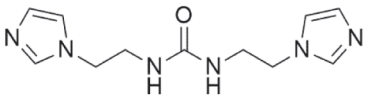

31

The urea moiety is often used for the design of gelators for the formation of supramolecular gels. The gelator **28** is able to bind both anions and metal ions, and preferentially gelates in MeOH in the presence of $CuBr_2$ while other copper(II) salts such as $CuCl_2$, $Cu(AcO)_2$, $Cu(NO_3)_2$ and $Cu(BF_4)_2$ inhibit the process [86]. Upon shaking the gel strengthened and a morphological change was observed *via* cryoSEM (Fig. 33B). This work highlights the importance of morphology and connectivity in gel formation. The initial fibres are "too perfect" and lack cross links. It is only when the fibres are sheared and recombine in a more entangled way that a self-supporting gel network results. A reversible anion-dependent gel-sol transition was observed in the presence of TBAAcO and $Cu(BF_4)_2$ (Fig. 33A).

The family of pyridinylmethyl ureas **29a–e** were reported by Steed and co-workers [87]. Gelators **29b** and **29c** form stable gels in aromatic solvents such as toluene, nitrobenzene and 1,3-dichlorobenzene and metallogels in the presence of 0.5 equivs. of chloride salts of Cu^{2+} and Co^{2+} and the tetrafluroborate salt of Ag^{+} in the same solvents. Upon the addition of the nitrate salts of Zn^{2+} and Co^{2+} the gels are destroyed. However, in the presence of TBABr a gel-sol–gel transition was observed. In particular, after 5 min of sonication, the addition of 0.3 equivs. or more of TBABr promoted the formation of the two metallogels Zn^{2+}-**29b** and Co^{2+}-**29c**. and in the latter case the gel turned from pink to blue upon the addition of the anion (Fig. 34). Interestingly, when an excess of bromide was added the metallogel remained stable.

More recently also squaramides have attracted the attention of supramolecular chemists [88–92]. Wu, You and collaborators reported two new compounds (**30** and **31**) with a squaramide or an urea motif featuring two imidazole functionalized pendant arms [93]. These ligands have been studied as possible gelator in various solvents, also in the presence of different metals. The green opaque metallogel Cu^{2+}-**30**-Cl was obtained by shaking gelator **30** in the presence of various amount (between 1:0.6–1.4 molar ratio) of $CuCl_2{\cdot}2H_2O$ in MeOH. In the same experimental conditions urea **31** formed a precipitate probably because of the lack of π-π interactions that can be established in the squaramide derivative.

The possibility to form metallogels was tested by using different copper(II) salts. These tests demonstrated that also $CuBr_2$ formed a dark purple gel (Cu^{2+}-**30**-Br), while in the presence of other copper(II) salts no metallogels were obtained. Gelation tests have been carried out in H_2O/MeOH with a maximum ratio of H_2O/MeOH of 1:10 (v/v). SEM and TEM images of Cu^{2+}-**30**-Cl gel are reported in Fig. 35.

The authors tested the ability of gel Cu^{2+}-**30**-Cl to sense anions. Upon the addition of aqueous solutions of various sodium salts to metallogel Cu^{2+}-**30**-Cl a pale purple colour was observed only in the presence of NaBr solution, while other anions gave a blue colour (Fig. 36). The same colour change was observed when different bromide salts were used. When bromide salts were added as powders into Cu^{2+}-**30**-Cl gel the colour change was even more intense than in solution (Fig. 36).

5. Metallogels for neutral species sensing

In addition to charged species, in literature it is possible to find interesting examples of metallogel for neutral species sensing. Lin and co-workers reported a novel supramolecular polymer metallogel based on the complex of Al^{3+} with the pillar[5]arene **31** functionalised with bis-8-hydroxyquinoline (Fig. 37) [94]. In DMSO/H_2O mixture (at 20% H_2O) metallogel Al^{3+}-**31** showed a light blue emission due to AIE and a multi stimuli-responsive behaviour (temperature changing, addition of acids, bases or guest compounds).

The metallogel Al^{3+}-**31** could be used to detect acids such as trifluoroacetic acid (TFA). A fluorescence quenching was observed by

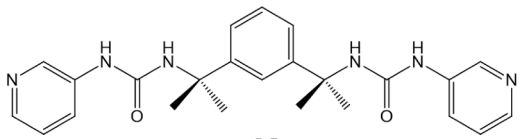

28

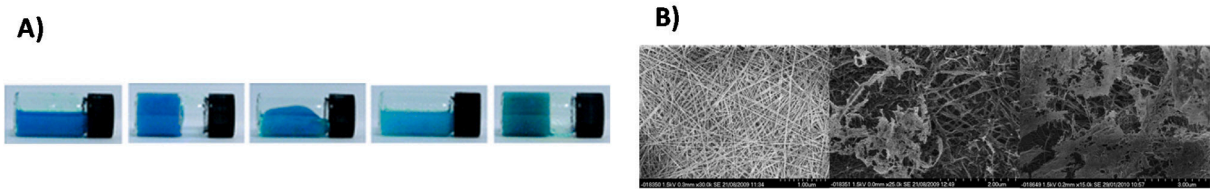

Fig. 33. A) Behaviour of the metallogel Cu^{2+}-**28** formed by $CuBr_2$ (0.3 equivs.) in MeOH (from left to right) before shaking, after shaking, 5 min. after the addition of 1 equiv. of TBAAcO, 30 min. after the addition of TBAAcO, and 5 min after the addition of 1 equiv. of $Cu(BF_4)_2$; B) cryo-SEM pictures of the metallogel Cu^{2+}-**28** formed by $CuBr_2$ (left) before shaking, (middle) after shaking, and (right) after 1 week resting. Copyright RSC 2010. Reproduced with permission form ref [86].

Fig. 34. Picture of the Co^{2+}-**29c** metallogel in nitrobenzene and colour changed triggered by the addition of TBABr [(a) 0.2, (b) 0.3, (c) 0.4, (d) 0.5, (e) 1, (f) 2, (g) 4 equivs.]. Copyright RSC 2017. Reproduced with permission form ref [87].

adding increasing concentrations of TFA (Fig. 38A). However, when a base, in this case triethylamine (TEA) was added, the blue emission of metallogel was restored (Fig. 38B).

As already described above, lanthanide complexes can be successfully used to form luminescent metallogels. In some case this class of materials can be used for the detection of neutral species. As an example, Maitra and co-workers described a class of lanthanide cholate hydrogels, characterised by a fibrillar network deriving from the self-assembling of the two components [95]. These materials have been successfully used as white-light-emitting gels and for sensing enzymes [96–98]. On the basis of these results, the same group developed the hydrogel Tb^{3+}–**32** (using the nitrate salt of Tb^{3+}) for the detection of naphthalene-containing drugs such as naproxen and propranolol [99].

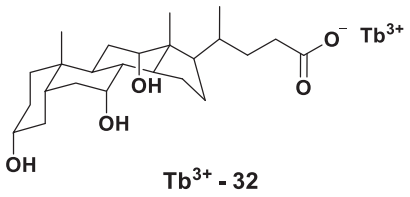

Indeed, upon the addition of naproxen and propranolol, an enhancement of the emission band at about 550 nm (corresponding to the excitation at 332 nm and 296 nm in the presence of naproxen and propranolol, respectively) was observed. The dramatic changes could be appreciated also at naked eye (Fig. 39A).

Ghosh and collaborators presented some symmetrical, neutral and charged pyridyl bisamides **33**–**36** gelators able to sense different species, including metals and aminoacids [100]. These molecules behaved also as drug delivery. Compounds **33** and **34** present metal coordinating pyridyl nitrogen while structures **35** and **36** presented a quaternization of nitrogen atoms with a cholesteryl unit.

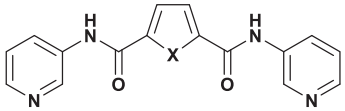

33 X= O
34 X= NH

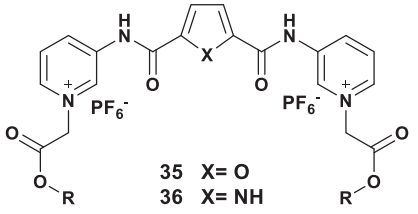

35 X= O
36 X= NH

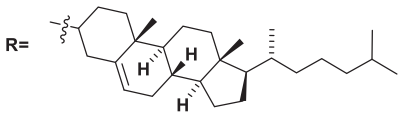

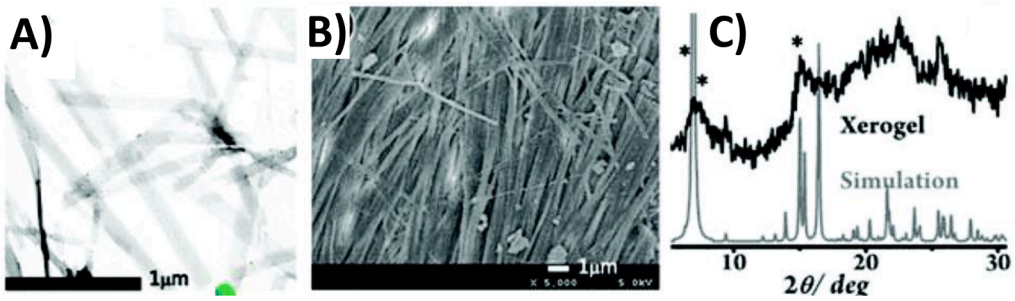

Fig. 35. A) TEM image of Cu^{2+}-**30**-Cl; B) SEM image; and C) PXRD pattern of the xerogel of Cu^{2+}-**30**-Cl. Copyright RSC 2016. Reproduced with permission from ref. [93].

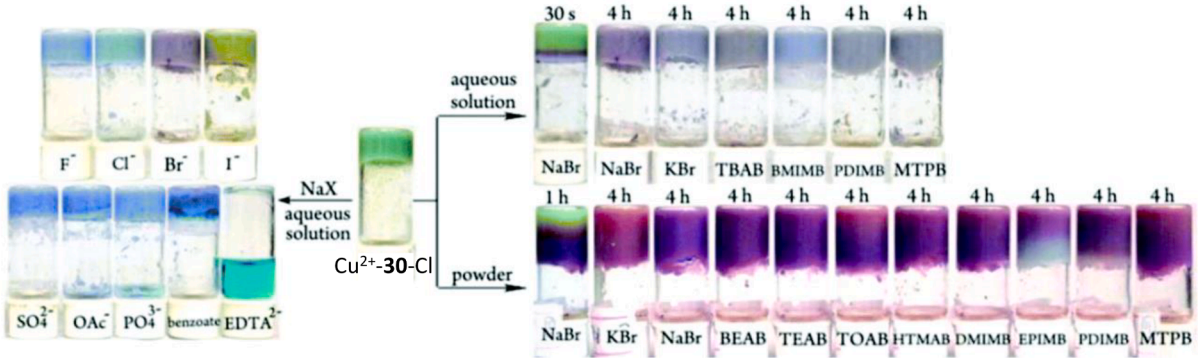

Fig. 36. Samples of gel Cu^{2+}-**30**-Cl upon addition of aqueous sodium salts, aqueous bromide salts and bromide salts as powders. Copyright RSC 2016. Adapted with permission from ref. [93].

The ability of these ligands to form metallogels was evaluated. As shown in Fig. 40 (left) when 2 equivs. of various metal ions were added to a solution of **33** in DMSO/H_2O (1:1 v/v), metallogels were formed only in the case of Ag^+ (pale yellow gel) and Cu^{2+} (green gel). Gelator **34** formed a metallogel only in the presence of Ag^+ ions. The morphology of the metallogels were studied by SEM. In Fig. 40 (right) SEM images of the metallogels are reported from which it is clear that the morphologies of the metallogels depend both on the nature of the gelators and the metal ions. The Ag^+-**33** metallogel showed non-twisted rod like networks while the Cu^{2+}-**33** metallogel revealed flower like matrices. Closely spaced globular microstructures were observed for Ag^+-**34** metallogel.

The three metallogels were tested as possible sensors for amino acid and carbohydrate recognition. When an aqueous solution of L-cysteine was added for Cu^{2+}–**33** metallogel a gel-sol transition was observed, probably because of the affinity of L-cysteine to Cu^{2+} ion (Fig. 41). All the other amino acids tested did not cause any appreciable changes to the material. To better understand the interaction between metallogel and amino acids, UV–Vis measurements were performed: only in presence of L-cysteine, DL-homocysteine and L-glutathione an increase of the absorption in the region of 290–300 nm was observed. Other amino acids weakly decreased the absorption. Cu^{2+}–**33** metallogel was also able to discriminates D-glucose from D-mannose by a gel-sol transition (Fig. 41).

An example of metallogel prepared by mixing gelator **37** with the iridium complex **38** and $EuCl_3{\cdot}6H_2O$ has been described by Cao, Wu and co-workers with the idea to couple the intriguing photophysical properties of Ir^{3+} with those of the lanthanide ion [101].

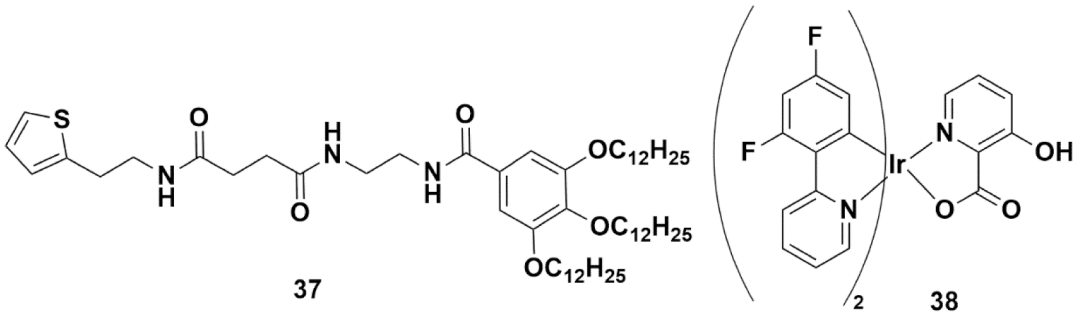

As shown in Fig. 42 the photophysical properties of the hybrid metallogel Eu^{3+}-**37**–**38** could be modulated in the presence of acids or bases. Indeed, in the presence of NaOH aqueous solution the metallogel Eu^{3+}-**37**–**38** was able to emit red light, but if a certain amount of trifluoroacetic acid, formic acid, acetic acid, propionic acid and organic amine vapours such as Et_3N, ammonium hydroxide, tripropylamine and

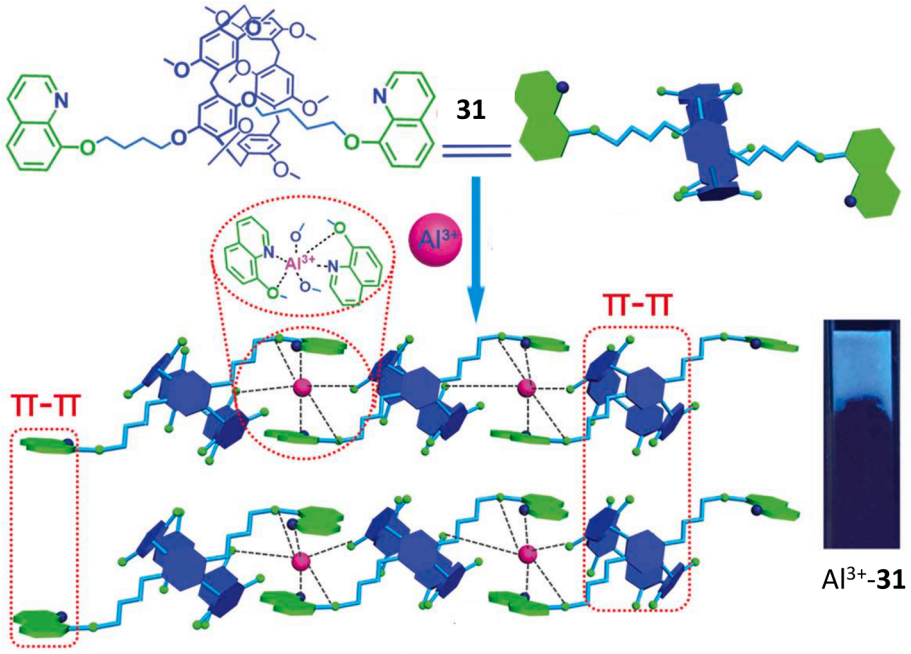

Fig. 37. Cartoon showing the formation of supramolecular metallogel Al^{3+}-**31**. Copyright Elsevier 2019. Adapted with permission from ref [94].

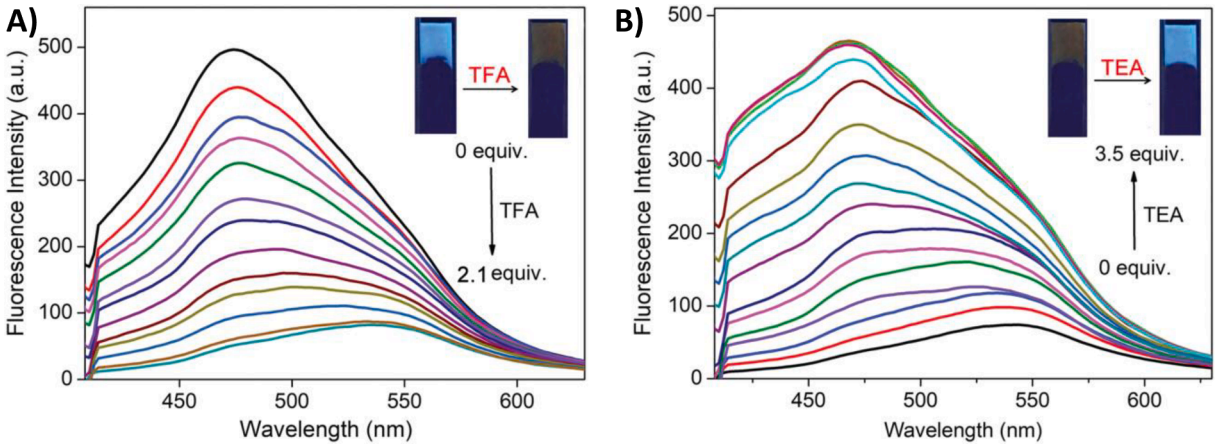

Fig. 38. A) Fluorescence titration of metallogel Al^{3+}-**31** with TFA ($\lambda_{ex} = 380$ nm) and pictures of Al^{3+}-**31** and Al^{3+}-**31** + TFA under 365 nm UV light; B) fluorescence titration of the gelator **31** + TFA with TEA ($\lambda_{ex} = 380$ nm) and pictures of Al^{3+}-**31** + TFA and Al^{3+}-**31** + TFA + TEA under 365 nm UV light. Copyright Elsevier 2019. Reproduced with permission from ref [94].

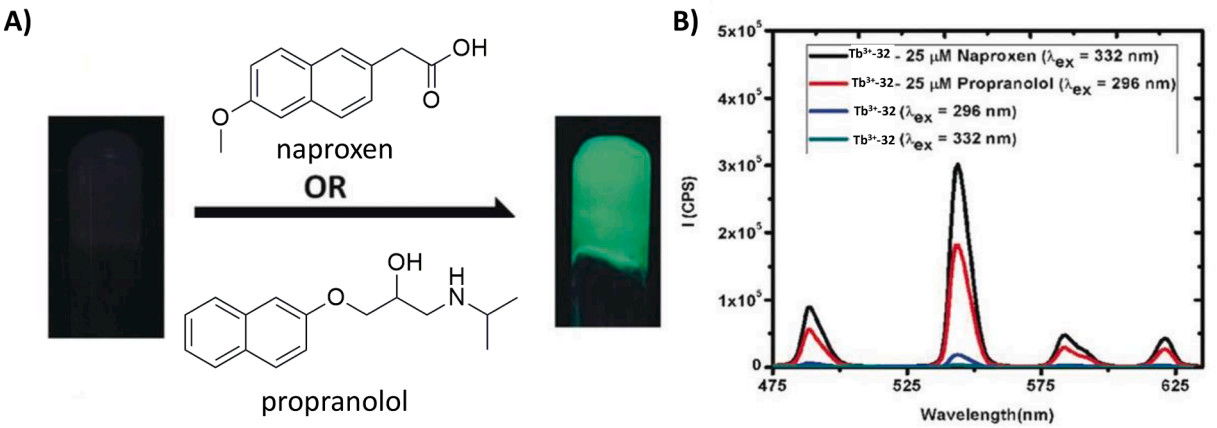

Fig. 39. A) Naked eye (under UV light) switching on of the fluorescence emission of Tb^{3+}-**32** metallogel in the presence of naproxen or propranolol; B) emission spectra of Tb^{3+}-**32** metallogel in the presence (black and red lines) or in the absence (blue and green lines) of naproxen or propranolol. Copyright Wiley 2017. Adapted with permission from ref. [99].

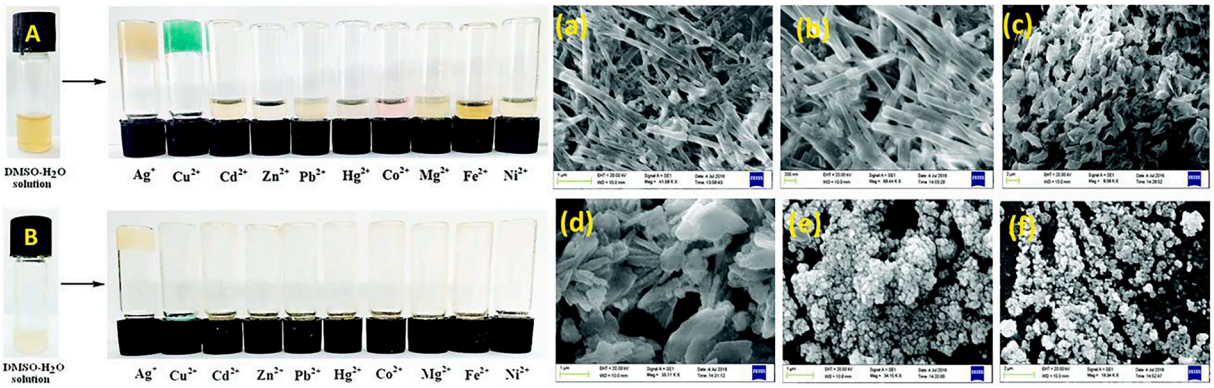

Fig. 40. Left: pictures showing the gel-sol transition of A) **33**; and B) **34** in DMSO/H_2O (1:1 v/v) upon the addition of 2 equivs. of various metal ions after 1 h; Right: SEM images of xerogels of Ag^+-**33** (a and b), Cu^{2+}-**33** (c and d) and Ag^+-**34** (e and f). Copyright RSC 2018. Reproduced with permission from ref. [100].

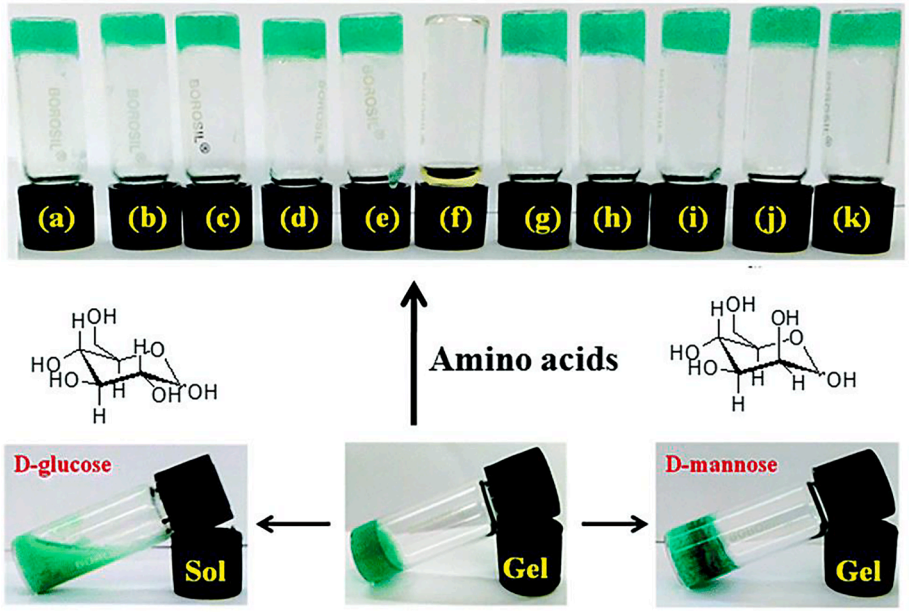

Fig. 41. Pictures of the Cu^{2+}-**33** metallogel in DMSO/H_2O (1:1 v/v) in the presence of 2 equivs. of different amino acids and D-glucose and D-mannose (0.03 M) [(a): glycine,(b): L-valine, (c): L-alanine, (d): L-phenylalanine, (e): L-proline, (f): L-cysteine, (g): L-lysine, (h): L-threonine, (i): L-histidine, (j): L-methionine, (k): L-glutamic acid]. Copyright RSC 2018. Reproduced with permission form ref [100].

ethylenediamine, were added to a mixture of the metallogel Eu^{3+}-**35**–**36** and NaOH a cyan light was observed. No changes in the absorption properties of the system were observed. The xerogel film of Eu^{3+}-**37**–**38** + NaOH can be used as a fast dual sensor for volatile gaseous amines and acid vapours recognition. The xerogel could respond to the presence of vapours of TFA and Et_3N for several cycles, with a decrease in the fluorescence emission, while the position of the emission band was unaffected.

An interesting system able to recognise chiral phosphine species such as binap (2,2′-Bis(diphenylphosphino)-1,1′-binaphthyl) was obtained from metallogel Pt^{2+}-**39a**-Cl in which the gelator is characterised by the presence of a steroidal skeleton connected to a nitrogen-containing pincer to coordinate the metal ion [102]. In particular, a gel-sol transition was observed only when metallogel Pt^{2+}-**39a**-Cl was in contact with 0.1 equivs. of (*R*)-binap (Fig. 43c), while in the presence of (*S*)-binap the material remained stable (Fig. 43b).

6. Metallogels for remediation, gas and dye absorption

Supramolecular metallogels have been successfully used as materials for environmental remediation. Indeed, their solid-like nature combined with the high degree of solvation facilitate the decontamination of polluted liquid phases from dyes, neutral molecules or toxic metal ions and anions due to an efficient contact with the contaminated samples [103].

An example of metallogel able to efficiently remove mercury ions from water was proposed by Lin, Wei, and co-workers. Their interest in the design of pillarenes led to the design of a thioacetohydrazide functionalized pillar[5]arene (**40**) which, in the presence of $Zn(ClO_4)_2$ formed a linear metal–organic polymer (Fig. 44) [104].

By dissolving **40** (150 mM) and $Zn(ClO_4)_2$ in 1:1 ratio in cyclohexanol at 75 °C and cooling down the resulting gluey solution a transparent gel was formed. The gel-sol transition could be achieved by several cooling-heating cycles as well as by addition of TBAOH (which formed $Zn(OH)_2$, destroying the coordination) to the gel. SEM images on the xerogel revealed a micro-sized cubic framework confirming the formation of the metal–organic framework (Phase B in Fig. 44). The metallogel Zn^{2+}-**40** showed a fluorescence emission band at 464 nm which disappeared in the presence of Hg^{2+} ions, suggesting that Hg^{2+} replace Zn^{2+} in the coordination to the thioacetohydrazide moieties due to its higher affinity towards S atoms. The xerogel was successfully used to capture Hg^{2+} ions from water. The xerogel was suspended in an

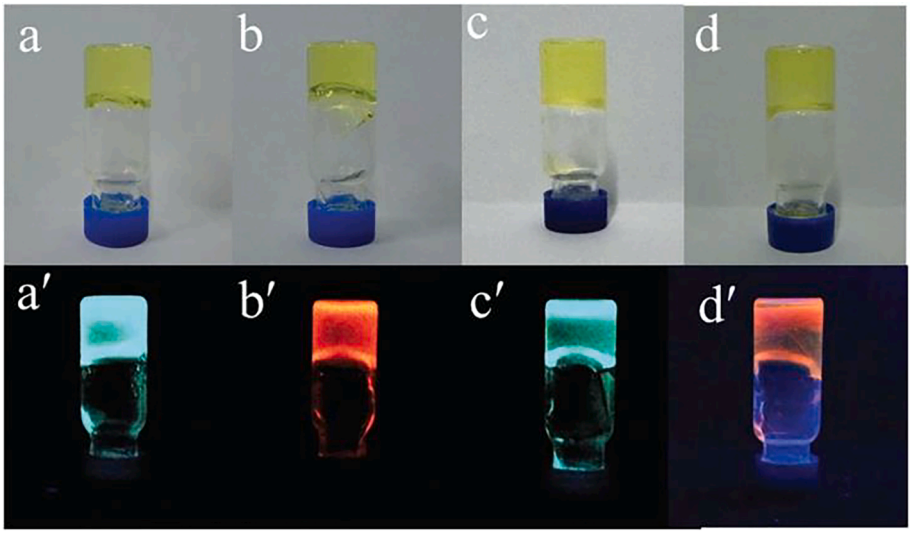

Fig. 42. Pictures of: (a) gel Eu^{3+}-**37**–**38** in DMSO; (b) gel Eu^{3+}-**37**–**38** in DMSO in the presence of NaOH solution; (c) b in the presence of TFA solution; and (d) c in the presence of NaOH solution. In the first row pictures were taken under daylight, in the second row pictures were taken under 365 nm light. Copyright RSC 2017. Adapted with permission form ref [101].

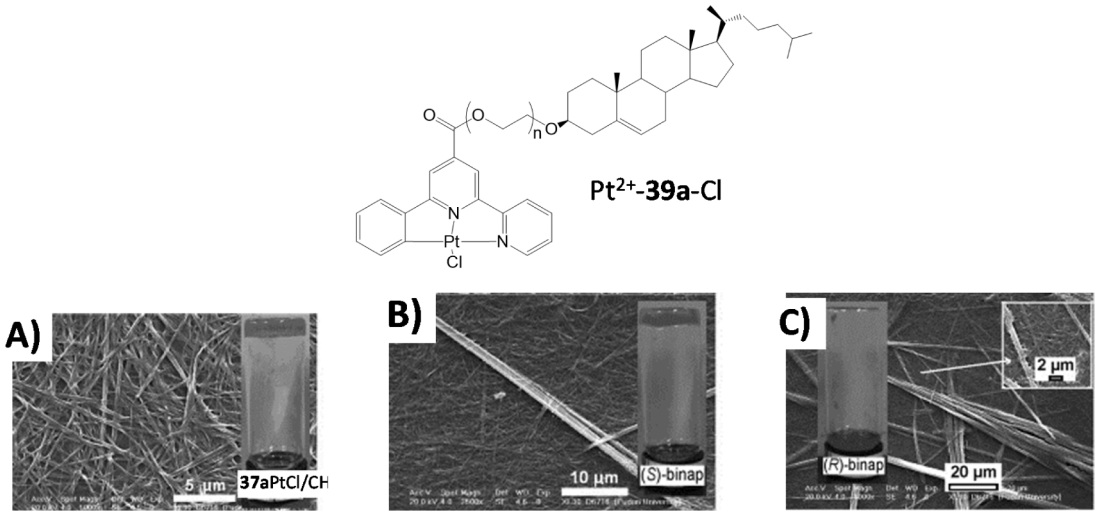

Fig. 43. Visual chiral recognition of (*R*)- and (*S*)-binap by metallogel Pt^{2+}-**39a**-Cl/$CHCl_3$ (1 wt%) SEM images of A) metallogel Pt^{2+}-**39a**-Cl; B) metallogel Pt^{2+}-**39a**-Cl + 0.1 equivs. of (*S*)-binap; C) metallogel Pt^{2+}-**39a**-Cl + 0.1 equivs. of (*R*)-binap. Copyright Wiley 2011. Reproduced with permission form ref [102].

aqueous solution of $Hg(ClO_4)_2$ for 1 h and then the supernatant solution was analysed by ICP to determine the concentration of the residual Hg^{2+} in water. ICP results showed that more than 90% of Hg^{2+} ions were removed by the xerogel.

Another example of metallogel for the removal of Hg^{2+} ions from water was proposed by Ballabh and Yadav [105]. In this case Hg^{2+} was the metal forming the metallogel when coordinating with 2-amino-4-methylthiazole (**41**). When an aqueous solution of $Hg(CH_3COO)_2$ was added to a solution of **41** in chloroform at 2.18% (w/v) concentration the aqueous layer gelled without any external stimulus. The gel showed an interesting thixotropic behaviour. The formation of the gel strongly depends on the nature of the metal ion (other metal ions such as Co^{2+}, Ni^{2+}, Cd^{2+}, Cu^{2+}, Zn^{2+}, Pb^{2+}, and Ag^{+} did not promote the formation of the gel) as well as the counter-anion (in the presence of $HgCl_2$ the gel did not form suggesting that the coordination of the oxygen atoms of the acetate on the metal centre has an important role in the formation of the coordination polymer). Rheological studies evidenced that the storage modulus (G′) was one order of magnitude higher than the loss modulus (G\prime\prime) demonstrating the viscoelastic properties of the new material. SEM images of the xerogel showed the formation of a continuous three-dimensional network (Fig. 45). The formation of a robust metallogel was proposed for the mercury removal from water. Indeed, as the gel formed at the interphase $H_2O/CHCl_3$, it could be easily skimmed off from polluted water. The experiment showed that when a water sample containing 1000 ppm of Hg^{2+} was treated with a chloroform solution of **41**, after the removal of the gel by filtration, water contained only 1.0–0.5 ppm of Hg^{2+} as demonstrated by AAS analysis.

Multi-stimuli responsive metallogels formed with the complexation of $Ni(CH_3COO)_2$ by 3,5-diamino-1,2,4-triazole (**42**) were reported by Mitra and Saha [106]. Gels were formed in DMF or in a DMF/H_2O (1:1, 2:1, 3:1 v/v) mixture and UV–Vis solution studies suggested the presence of hexacoordinated high-spin Ni^{2+} with a distorted octahedral geometry, while PXRD studies on the xerogels and the gels suggested the presence of metal–metal interactions. Interestingly, these gels showed impressive self-healing, self-sustainable and modulable properties attributed to a strong network of HBs between the constituents of the gel within the network. The gels also exhibited a chemo-responsive behaviour in terms of sol–gel transformation in the presence of

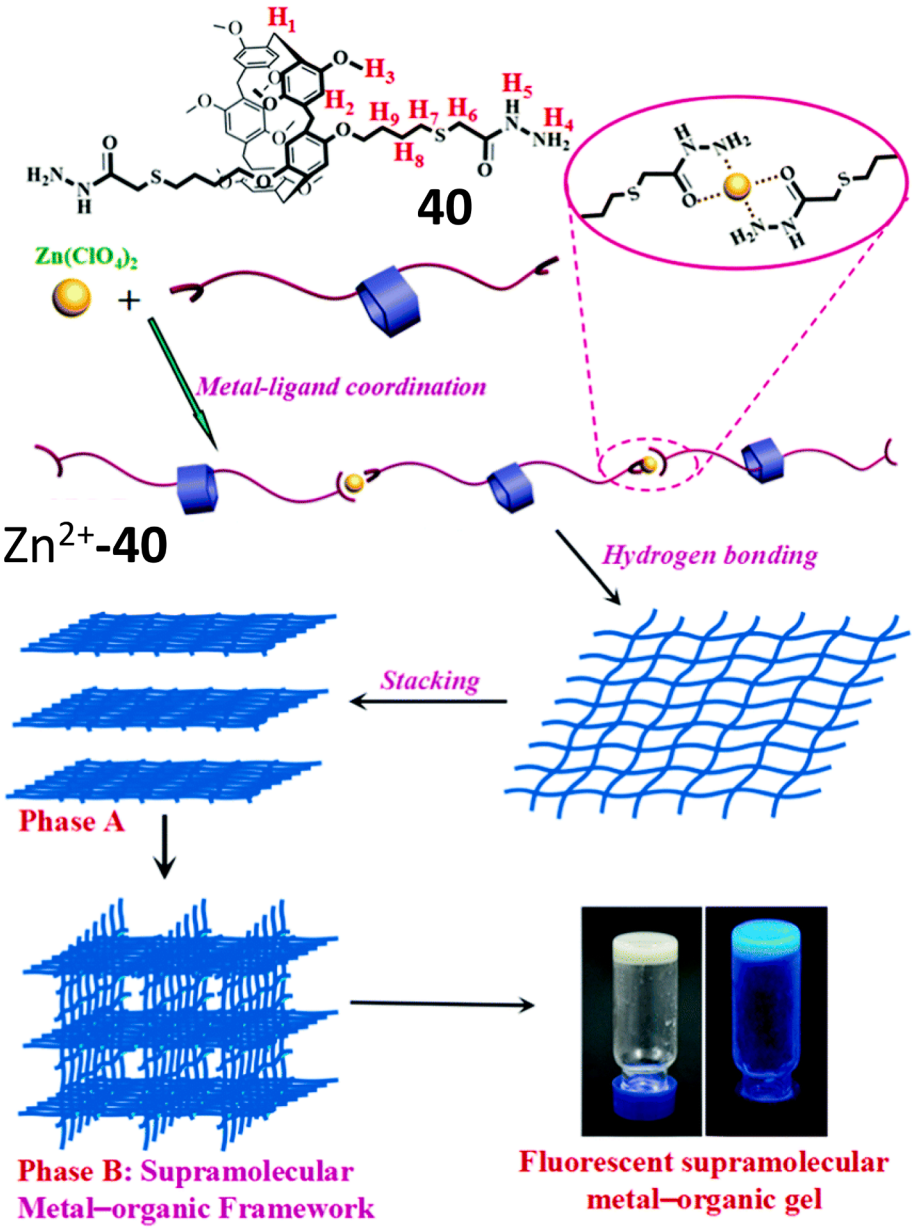

Fig. 44. Representation of the formation of the metal–organic gel of Zn^{2+}-**40**. Copyright RSC 2018. Reproduced with permission from ref. [104].

tetrabutylammonium bromide (the bulky cation and the anion disrupt the HB network of the gel), PPh_3 (the great affinity of phosphine for nickel(II) caused the sequestration of the metal, and thus the collapse of the gel structure), pH (both acid and basic), EDTA and dimethylglyoxime (both chelating the metal). Finally, a rare gel-to-gel transformation with detectable colour change was obtained from Ni^{2+}-**42** Gel 1 (obtained from DMF) and Ni^{2+}-**42** Gel 2 [obtained from DMF/H_2O (1:1 v/v)] (Fig. 46) upon the uptake of metal ions (Na^+, Mg^{2+}, Cr^{3+}, Mn^{2+}, Fe^{2+}, Co^{2+}, Cu^{2+}, Zn^{2+}, and Pd^{2+}) from solution. In the presence of a solution of the metal ions the upper layer of the gels changed colour during time for the percolation of the metal ion solutions in the gel (Fig. 46A and B). A similar behaviour was observed with the xerogels. The metal solutions were then analysed to evaluate the residual concentration of the metal ions and the best results were obtained for both gels in the case of Pd^{2+}. The authors demonstrated that Pd^{2+} was adsorbed into the fibres of the gels and no release of Ni^{2+} was observed (Fig. 46C, D).

An interesting example of copper-based metallogel for the removal of Sb^{3+} and Sb^{5+} from contaminated water samples using 1,3-dicarboxymethyl-2-methyl benzimidazole (**43**) as a gelator was proposed by Luo and collaborators [107]. The metallogel was prepared by reacting gelator **43** in the presence of 2 equivs. of $CuCl_2$ in EtOH/H_2O (1:1 v/v) at pH = 5. 3.2% ethyleneglycol dimethacrylate (EGDMA) was added to reinforce the metallogel network. The metallogel Cu^{2+}-**43** showed excellent adsorption capacity for aqueous antimony with a preference for Sb^{5+} over Sb^{3+}. This major drawback was overcome by the *in situ* oxidation of Sb^{3+} to Sb^{5+}. The adsorption showed to be fast and efficient with 90% Sb removal in 30 min. Competitive adsorption experiments showed that the adsorption capacity followed the order $Sb^{5+} > P^{5+} > As^{5+} > As^{3+}$. DFT calculations demonstrated that the copper valence electron orbitals were the adsorption sites for Sb^{3+} and Sb^{5+}.

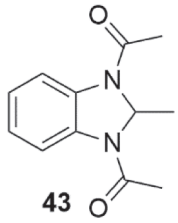

43

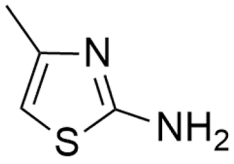

41

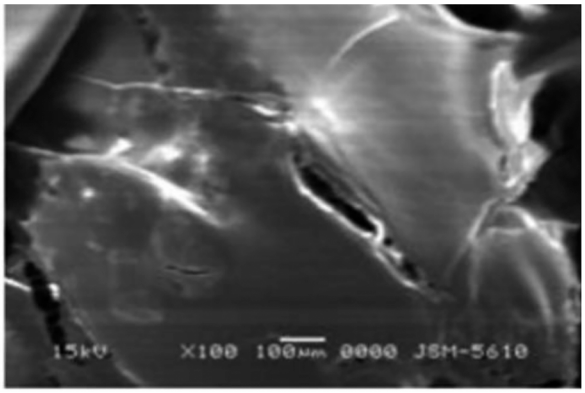

Fig. 45. 2-amino-4-methylthiazole (**41**) structure and SEM image of the xerogels formed from a mixture of **41** and $Hg(CH_3COO)_2$ in 1:1 molar ratio. Copyright RSC 2014. Reproduced with permission from ref. [105].

As mentioned above metallogels could also be used as efficient decontaminants for neutral molecules. An example was reported by Gosh and Panja who developed an efficient Fe^{3+}-based metallogel using **44** as LMWG [108].

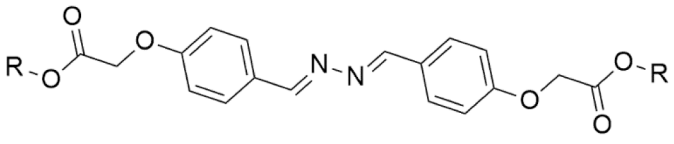

44

R =

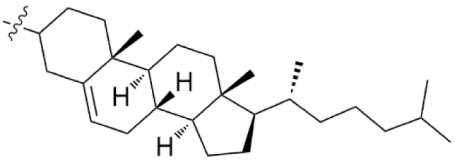

Compound **44** contains cholesterol to enhance self-aggregation *via* hydrophobic interactions and a diazine bridge as the metal coordination site. An orange metallogel Fe^{3+}-**44** with an interlinked porous fibrillar network (as shown by SEM, Fig. 47A) was formed by mixing **44** with 1 equiv. of $Fe(ClO_4)_3$ or $Fe(NO_3)_3$ in a mixture of $CHCl_3$/MeOH (3:1 v/v). The metallogel was used as adsorbent of picric acid (PA), a strong explosive used as a constituent of landmines, which, due to its high solubility in water could cause serious damages to the environment. After assessing the stability of the metallogel in the presence of PA, authors carried out adsorption experiments by exposing the metallogel to an aqueous solution of the acid (Fig. 47B) and monitored the PA absorbance during time (Fig. 47C). After one hour a removal of PA of 83% was observed while negligible adsorption was found for similar analytes 2,4-dinitrotoluene and *m*-dinitrobenzene.

Metallogels can also be useful for the adsorption of toxic dyes. This is a serious problem as this class of compounds are largely used in industry and disposed. Mondal and Sengupta described a system that in one shot is able to gel toxic metal ions such as cadmium and lead, but it can also adsorb methyl orange, a toxic dye from water [109]. The LMWG used in this case was N^2,N^6-bis(3-(pyridin-2-yl)-1H-pyrazol-5-yl)-pyridine-2,6-dicarboxamide (**45**). Immediate formation of metallogels was observed upon addition of $Cd(NO_3)_2$ (1.5 equivs.) or $Pb(CH_3COO)_2$ (from 1 to 4 equivs.) in a mixture of DMF/H_2O (1:1 v/v) at 1 wt% concentration. Both gels showed a thixotropic behaviour and thermoreversibility. From a structural point of view SEM images revealed a presence of highly entangled cross-linked fibrous networks with an average fibres' diameter of 20 nm. IR spectroscopy results suggested the participation of the amide groups into the formation of HBs that led to the self-assembly of the gels, while UV–Vis titrations with both Cd^{2+} and Pb^{2+} confirmed the formation of the metal complexes. The chemical responsiveness of the metallogels to EDTA was tested by adding an equimolar amount (with respect to the metal ion) of the chelator to the vial containing the gel. After a few days, once the EDTA penetrated into the lead metallogel, a transformation into solution was observed. In the case of cadmium(II), instead no transformation was observed due to the lower formation

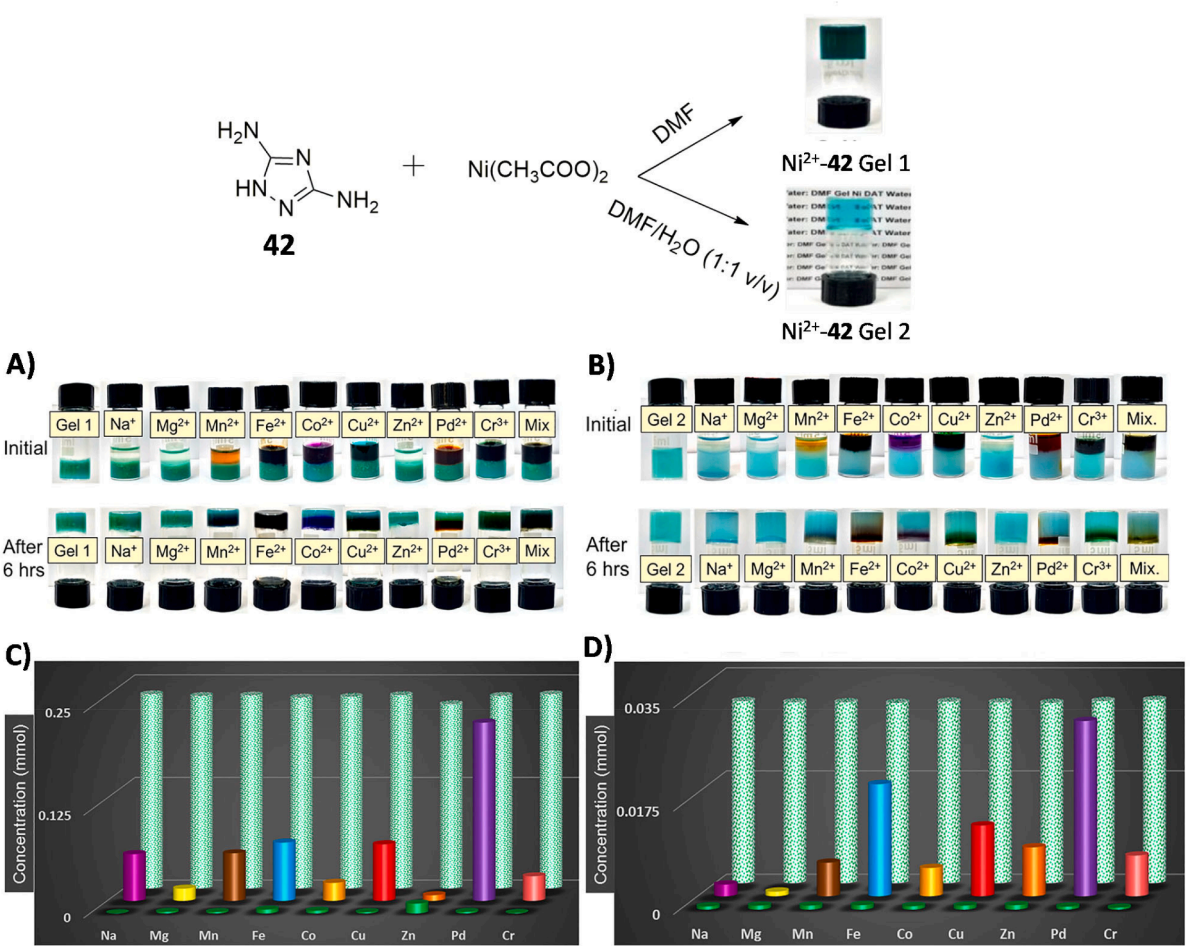

Fig. 46. Synthetic pathway for the formation of Ni^{2+}-**42** Gel 1 and Ni^{2+}-**42** Gel 2; colour changes for Ni^{2+}-**42** Gel 1 in A); and for Ni^{2+}-**42** Gel 2 in B) upon metal ion uptake and corresponding graphical representations C) and D), respectively, after 6 h. The green bars at the foreground correspond to the amount of Ni^{2+} released in the supernatant solution, the green textured bars at the background indicate the amount of Ni^{2+} remaining. Copyright ACS 2019. Adapted with permission from ref. [106].

constant of the Cd^{2+}-EDTA complex. The metallogels were also used to adsorb methyl orange due to the formation of additional HBs between the ligand and the dye.

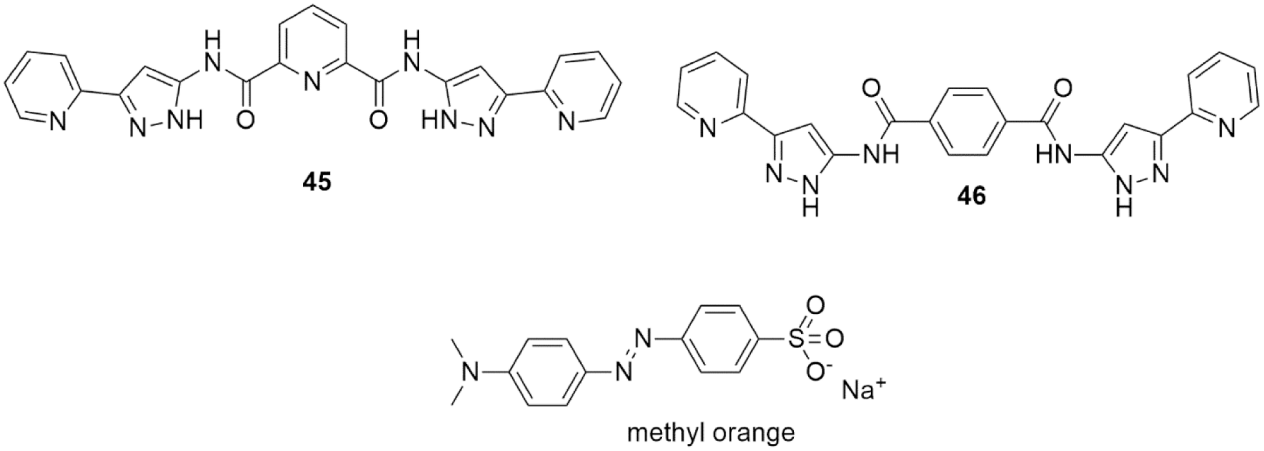

More recently the same authors developed a similar ligand (**46**) containing the pyridine-pyrazole core with a phenyl spacer able to form a strong metallogel with copper triflate in DMSO in the presence of 3 equivs. of metal ion with a concentration as low as 0.3 wt% [110]. The formation of the metallogel Cu^{2+}-**46** was attributed to the coordination of the metal ion to the pyridine and pyrazole nitrogens in a square planar geometry and to the formation of intermolecular HBs and π-π interactions with the other portions of the ligand molecule. Also in this case methyl orange was adsorbed by the system in the form of xerogel

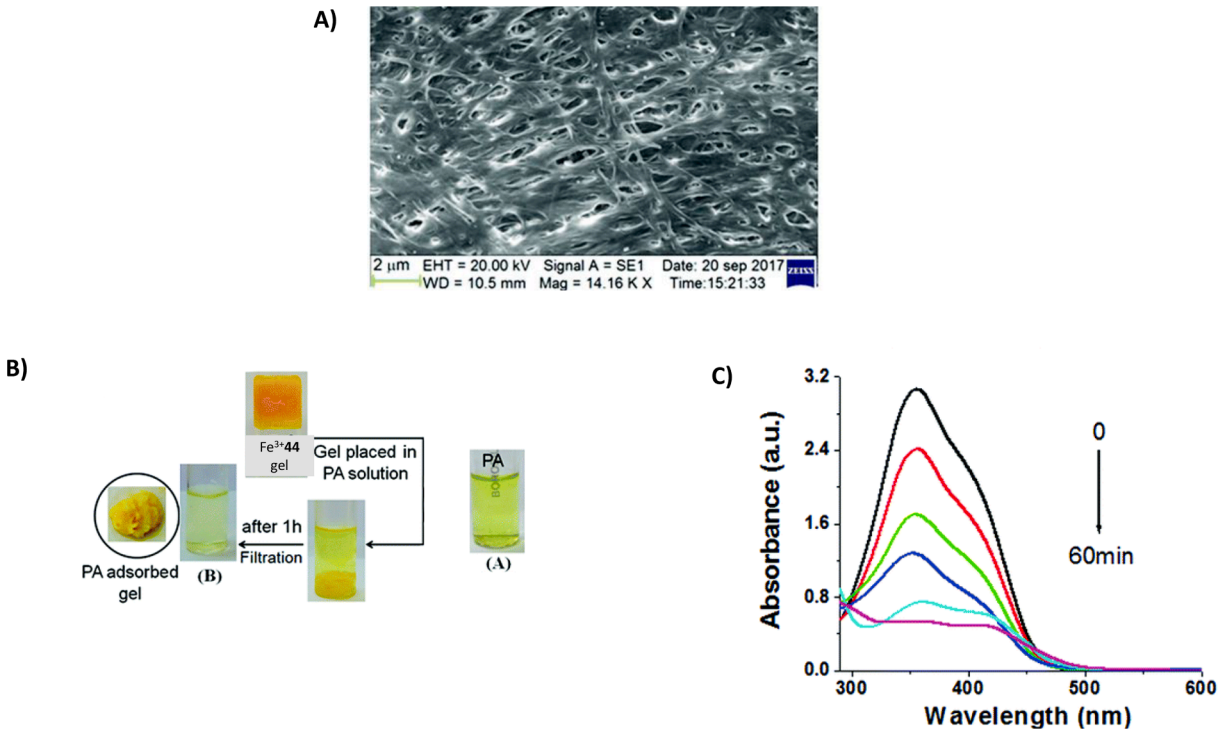

Fig. 47. A) SEM image of the Fe^{3+}-**44** xerogel; B) photographs showing the adsorption experiment of the metallogel Fe^{3+}-**44** in the presence of PA; C) changes in the absorbance of the PA solution after gel exposure. Copyright RSC 2018. Adapted with permission from ref. [108].

with a dye adsorption capacity of about 5 mg/g over a period of 8 h. The dye adsorption was found to be reversible as after washing the xerogel with HCl, NaOH and then neutralising the pH, several cycles of adsorption/desorption could be performed. The copper metallogel of **46** was reported to be the first example of a metallogel able to calorimetrically sense vapours of amines. When the metallogel was exposed to ammonia, diethylamine, triethyl amine and pyridine vapours a colour change (attributed to a change in the coordination sphere of the copper (II) ion) from green to red was observed. As shown in Fig. 48 in the presence of HCl vapour the gel reverted back to its original state.

The pyridine-pyrazole motif have also been used by the same group to design a tripodal system that forms a gel in the presence of various silver(I) salts in H_2O/DMF (4:1 v/v). Interestingly this platform was used to grow silver nanoparticles which were able to improve the mechanic properties of the material and its stability [111].

A coordination polymer able to form a gel was obtained by the self-assembling of two tripodal receptors **47** and **48** and Fe^{3+} (as its perchlorate salt) in DMSO/H_2O (66:34 v/v) [112]. Authors had previously shown that in the same experimental conditions **47** and **48** are able to form a AIE supramolecular polymer with a rod-like structure [113]. In the presence of Fe^{3+}, the polymer folds, forming a coordination polymer with a micro-acanthosphere structure as revealed by SEM (Fig. 49A). FT-IR spectrum suggested that cation-π interactions and coordination with the nitrogen atom of the pyridine moieties are involved in the coordination process of the metal ion (Fig. 49B). The xerogel was then used to adsorb methylene blue (MB) form aqueous solution and it showed an absorption rate of 96% while with other dyes [crystal violet (CV), rhodamine (Rh), sudan I (Su I), and methyl orange (MO)] the adsorption rate was less than 30% (Fig. 49c).

A very interesting class of materials is represented by MOGs (metal organic gels) which are MOF (metal organic framework)-like materials, containing organic solvents with sponge-like gel matrixes [114]. MOGs formed by the reaction of carboxymethyl-(3,5-di-*tert*-butyl-2-hydroxybenzyl)-amino sodium acetate (**49**) and CdX_2 (X = Cl, Br, I) and $ZnCl_2$ in MeOH were described by Bhattacharjee and Karan [115]. The idea behind the design of the receptor is that carboxylate groups as well as phenolic oxygens and the nitrogen should be able to coordinate the metal centre and at the same time the same functional groups should be able to form HBs with protic solvents and form a gel. A white opaque Cd^{2+}-**49** MOG (Fig. 50A) with very interesting features was obtained upon the reaction of **49** with $CdCl_2$ in 1:0.7 molar ratio in MeOH after 60 s standing at room temperature with minimum gelation concentration of 0.89% (w/v). The Cd^{2+}-**49** MOG showed excellent thixotropic response, stable in the pH range 6–8 and chemoresponsive properties as addition of NH_3 caused the disruption of the gel and trifluoroacetic acid restored the material. When Cd^{2+}-**49** was treated with Na_2S a yellow precipitate of CdS was formed. Moreover, it exhibited good self-sustainability as the gel formed in a vial and then taken out retained

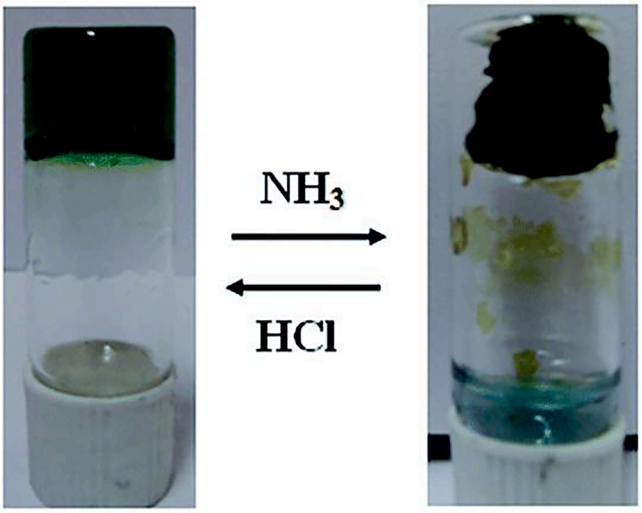

Fig. 48. Reversible colorimetric change of the metallogel Cu^{2+}-**46** in presence of ammonia and HCl vapour. Copyright RSC 2016. Reproduced with permission from ref. [110].

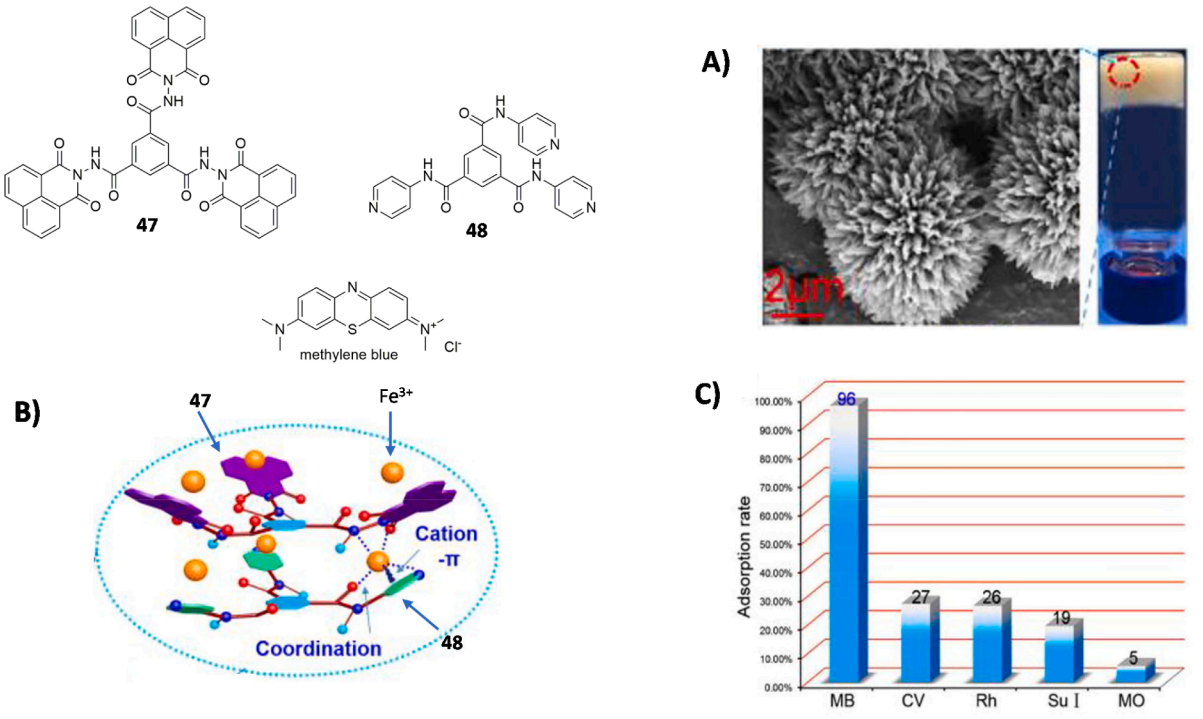

Fig. 49. A) SEM image of the xerogel formed by the coordination polymer generated by the self-assemble of **47**, **48** and Fe^{3+} and picture of the gel; B) proposed coordination sphere for Fe^{3+} in the coordination polymer; C) adsorption rate comparison for the xerogel in the presence of different dyes (MB = methylene blue, CV = crystal violet, Rh = rhodamine, Su I = sudan I, MO = methyl orange). Copyright Elsevier 2020. Adapted with permission from ref. [112].

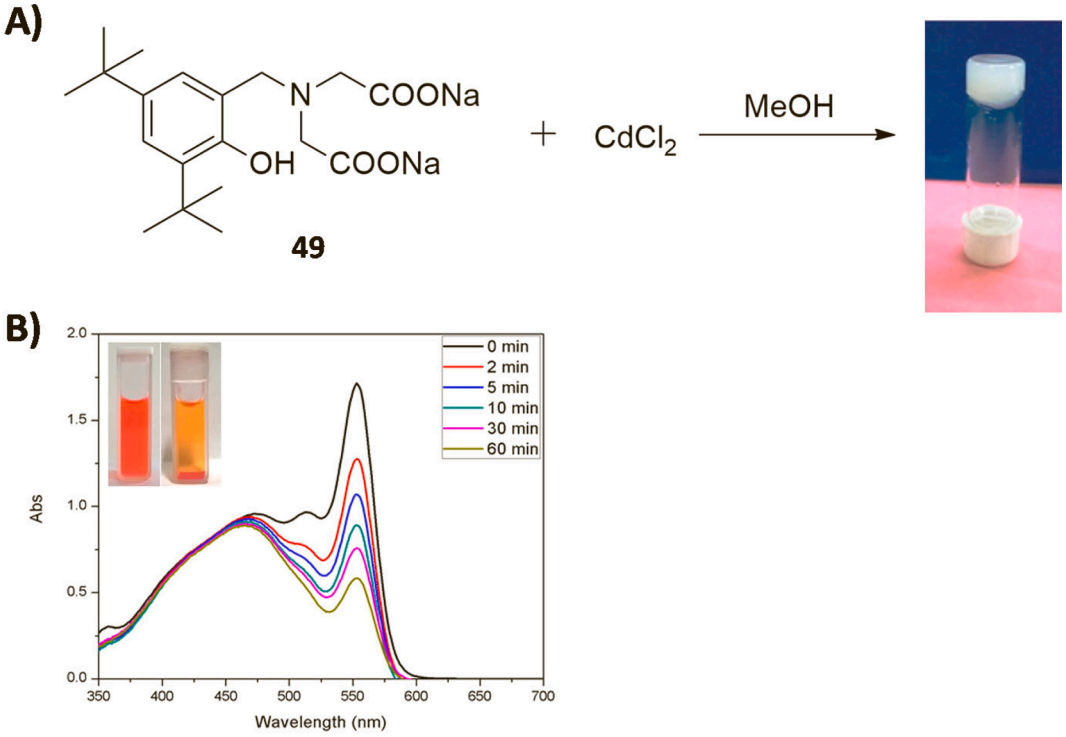

Fig. 50. A) Synthetic pathway for obtaining the MOG based on **49** and $CdCl_2$; B) absorption spectra of an aqueous solution mixture of Rh and MO in the presence of the Cd^{2+}-**49** xerogel, inset before (left) and after dye adsorption (right). Copyright ACS 2016. Reproduced with permission from ref. [115].

its initial shape. The xerogel dyes adsorption and dyes separation properties were also tested using aqueous solutions of cationic dyes MB, CV, Rh, anionic dyes MO, fluorescein (Fl), and a neutral dye, neutral red (NR). The system selectively adsorbed cationic dyes over anionic and neutral ones as shown in Fig. 50B. Indeed, UV–Vis spectroscopy revealed that when the xerogel was exposed to an aqueous mixture of Rh and MO, the absorption band of Rh at 554 nm decreased with time, while the absorption band of MO at 464 nm remains unchanged.

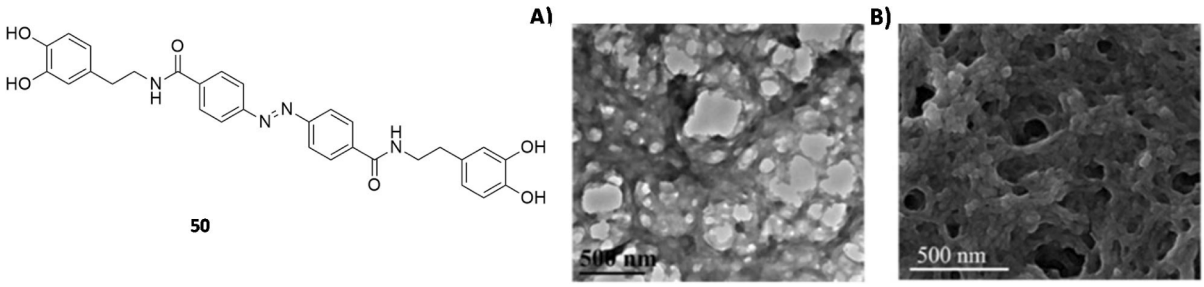

Fig. 51. Structure of gelator **50**, A) TEM; and B) SEM images of the Ni^{2+}-containing MOG. Copyright ACS 2018. Adapted with permission from ref. [116].

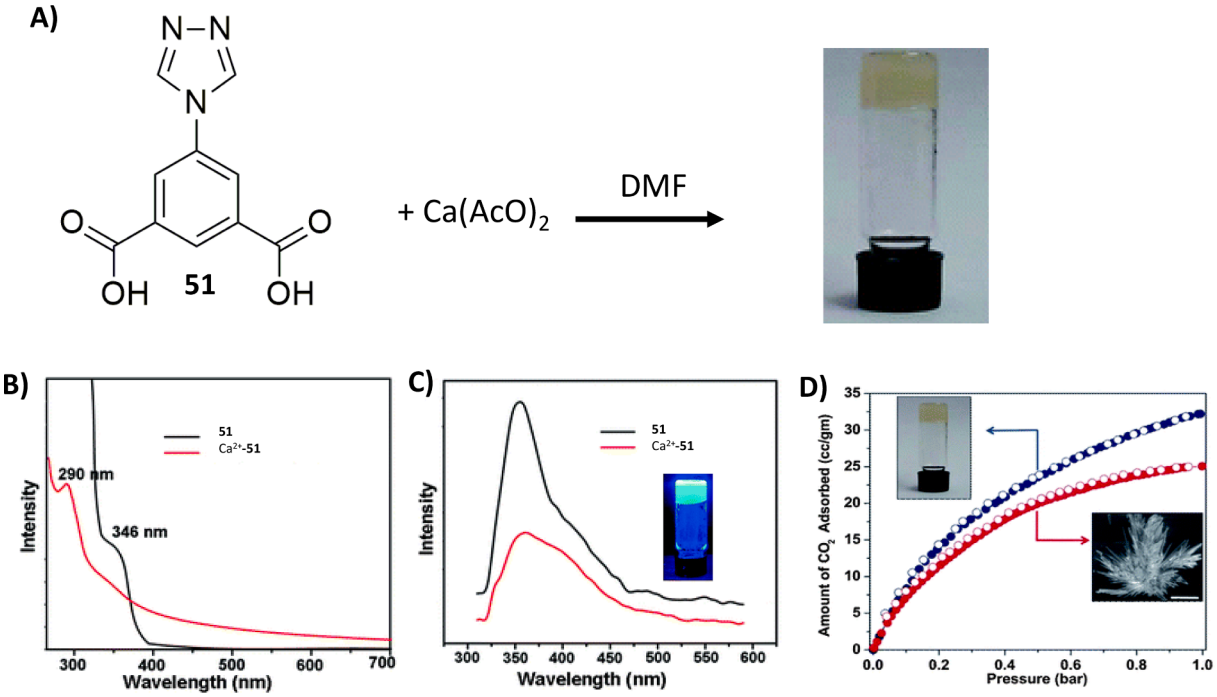

Fig. 52. A) Synthetic pathway for obtaining the Ca^{2+}-**51** gel; B) UV–Vis spectra for **51** (black) and Ca^{2+}-**51** gel (red); C) fluorescence emission spectra for **51** (black) and Ca^{2+}-**51** gel (red, inset: picture of Ca^{2+}-**51** gel under UV irradiation); D) CO_2 adsorption (filled circles), and desorption (open cyrcles) data for Ca^{2+}-**51** xerogel (blue) and Ca^{2+}-**51** MOF (red) at 298 K. Copyright RSC 2012. Adapted with permission from ref. [117].

Another example of MOG able to adsorb organic dyes was reported by Dong and co-workers [116]. The components were the catechol derivative **50**, nickel acetate, and DMF. TEM and SEM images revealed that the material has an irregular wormhole-like network consisting of agglomerated nanoparticles (Fig. 51). Its amorphous nature was determined by PXRD, while XPS allowed to identify the C═O and OH groups as the donors for the formation of the metal complex. In contrast to the previous example, when exposed to an aqueous solution of cationic or anionic organic dyes, the xerogel did not show any preference on the base of the ionic nature of the dye.

By reacting 5-(1,2,4-triazoleyl)isophthalic acid (**51**) and calcium acetate in DMF in equimolar ratio, Banerjee, Diaz and co-workers were able to obtain the first example of Ca^{2+}-based LMW metallogel (Fig. 52A) [117]. The gel showed a phenyl ring absorption peak at 298 nm (Fig. 52B) and an emission band at 356 nm less intense of that of **51** (Fig. 52C). Interestingly, in the presence of water, the system formed a stable MOF and the comparison of the CO_2 adsorption isotherms (Fig. 52D) of the xerogel of Ca^{2+}-**51** and the crystalline MOF showed a 20% increase in the CO_2 adsorption ability of the xerogel (1.45 and 1.12 mmol g^{-1} of CO_2 at 298 K and 1 atm pressure for the xerogel and the MOF, respectively).

A systematic study on the ability to form metallogels with iron(III) by a family of carboxylates containing single pyridyl or phenyl rings was carried out by Bourne and co-workers [118]. After a detailed characterization of the gels and the study of the influence of different factors (such as temperature, metal ion employed, solvent and type of gelator) the authors demonstrated that these systems are able to respond to external stimuli such as gas (N_2, CO_2, and H_2O vapours) and dyes (bromocresol green and methyl orange) adsorption.

7. Metallogels for catalysis

Metallogels could have wide application in various aspects, such as redox sensor, self-healing properties, and in particular, in catalysis [74,115,119–123]. Jin Yong Lee, Jong Hwa Jung, and co-workers reported a tetrazole-based gelator **52** that formed a metallogel upon the addition of Ag^{+} ions [124].

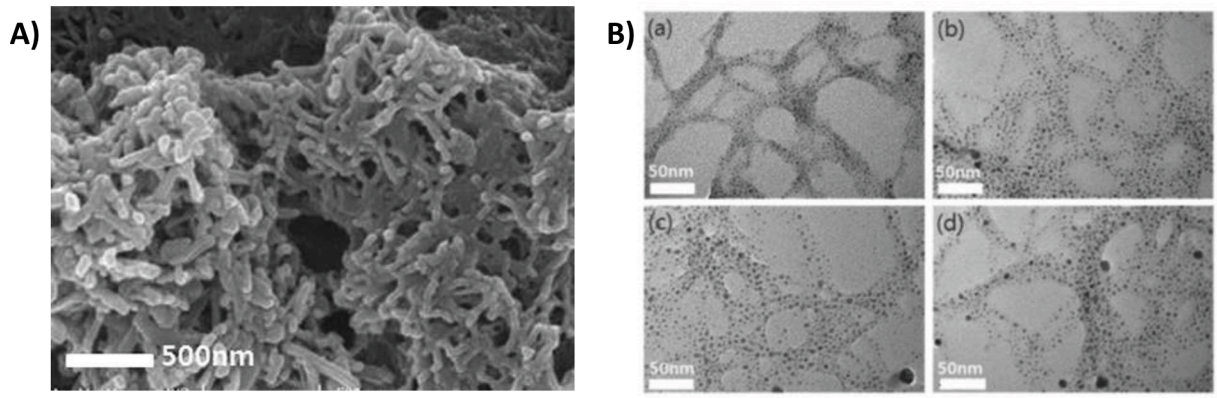

Fig. 53. A) SEM image of metallogel Ag^+-**52** in H_2O; B) TEM images of Ag^+-**52** upon the addition (a) 2, (b) 3, (c) 4, and (d) 5 equivs. of $AgClO_4$. Copyright RSC 2012. Adapted with permission from ref. [124].

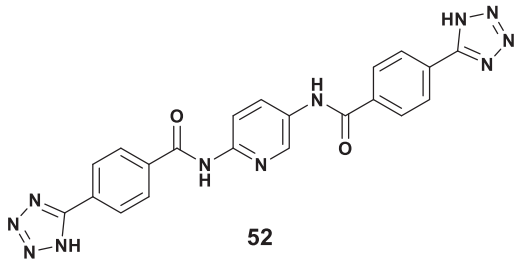

52

Indeed, upon the addition of more than 2 equivs. of Ag^+ as its perchlorate salt, compound **52** was found to gel in a basic aqueous solution. After its formation, the white metallogel Ag^+-**52** changed colour over time turning to brown due to reduction by NaOH and formation of metallic Ag nanoparticles (AgNPs).

Rheological studies highlighted how the metallogel is stable upon the addition of 5 equivs. of Ag^+, due to the complete coordination of the system. Furthermore, strain sweep studies demonstrated that the metallogel is stable in the presence of external forces, as suggested by the constant values of the two moduli G′ and G\prime\prime by increasing the frequency of the stress applied from 0.1 to 100 rad s^{-1}. The morphology of metallogel Ag^+-**52** in the presence of 2 equivs. of $AgClO_4$ in aqueous solution with basic conditions showed a fibre structure of 20–50 nm diameter and several mm in length (Fig. 53A). The presence of the nanoparticles was pointed out by means of TEM analysis; Indeed, TEM images (Fig. 53B) show a spherical particle exclusively formed in the gel fibres.

Interestingly, AgNPs present in the inner structure of the gel was found to be capable to catalyse in high conversion the reduction of 4-nitrophenol (4-NP) to 4-aminophenol (4-AP) by $NaBH_4$. Indeed, a conversion higher than 95% was achieved when a solution of 4-NP and $NaBH_4$ flushed into a column packed with the AgNPs/Ag^+-**52** gel fibre composite at a rate 0.60 mL cm^{-2} s^{-1}. The catalytic process was highly reproducible, and the catalytic reaction did not result in undesired system alterations and/or detachment of AgNPs.

Another effective catalyst for nitro-arene reduction in presence of $NaBH_4$ was reported by Bania and collaborators [125]. Indeed, the Fe^{3+}-metallogel based on *trans*-1,2-cyclohexanedicarboxylic acid **53** was used to grown cubical shape silver particles that were found to have high efficiency in catalysing the reduction of 4-NP to 4-AP in the presence of $NaBH_4$.

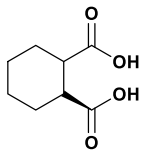

53

Dastidar and co-workers reported the novel C_3-symmetric based bowl-shaped tris(pyridylamide) **54** and **55**, containing potential HB sites suitable for the formation of metallogels [126].

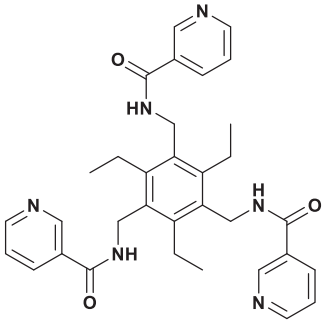

54

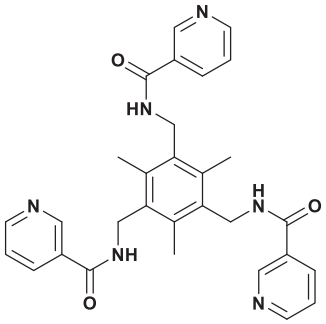

55

Compounds **54** and **55** formed gels in DMSO/H_2O (2:3 v/v), DMF/H_2O (2:3 v/v), and nitrobenzene. They were able to form metallogels with all the silver(I) salts considered (PF_6^-, BF_4^-, and NO_3^-), except

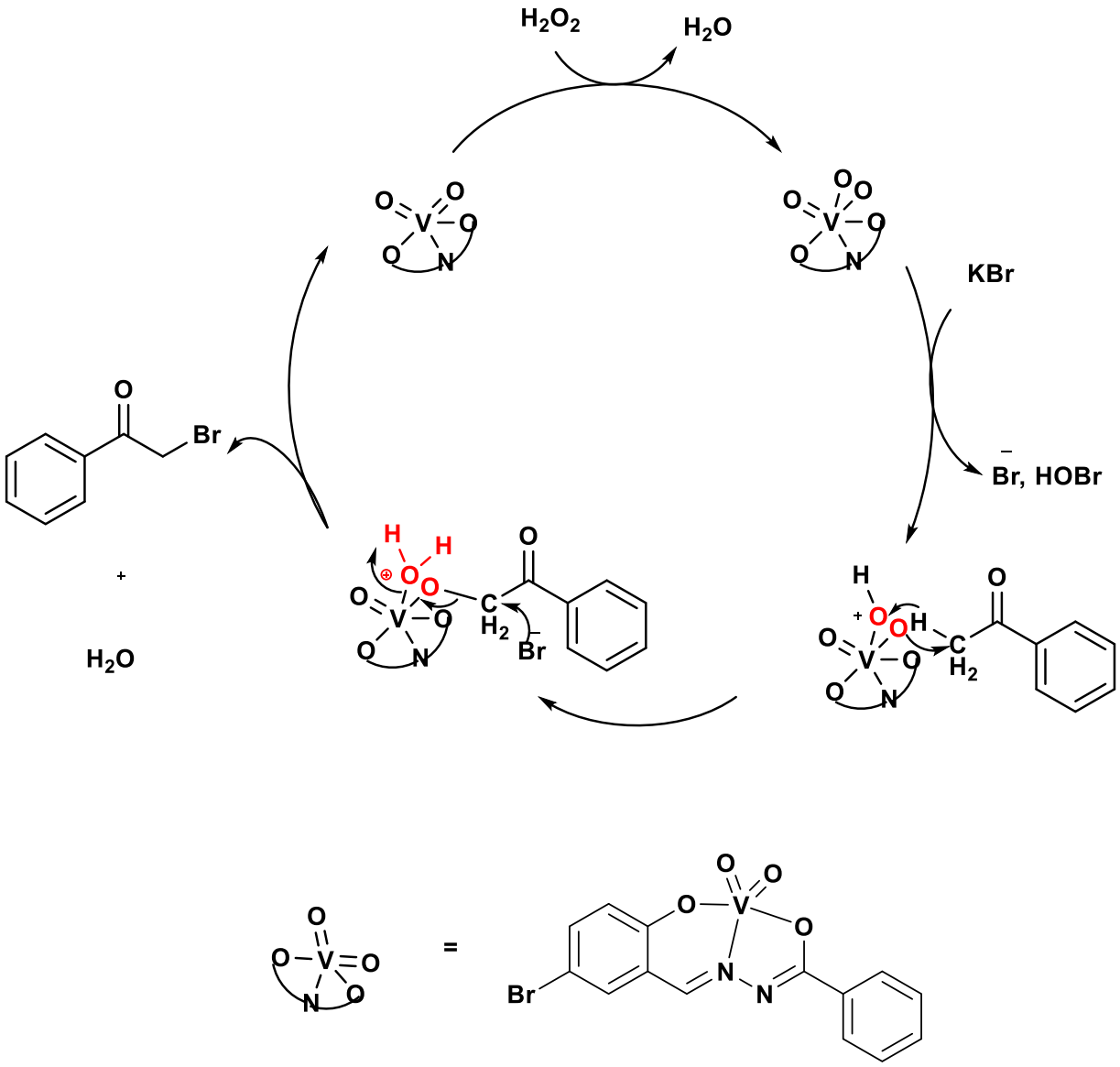

Scheme 1. Possible mechanism for the oxidative bromination catalysed by VO_2^+-**56** metallogel. Copyright RSC 2020. Reproduced with permission from ref. [127] (Scheme 2).

$AgCF_3CO_2$, suggesting the important role of the counter ion in the gelation process. Interestingly, also in this case the metallogels were capable to produce AgNPs, at 298 K upon light exposition, as the result of the reduction of Ag^+ to Ag^0 without any reducing agent like $NaBH_4$. After the characterization of AgNPs, their catalytic behaviour was investigated. The AgNPs present within the inner structure of metallogel were capable to catalyse the reaction 4-NP to 4-AP without the use of any other reducing agent like $NaBH_4$. It is worth to evidence how the same procedure in the presence of separately prepared AgNPs, did not provide the same conversion indicating the fundamental activity of the ligand-AgNPs cooperativity in the metallogel in catalysing the reaction. The catalytic process could be also appreciate by naked eyes, with a dramatic chromatic change: the well-known yellow colour of 4-nitrophenolate turned to colourless within a few seconds, due to the adsorption of the 4-nitrophenolate over the metallogel at room temperature.

Kurbah and co-workers presented the VO_2^+-**56** metallogel derived from a hydrazone gelator **56** able to catalyse the oxidative bromination of some organic substrates in presence of hydrogen peroxide [127].

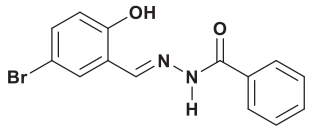

56

The reaction between **56** and vanadium pentoxide in a 2:1 molar ratio in methanol led to the formation of VO_2^+-**56**, enable to gelate in a MeOH/H_2O mixture (9:1 v/v) by sonicating for 5 min, obtaining a thermo-reversible gel. Rheological measurements evidenced a high mechanical strength of the material (yield stress was found around 312 Pa). VO_2^+-**56** metallogel was found to catalyse the oxidative bromination of some organic substrate. Indeed, by using the phenol red as a model substrate, the model reaction allowed to identify the best conditions to obtain the optimum yield for the reaction. It was found that a 1:10 molar ratio of VO_2^+-**56** metallogel/substrate, VO_2^+-**56** metallogel/substrate/KBr in a 1:10:40 molar ratio, 1:10:40:40 molar ratio of VO_2^+-**56** metallogel/substrate/KBr/H_2O_2 gave the maximum yield, and

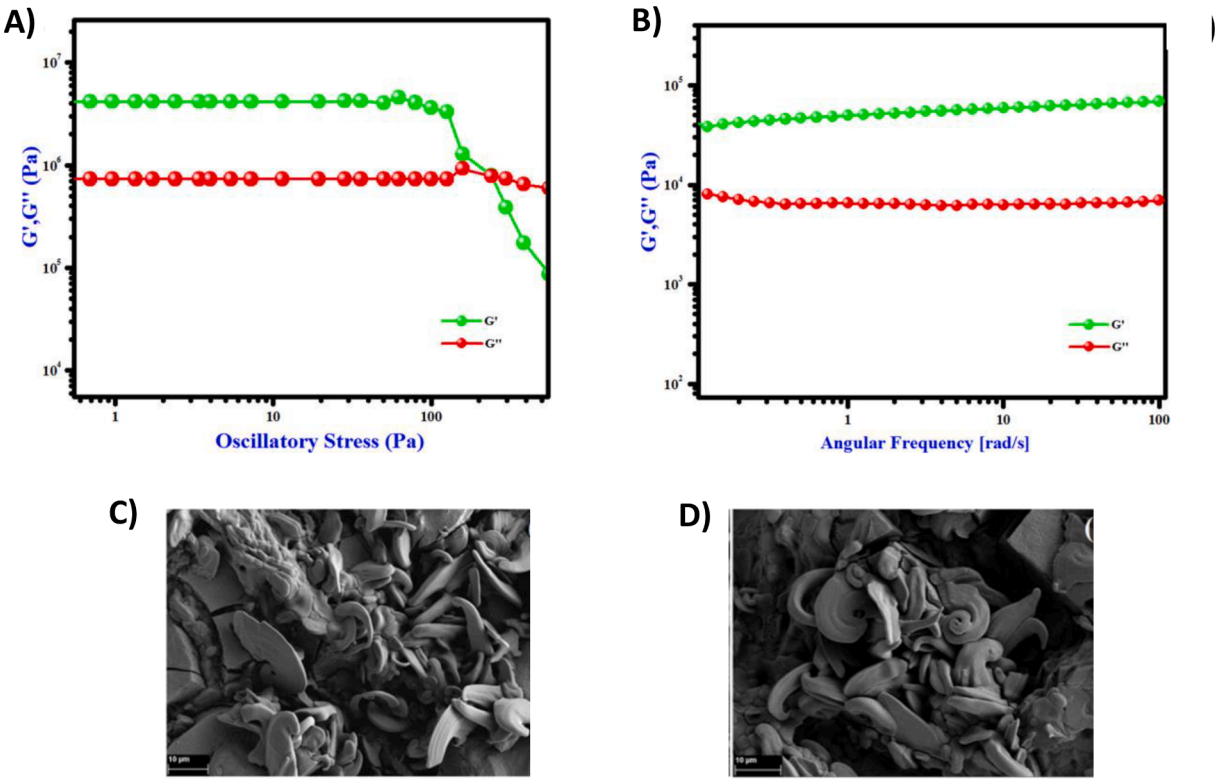

Fig. 54. A) Oscillatory stress rheology; and B) oscillatory frequency sweeps of the Fe^{3+}-**57**; C) and D) FESEM microstructural images of Fe^{3+}-**57**. Copyright © 2020 American Chemical Society. Adapted from ref. [128].

was also demonstrated that the effect of $HClO_4$ improved the performance of the reaction when presence at the concentration of 4 M. VO_2^+-**56** metallogel was tested on different substrates, achieving high yield (85–93%) and reaction times onto a range of 25′−40′. Moreover, the present catalytic approach provided efficient and simple access to a-bromoketones. Based on the results obtained, authors proposed a catalytic mechanism considering acetophenone as substrate (Scheme 1). The dissolution of the VO_2^+-**56** metallogel on 15% of H_2O_2 caused the formation of peroxo species. Thus, the bromine is oxidized forming HOBr, Br_3^-, Br_2^- or "V–OBr" species under acid conditions, followed by the oxidation of bromide by hydrogen peroxide in aqueous solution. In the final step, the oxidized bromide species is then trapped by organic substrates releasing the brominated products.

Ray, Dey and co-workers reported the triethylenetetramine Fe^{3+}-**57** metallogel prepared by mixing of **57** and iron(III) salt in water [128].

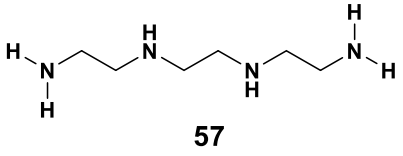

57

The rheology demonstrated the viscoelastic solid-like nature of Fe^{3+}-**57** metallogel in water (Fig. 54 A and 54B), whereas FESEM structural analysis evidenced cashew-shaped microstructure of the metallogel (Fig. 54 C and 54 D). Particularly, the iron(III) acts as a cross-linker and strengthening agent into the gel network, increasing the stability of the

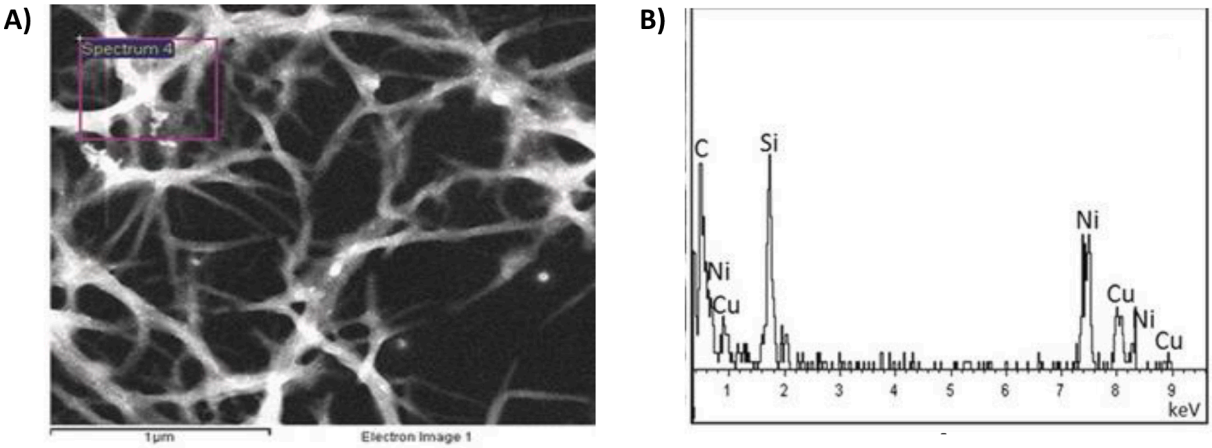

Fig. 55. A) STEM analysis of the metallogel Cu^+-**58**, and B) EDS analysis without staining. © 2017 Wiley-VCH Verlag GmbH & Co. KGaA, Weinheim. Adapted with the permission from ref. [129].

metallogel.

Fe^{3+}-**57** metallogel was capable to economically catalyse the aryl − S coupling reaction. In particular, the possibility to use this metallogel as a solvent-free catalyst toward C–S cross-coupling reactions was investigated. Fe^{3+}-**57** metallogel was found to be able to catalyse the coupling reaction within 12 h at 80 °C, providing a solvent-free synthetic strategy of aryl thioethers through a C–S coupling reaction. The possible recycle of the metallogel was also examined, the recovery rate gradually decreased from the second, third, to fourth runs.

Escuder and collaborators presented a dynamic catalytic system based on the amphiphilic gelator functionalized with an azidocoumarine triazole fragment **58**, able to catalyse model "click" reactions [129].

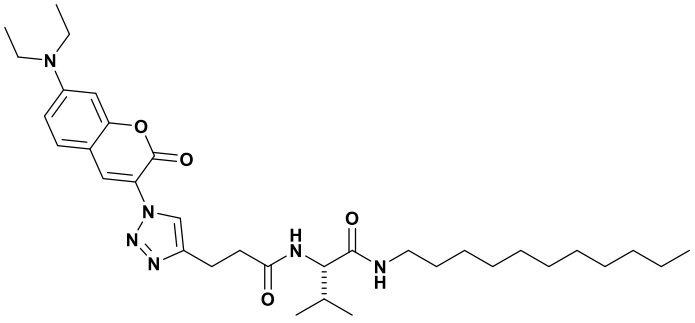

58

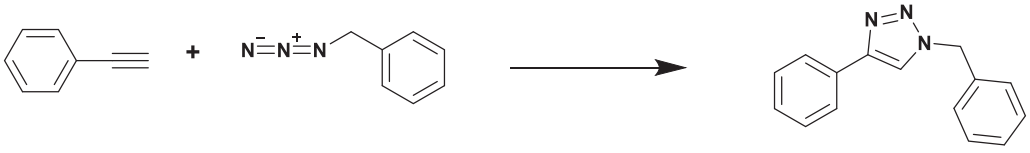

Scheme 2. Click reaction catalised by Cu^{+}-**58**.

Gelator **58** formed gels in 1:1 H_2O/t-BuOH (v/v) at a concentration of 10.7 mM, but the addition of copper(I) caused a decrease in the minimum gelation concentration to 7.1 mM, suggesting some cooperativity from the metal centre on the gelation process. The presence of copper(I) in the metallogel Cu^{+}-**58** has been observed by means of STEM picture and supported by EDS analysis, with a good distribution of the copper(I) along the fibres, resulting in the formation of an extended organometallic network (Fig. 55A and B).

The STEM image reported in Fig. 55A highlighted the bright contrast due to the presence of copper(I), whereas the EDS analysis reported in Fig. 55B confirmed the distribution of the copper(I) along the fibres, facilitating/aiding the formation of organometallic networks.

The metallogel Cu^{+}-**58** was found to be a heterogeneous gel catalyst for the model "click" reaction between benzylazide and phenylacetylene represented in Scheme 2, with the 92% conversion after 8 h reaction conducted in a 1:1 H_2O/t-BuOH mixture. Upon the addition of the two reactants, Cu^{+}-**58** disassembled and moved to the solution. Once the reaction ended, the product obtained as a crystal precipitate switched on/prompted the reformation of the metallogel. Furthermore, Cu^{+}-**58** could be recycled for three runs, maintaining its catalytic activity. In addition, during the whole disassembly/assembly process the gelator molecule was not subjected to any chemical transformation.

8. Conclusions

We have shown here that in the last decade supramolecular metallogels have hold the promise to be versatile, smart, innovative materials that can find application in various fields. In particular, the possibility to modulate the properties of the materials by the right combination of metal ion/gelator opens infinite combinations. Clearly the field has not been fully explored yet and still much work on the fine control of the properties of these materials in which strong and weak interactions concur in the formation of complex supramolecular architectures. We hope this review will be of inspiration for the researchers in the field and these materials will move from lab bench to real life application in the near future.

Declaration of Competing Interest

The authors declare that they have no known competing financial interests or personal relationships that could have appeared to influence the work reported in this paper.

Data availability

No data was used for the research described in the article.

Acknowledgements

Financial support from MIUR (PRIN 2017 project 2017EKCS35, NextGeneration EU, Return project PE0000005 CUP: F53C22000730002), and FdS (annualità 2020) is gratefully acknowledged. J.M. thanks Regione Autonoma della Sardegna PN-RI project for her PhD scholarship. JWS thanks the Engineering and Physical Sciences Research Council for funding (EP/S035877/1).

References

[1] P. Terech, R.G. Weiss, Low molecular mass gelators of organic liquids and the properties of their gels, Chem. Rev. 97 (1997) 3133–3160, https://doi.org/10.1021/cr9700282.
[2] J. Lloyd, D. In, Colloid chemistry, Red. Alexander J.), Chem. Cat. Co., New York. 1 (1926).
[3] J.W. Steed, J.L. Atwood, Supramolecular Chemistry, 3rd edition, Wiley, 2022.

[4] M. Coppola, M. Djabourov, M. Ferrand, Unified phase diagram of gelatin films plasticized by hydrogen bonded liquids, Polymer (Guildf) 53 (2012) 1483–1493, https://doi.org/10.1016/j.polymer.2012.02.016.
[5] B. Rogers, T. Mikulchyk, M. Oubaha, D. Cody, S. Martin, I. Naydenova, Improving the holographic recording characteristics of a water-resistant photosensitive sol-gel for use in volume holographic optical elements, Photonics 9 (2022), https://doi.org/10.3390/photonics9090636.
[6] K. Baskaran, M. Ali, K. Gingrich, D.L. Porter, S. Chong, B.J. Riley, C.W. Peak, S. E. Naleway, I. Zharov, K. Carlson, Sol-gel derived silica: a review of polymer-tailored properties for energy and environmental applications, Microporous Mesoporous Mater. 336 (2022), 111874, https://doi.org/10.1016/j.micromeso.2022.111874.
[7] L. Trupp, M.C. Marchi, B.C. Barja, Lanthanide–based luminescent hybrid silica materials prepared by sol-gel methodologies: a review, J. Sol-Gel Sci. Technol. 102 (2022) 63–85, https://doi.org/10.1007/s10971-021-05678-9.
[8] H.O. Simila, A.R. Boccaccini, Sol-gel bioactive glass containing biomaterials for restorative dentistry: a review, Dent. Mater. 38 (2022) 725–747, https://doi.org/10.1016/j.dental.2022.02.011.
[9] P. Karasiński, M. Zięba, E. Gondek, J. Nizioł, S. Gorantla, K. Rola, A. Bachmatiuk, C. Tyszkiewicz, Sol-gel derived silica-titania waveguide films for applications in evanescent wave sensors—comprehensive study, Materials (Basel). 15 (2022), https://doi.org/10.3390/ma15217641.
[10] R. Fan, Y. Cheng, R. Wang, T. Zhang, H. Zhang, J. Li, S. Song, A. Zheng, Thermosensitive hydrogels and advances in their application in disease therapy, Polymers (Basel) 14 (2022), https://doi.org/10.3390/polym14122379.
[11] A.C. Marques, M. Vale, Macroporosity control by phase separation in sol-gel derived monoliths and microspheres, Materials (Basel) 14 (2021), https://doi.org/10.3390/ma14154247.
[12] X.-W. Zhang, Y.-J. Chu, Y.-H. Li, X.-J. Li, Matrix compatibility of typical sol–gel solid-phase microextraction coatings in undiluted plasma and whole blood for the analysis of phthalic acid esters, Anal. Bioanal. Chem. 414 (2022) 2493–2503, https://doi.org/10.1007/s00216-022-03890-2.
[13] M. Yokoya, S. Kimura, M. Yamanaka, Urea derivatives as functional molecules: supramolecular capsules, supramolecular polymers, supramolecular gels, artificial hosts, and catalysts, Chem. – A Eur. J. 27 (2021) 5601–5614, https://doi.org/10.1002/chem.202004367.
[14] G. Picci, M.T. Mulvee, C. Caltagirone, V. Lippolis, A. Frontera, R.M. Gomila, J. W. Steed, Anion-responsive fluorescent supramolecular gels, Molecules 27 (2022), https://doi.org/10.3390/molecules27041257.
[15] T. Das, M. Häring, D. Haldar, D. Díaz Díaz, Phenylalanine and derivatives as versatile low-molecular-weight gelators: design, structure and tailored function, Biomater. Sci. 6 (2018) 38–59, https://doi.org/10.1039/C7BM00882A.
[16] N. Singh, M. Kumar, J.F. Miravet, R.V. Ulijn, B. Escuder, Peptide-based molecular hydrogels as supramolecular protein mimics, Chem. – A Eur. J. 23 (2017) 981–993, https://doi.org/10.1002/chem.201602624.
[17] N. Maldonado, P. Amo-Ochoa, Advances and novel perspectives on colloids, hydrogels, and aerogels based on coordination bonds with biological interest ligands, Nanomaterials 11 (2021), https://doi.org/10.3390/nano11071865.
[18] T. Giraud, S. Bouguet-Bonnet, M.-J. Stébé, L. Richaudeau, G. Pickaert, M.-C. Averlant-Petit, L. Stefan, Co-assembly and multicomponent hydrogel formation upon mixing nucleobase-containing peptides, Nanoscale 13 (2021) 10566–10578, https://doi.org/10.1039/D1NR02417E.
[19] F. Khan, S. Das, Modified low molecular weight pure and engineered gels: a review of strategies towards their development, ChemistrySelect. 7 (2022) e202200205.
[20] E. Impresari, A. Bossi, E.M. Lumina, M.A. Ortenzi, J.M. Kothuis, G. Cappelletti, D. Maggioni, M.S. Christodoulou, R. Bucci, S. Pellegrino, Fatty acids/tetraphenylethylene conjugates: hybrid aiegens for the preparation of peptide-based supramolecular gels, Front. Chem. 10 (2022) 1–14, https://doi.org/10.3389/fchem.2022.927563.
[21] G. Fernandes, A. Pandey, S. Kulkarni, S.P. Mutalik, A.N. Nikam, R.N. Seetharam, S.S. Kulkarni, S. Mutalik, Supramolecular dendrimers based novel platforms for effective oral delivery of therapeutic moieties, J. Drug Deliv. Sci. Technol. 64 (2021), 102647, https://doi.org/10.1016/j.jddst.2021.102647.
[22] Y. Feng, Z.-X. Liu, H. Chen, Q.-H. Fan, Functional supramolecular gels based on poly(benzyl ether) dendrons and dendrimers, Chem. Commun. 58 (2022) 8736–8753, https://doi.org/10.1039/D2CC03040C.
[23] X. Feng, C. Liu, X. Wang, Y. Jiang, G. Yang, R. Wang, K. Zheng, W. Zhang, T. Wang, J. Jiang, Functional supramolecular gels based on the hierarchical assembly of porphyrins and phthalocyanines, Front. Chem. 7 (2019) 1–20, https://doi.org/10.3389/fchem.2019.00336.
[24] E.R. Draper, D.J. Adams, Low-molecular-weight gels: the state of the art, Chem. 3 (2017) 390–410, https://doi.org/10.1016/j.chempr.2017.07.012.
[25] D. Núñez-Villanueva, M.A. Jinks, J. Gómez Magenti, C.A. Hunter, Ultrasound-induced gelation of a giant macrocycle, Chem. Commun. 54 (2018) 10874–10877, https://doi.org/10.1039/C8CC04742A.
[26] V.K. Pandey, M.K. Dixit, S. Manneville, C. Bucher, M. Dubey, A multi-stimuli responsive conductive sonomettallogel: a mechanistic insight into the role of ultrasound in gelation, J. Mater. Chem. A 5 (2017) 6211–6218, https://doi.org/10.1039/c7ta00854f.
[27] C.D. Jones, J.W. Steed, Gels with sense: Supramolecular materials that respond to heat, light and sound, Chem. Soc. Rev. 45 (2016) 6546–6596, https://doi.org/10.1039/c6cs00435k.
[28] G. Biscari, G. Pitarresi, C. Fiorica, D. Schillaci, V. Catania, F.S. Palumbo, G. Giammona, Near-infrared light-responsive and antibacterial injectable hydrogels with antioxidant activity based on a Dopamine-functionalized Gellan Gum for wound healing, Int. J. Pharm. 627 (2022), 122257, https://doi.org/10.1016/j.ijpharm.2022.122257.
[29] R. Brighenti, M.P. Cosma, Mechanics of multi-stimuli temperature-responsive hydrogels, J. Mech. Phys. Solids 169 (2022), 105045, https://doi.org/10.1016/j.jmps.2022.105045.
[30] F. Billeci, F. D'Anna, H.Q.N. Gunaratne, N.V. Plechkova, K.R. Seddon, "Sweet" ionic liquid gels: materials for sweetening of fuels, Green Chem. 20 (2018) 4260–4276, https://doi.org/10.1039/C8GC01615A.
[31] S. Marullo, C. Rizzo, N.T. Dintcheva, F. Giannici, F. D'Anna, Ionic liquids gels: Soft materials for environmental remediation, J. Colloid Interface Sci. 517 (2018) 182–193, https://doi.org/10.1016/j.jcis.2018.01.111.
[32] C. Rizzo, S. Marullo, P.R. Campodonico, I. Pibiri, N.T. Dintcheva, R. Noto, D. Millan, F. D'Anna, Self-sustaining supramolecular ionic liquid gels for dye adsorption, ACS Sustain. Chem. Eng. 6 (2018) 12453–12462, https://doi.org/10.1021/acssuschemeng.8b03002.
[33] C. Rizzo, A. Mandoli, S. Marullo, F. D'Anna, Ionic liquid gels: supramolecular reaction media for the alcoholysis of anhydrides, J. Org. Chem. 84 (2019) 6356–6365, https://doi.org/10.1021/acs.joc.9b00684.
[34] S. Marullo, A. Meli, F. Giannici, F. D'Anna, Supramolecular eutecto gels: fully natural soft materials, ACS Sustain. Chem. Eng. 6 (2018) 12598–12602, https://doi.org/10.1021/acssuschemeng.8b04278.
[35] B. Saavedra, A. Meli, C. Rizzo, D.J. Ramón, F. D'Anna, Natural eutectogels: sustainable catalytic systems for C-C bond formation reactions, Green Chem. 23 (2021) 6555–6565, https://doi.org/10.1039/D1GC01647D.
[36] S. Marullo, M. Tiecco, R. Germani, F. D'Anna, Highly recyclable surfactant-based supramolecular eutectogels for iodine removal, J. Mol. Liq. 362 (2022), 119712, https://doi.org/10.1016/j.molliq.2022.119712.
[37] P. Dastidar, S. Ganguly, K. Sarkar, Metallogels from coordination complexes, organometallic, and coordination polymers, Chem. – An Asian J. 11 (2016) 2484–2498, https://doi.org/10.1002/asia.201600814.
[38] A.V. Lipowitz, No Title, Liebigs Ann. Chem. 38 (1841) 348–355.
[39] D.D. Díaz, D. Kühbeck, R.J. Koopmans, Stimuli-responsive gels as reaction vessels and reusable catalysts, Chem. Soc. Rev. 40 (2011) 427–448, https://doi.org/10.1039/c005401c.
[40] Q. Lin, T.-T. Lu, X. Zhu, B. Sun, Q.-P. Yang, T.-B. Wei, Y.-M. Zhang, A novel supramolecular metallogel-based high-resolution anion sensor array, Chem. Commun. 51 (2015) 1635–1638, https://doi.org/10.1039/C4CC07814D.
[41] M.H. Filby, J.W. Steed, A modular approach to organic, coordination complex and polymer based podand hosts for anions, Coord. Chem. Rev. 250 (2006) 3200–3218, https://doi.org/10.1016/j.ccr.2006.06.004.
[42] M.O.M. Piepenbrock, N. Clarke, J.W. Steed, Metal ion and anion-based "tuning" of a supramolecular metallogel, Langmuir 25 (2009) 8451–8456, https://doi.org/10.1021/la900145n.
[43] M. Dudek, J.K. Clegg, C.R.K. Glasson, N. Kelly, K. Glou, K. Gloe, A. Kelling, H. J. Buschmann, K.A. Jolliffe, L.F. Lindoy, G.V. Meehan, Interaction of copper(II) with ditopic pyridyl-β-diketone ligands: dimeric, framework, and metallogel structures, Cryst. Growth Des. 11 (2011) 1697–1704, https://doi.org/10.1021/cg101629w.
[44] A. Fortunato, M. Mba, Metal cation triggered peptide hydrogels and their application in food freshness monitoring and dye adsorption, Gels. 7 (2021), https://doi.org/10.3390/gels7030085.
[45] X. Ma, Y. Wang, Y. Lai, T. Ren, J. Tang, Y. Gao, Y. Geng, J. Zhang, Artificial light-harvesting systems based on supramolecular self-assembly multi-component metallogels, Soft Matter. 18 (48) (2022) 9283–9290.
[46] G. Yang, S. Li, N. Li, P. Zhang, C. Su, L. Gong, B. Chen, C. Qu, D. Qi, T. Wang, J. Jiang, Enhanced photocatalytic CO2 reduction through hydrophobic microenvironment and binuclear cobalt synergistic effect in metallogels, Angew. Chemie Int. Ed. 61 (2022) e202205585.
[47] F. Fages, Metal coordination to assist molecular gelation, Angew. Chemie Int. Ed. 45 (2006) 1680–1682, https://doi.org/10.1002/anie.200503704.
[48] W.S. Compel, Metallogels through glyme coordination, Dalt. Trans. 45 (2016) 4509–4512, https://doi.org/10.1039/c6dt00255b.
[49] A.Y.Y. Tam, V.W.W. Yam, Recent advances in metallogels, Chem. Soc. Rev. 42 (2013) 1540–1567, https://doi.org/10.1039/c2cs35354g.
[50] Y. Zhao, J.B. Beck, S.J. Rowan, A.M. Jamieson, Rheological behavior of shear-responsive metallo-supramolecular gels, Macromolecules 37 (2004) 3529–3531, https://doi.org/10.1021/ma0497005.
[51] W. Weng, A.M. Jamieson, S.J. Rowan, Structural origin of the thixotropic behavior of a class of metallosupramolecular gels, Tetrahedron 63 (2007) 7419–7431, https://doi.org/10.1016/j.tet.2007.03.119.
[52] W. Weng, Z. Li, A.M. Jamieson, S.J. Rowan, Control of gel morphology and properties of a class of metallo- supramolecular polymers by good/poor solvent environments, Macromolecules 42 (2009) 236–246, https://doi.org/10.1021/ma801046w.
[53] M.O.M. Piepenbrock, N. Clarke, J.W. Steed, Rheology and silver nanoparticle templating in a bis(urea) silver metallogel, Soft Matter. 7 (2011) 2412–2418, https://doi.org/10.1039/c0sm00647e.
[54] Q. Wei, S.L. James, A metal-organic gel used as a template for a porous organic polymer, Chem. Commun. (2005) 1555–1556, https://doi.org/10.1039/b418554d.
[55] B. Adhikari, R. Afrasiabi, H.B. Kraatz, Ferrocene-tryptophan conjugate: An example of a redox-controlled reversible supramolecular nanofiber network, Organometallics 32 (2013) 5899–5905, https://doi.org/10.1021/om4004779.
[56] R. Afrasiabi, H.B. Kraatz, Stimuli-responsive supramolecular gelation in ferrocene-peptide conjugates, Chem. – A Eur. J. 19 (2013) 17296–17300, https://doi.org/10.1002/chem.201302450.

[57] R. Afrasiabi, H.B. Kraatz, Small-peptide-based organogel kit: towards the development of multicomponent self-sorting organogels, Chem. – A Eur. J. 19 (2013) 15862–15871, https://doi.org/10.1002/chem.201303116.
[58] Y. Wang, W. Qi, R. Huang, X. Yang, M. Wang, R. Su, Z. He, Rational design of chiral nanostructures from self-assembly of a ferrocene-modified dipeptide, J. Am. Chem. Soc. 137 (2015) 7869–7880, https://doi.org/10.1021/jacs.5b03925.
[59] B. Adhikari, C. Singh, A. Shah, A.J. Lough, H.B. Raatz, Amino acid chirality and ferrocene conformation guided self-assembly and gelation of ferrocene-peptide conjugates, Chem. – A Eur. J. 21 (2015) 11560–11572, https://doi.org/10.1002/chem.201501395.
[60] Z. Sun, Z. Li, Y. He, R. Shen, L. Deng, M. Yang, Y. Liang, Y. Zhang, Ferrocenoyl phenylalanine: A new strategy toward supramolecular hydrogels with multistimuli responsive properties, J. Am. Chem. Soc. 135 (2013) 13379–13386, https://doi.org/10.1021/ja403345p.
[61] N. Falcone, S. Basak, B. Dong, J. Syed, A. Ferranco, A. Lough, Z. She, H.B. Kraatz, A ferrocene-tryptophan conjugate: the role of the indolic nitrogen in supramolecular assembly, Chempluschem 82 (2017) 1282–1289, https://doi.org/10.1002/cplu.201700407.
[62] S. Basak, N. Falcone, A. Ferranco, H.B. Kraatz, Remarkable morphology transformation from fiber to nanotube of a histidine organogel in presence of a binuclear iron(III)–sulfur complex, J. Inorg. Organomet. Polym. Mater. 30 (2020) 121–130, https://doi.org/10.1007/s10904-019-01299-6.
[63] M. Ma, T. Luan, M. Yang, B. Liu, Y. Wang, W. An, B. Wang, R. Tang, A. Hao, Self-assemblies of cyclodextrin derivatives modified by ferrocene with multiple stimulus responsiveness, Soft Matter. 13 (2017) 1534–1538, https://doi.org/10.1039/c7sm00017k.
[64] S. Collavini, S.F. Völker, A. Cabrera-Espinoza, M.A. Martínez, A. De Cózar, L. San Felices, L. Sánchez, J.L. Delgado, Triarylamine enriched organostannoxane drums: synthesis, optoelectrochemical properties, association studies, and gelation behavior, Inorg. Chem. 61 (2022) 4046–4055, https://doi.org/10.1021/acs.inorgchem.1c03761.
[65] J. Park, J.H. Lee, J. Jaworski, S. Shinkai, J.H. Jung, Luminescent Calix[4]arene-based metallogel formed at different solvent composition, Inorg. Chem. 53 (2014) 7181–7187, https://doi.org/10.1021/ic500266f.
[66] K. Kolari, E. Bulatov, R. Tatikonda, K. Bertula, E. Kalenius, N. Nonappa, M. Haukka, Self-healing, luminescent metallogelation driven by synergistic metallophilic and fluorine-fluorine interactions, Soft Matter. 16 (2020) 2795–2802, https://doi.org/10.1039/c9sm02186h.
[67] K.C. Chang, J.L. Lin, Y.T. Shen, C.Y. Hung, C.Y. Chen, S.S. Sun, Synthesis and photophysical properties of self-assembled metallogels of platinum(II) acetylide complexes with elaborate long-chain pyridine-2,6- dicarboxamides, Chem. – A Eur. J. 18 (2012) 1312–1321, https://doi.org/10.1002/chem.201103030.
[68] V.-K.-M. Au, N. Zhu, V.-W.-W. Yam, Luminescent metallogels of bis-cyclometalated alkynylgold(III) complexes, Inorg. Chem. 52 (2013) 558–567, https://doi.org/10.1021/ic3007519.
[69] O. Kotova, R. Daly, C.M.G. Dos Santos, M. Boese, P.E. Kruger, J.J. Boland, T. Gunnlaugsson, Europium-directed self-assembly of a luminescent supramolecular gel from a tripodal terpyridine-based ligand, Angew. Chemie Int. Ed. 51 (2012) 7208–7212, https://doi.org/10.1002/anie.201201506.
[70] W.J. Gee, S.R. Batten, Instantaneous gelation of a new copper(II) metallogel amenable to encapsulation of a luminescent lanthanide cluster, Chem. Commun. 48 (2012) 4830–4832, https://doi.org/10.1039/c2cc30170a.
[71] X. Ma, Y. Cui, S. Liu, J. Wu, A thermo-responsive supramolecular gel and its luminescence enhancement induced by rare earth Y3+, Soft Matter. 13 (2017) 8027–8030, https://doi.org/10.1039/c7sm01726j.
[72] M. Martínez-Calvo, O. Kotova, M.E. Möbius, A.P. Bell, T. McCabe, J.J. Boland, T. Gunnlaugsson, Healable luminescent self-assembly supramolecular metallogels possessing lanthanide (Eu/Tb) dependent rheological and morphological properties, J. Am. Chem. Soc. 137 (2015) 1983–1992, https://doi.org/10.1021/ja511799n.
[73] Y. Yang, W. Liu, Q. Zhong, J. Zhang, B. Yao, X. Lian, H. Niu, Self-assembly of lanthanide-based metallogel nanoplates into microcubic blocks as self-calibrating luminescent methanol sensors, ACS Appl. Nano Mater. 4 (2021) 4735–4745, https://doi.org/10.1021/acsanm.1c00343.
[74] P. Chen, Q. Li, S. Grindy, N. Holten-Andersen, White-light-emitting lanthanide metallogels with tunable luminescence and reversible stimuli-responsive properties, J. Am. Chem. Soc. 137 (2015) 11590–11593, https://doi.org/10.1021/jacs.5b07394.
[75] T. Singha Mahapatra, H. Singh, A. Maity, A. Dey, S.K. Pramanik, E. Suresh, A. Das, White-light-emitting lanthanide and lanthanide-iridium doped supramolecular gels: modular luminescence and stimuli-responsive behaviour, J. Mater. Chem. C. 6 (2018) 9756–9766, https://doi.org/10.1039/C8TC03487G.
[76] Q. Zhou, X. Dong, J. Yuan, B. Zhang, S. Lu, Y. Xiong, Y. Liao, Q. Wang, Y. Yang, H. Wang, Supramolecular lanthanide metallogels rapidly formed at room temperature and their thermally stable luminescence behavior, J. Mol. Liq. 292 (2019), 111373, https://doi.org/10.1016/j.molliq.2019.111373.
[77] M. Xue, M. Chen, W. Chang, R. Chen, P. Li, Luminescent lanthanide metallogels: situ fabrication, self-healing and rheological properties, Colloid Polym. Sci. 298 (2020) 233–241, https://doi.org/10.1007/s00396-020-04598-4.
[78] B. Zhang, X. Dong, Y. Xiong, Q. Zhou, S. Lu, Y. Liao, Y. Yang, H. Wang, A heat-set lanthanide metallogel capable of emitting stable luminescence under thermal, mechanical and water stimuli, Dalt. Trans. 49 (2020) 2827–2832, https://doi.org/10.1039/c9dt04713a.
[79] J. Shukla, Y. Kumar, M.K. Dixit, C. Mahendar, V.K. Sharma, A. Kalam, M. Dubey, Investigation of the mechanism behind conductive fluorescent and multistimuli-responsive Li^+-enriched metallogel formation, Chem. – An Asian J. 15 (2020) 3020–3028, https://doi.org/10.1002/asia.202000630.
[80] W. Miao, L. Zhang, X. Wang, L. Qin, M. Liu, Gelation-induced visible supramolecular chiral recognition by fluorescent metal complexes of quinolinol-glutamide, Langmuir 29 (2013) 5435–5442, https://doi.org/10.1021/la400562f.
[81] H. Mehdi, H. Pang, W. Gong, M.K. Dhinakaran, A. Wajahat, X. Kuang, G. Ning, A novel smart supramolecular organic gelator exhibiting dual-channel responsive sensing behaviours towards fluoride ion: *via* gel-gel states, Org. Biomol. Chem. 14 (2016) 5956–5964, https://doi.org/10.1039/c6ob00600k.
[82] A. Sebastian, E. Prasad, Cyanide sensing in water using a copper metallogel through "turn-on" fluorescence, Langmuir 36 (2020) 10537–10547, https://doi.org/10.1021/acs.langmuir.0c01803.
[83] D. Ghosh, Deepa, K.K. Damodaran, Damodaran, metal complexation induced supramolecular gels for the detection of cyanide in water, Supramol. Chem. 32 (4) (2020) 276–286.
[84] N. Malviya, C. Sonkar, B.K. Kundu, S. Mukhopadhyay, Discotic organic gelators in ion sensing, metallogel formation, and bioinspired catalysis, Langmuir 34 (2018) 11575–11585, https://doi.org/10.1021/acs.langmuir.8b02352.
[85] J. Sun, Y. Liu, L. Jin, T. Chen, B. Yin, Coordination-induced gelation of an l-glutamic acid Schiff base derivative: The anion effect and cyanide-specific selectivity, Chem. Commun. 52 (2016) 768–771, https://doi.org/10.1039/c5cc07903a.
[86] M.O.M. Piepenbrock, N. Clarke, J.W. Steed, Shear induced gelation in a copper(ii) metallogel: new aspects of ion-tunable rheology and gel-reformation by external chemical stimuli, Soft Matter. 6 (2010) 3441–3457, https://doi.org/10.1039/c0sm00313a.
[87] C.A. Offiler, C.D. Jones, J.W. Steed, Metal "turn-off", anion "turn-on" gelation cascade in pyridinylmethyl ureas, Chem. Commun. 53 (2017) 2024–2027, https://doi.org/10.1039/c6cc09126a.
[88] G. Picci, M. Kubicki, A. Garau, V. Lippolis, R. Mocci, A. Porcheddu, R. Quesada, P. C. Ricci, M.A. Scorciapino, C. Caltagirone, Simple squaramide receptors for highly efficient anion binding in aqueous media and transmembrane transport, Chem. Commun. 56 (2020) 11066–11069, https://doi.org/10.1039/d0cc04090h.
[89] R.I. Storer, C. Aciro, L.H. Jones, Squaramides: physical properties, synthesis and applications, Chem. Soc. Rev. 40 (2011) 2330–2346, https://doi.org/10.1039/c0cs00200c.
[90] J.I. Lachowicz, G. Picci, P. Coni, V. Lippolis, M. Mamusa, S. Murgia, G. Pichiri, C. Caltagirone, Fluorescent squaramide ligands for cellular imaging and their encapsulation in cubosomes, New J. Chem. 43 (2019) 10336–10342, https://doi.org/10.1039/c9nj01548e.
[91] L.A. Marchetti, L.K. Kumawat, N. Mao, J.C. Stephens, R.B.P. Elmes, The versatility of squaramides: from supramolecular chemistry to chemical biology, Chem 5 (2019) 1398–1485, https://doi.org/10.1016/j.chempr.2019.02.027.
[92] G. Picci, J. Milia, M.C. Aragoni, M. Arca, S.J. Coles, A. Garau, V. Lippolis, R. Montis, J.B. Orton, C. Caltagirone, A Case Study with a Pyrene-Functionalized Squaramide, Molecules. 1–16 (2021).
[93] D. Wu, R. Jiang, L. Luo, Z. He, J. You, Bromide anion-triggered visible responsive metallogels based on squaramide complexes, Inorg. Chem. Front. 3 (2016) 1597–1603, https://doi.org/10.1039/c6qi00386a.
[94] Y.M. Zhang, J.X. He, W. Zhu, Y.F. Li, H. Fang, H. Yao, T.B. Wei, Q. Lin, Novel pillar[5]arene-based supramolecular organic framework gel for ultrasensitive response Fe 3+ and F − in water, Mater. Sci. Eng. C 100 (2019) 62–69, https://doi.org/10.1016/j.msec.2019.02.094.
[95] S. Bhowmik, S. Banerjee, U. Maitra, A self-assembled, luminescent europium cholate hydrogel: a novel approach towards lanthanide sensitization, Chem. Commun. 46 (2010) 8642–8644, https://doi.org/10.1039/c0cc02939d.
[96] T. Gorai, U. Maitra, Supramolecular approach to enzyme sensing on paper discs using lanthanide photoluminescence, ACS Sens. 1 (2016) 934–940, https://doi.org/10.1021/acssensors.6b00341.
[97] S. Bhowmik, U. Maitra, A novel "pro-sensitizer" based sensing of enzymes using Tb(III) luminescence in a hydrogel matrix, Chem. Commun. 48 (2012) 4624–4626, https://doi.org/10.1039/c2cc30904a.
[98] R. Laishram, S. Bhowmik, U. Maitra, White light emitting soft materials from off-the-shelf ingredients, J. Mater. Chem. C 3 (2015) 5885–5889, https://doi.org/10.1039/c5tc01072a.
[99] R. Laishram, U. Maitra, Rapid sensing of specific drugs at sub-ppb levels by using a hybrid organic-inorganic photoluminescent soft material, asian, J. Org. Chem. 6 (2017) 1235–1239, https://doi.org/10.1002/ajoc.201700156.
[100] S. Panja, S. Ghosh, K. Ghosh, Pyridine/pyridinium symmetrical bisamides as functional materials: aggregation, selective sensing and drug release, New J. Chem. 42 (2018) 6488–6497, https://doi.org/10.1039/c7nj03931j.
[101] X. Cao, N. Zhao, G. Zou, A. Gao, Q. Ding, G. Zeng, Y. Wu, A dual response organogel system based on an iridium complex and a Eu(III) hybrid for volatile acid and organic amine vapors, Soft Matter. 13 (2017) 3802–3811, https://doi.org/10.1039/c7sm00714k.
[102] T. Tu, W. Fang, X. Bao, X. Li, K.H. Dötz, Visual chiral recognition through enantioselective metallogel collapsing: Synthesis, characterization, and application of platinum-steroid low-molecular-mass gelators, Angew. Chemie Int. Ed. 50 (2011) 6601–6605, https://doi.org/10.1002/anie.201100620.
[103] B.O. Okesola, D.K. Smith, Applying low-molecular weight supramolecular gelators in an environmental setting-self-assembled gels as smart materials for pollutant removal, Chem. Soc. Rev. 45 (2016) 4226–4251, https://doi.org/10.1039/c6cs00124f.
[104] J.F. Chen, X. Liu, J.F. Ma, B.B. Han, J.D. Ding, Q. Lin, H. Yao, Y.M. Zhang, T. B. Wei, A pillar[5]arene-based multiple-stimuli responsive metal-organic gel was

constructed for facile removal of mercury ions, Soft Matter. 13 (2017) 5214–5218, https://doi.org/10.1039/c7sm01118k.
[105] P. Yadav, A. Ballabh, Room temperature metallogelation for a simple series of aminothiazole ligands with potential applications in identifying and scavenging mercury ions, RSC Adv. 4 (2014) 563–566, https://doi.org/10.1039/c3ra45024d.
[106] E. Saha, J. Mitra, Multistimuli-responsive self-healable and moldable nickel(II)-based gels for reversible gas adsorption and palladium sequestration *via* gel-to-gel transformation, ACS Appl. Mater. Interfaces. 11 (2019) 10718–10728, https://doi.org/10.1021/acsami.8b21606.
[107] D. You, X. Min, L. Liu, Z. Ren, X. Xiao, S.G. Pavlostathis, J. Luo, X. Luo, New insight on the adsorption capacity of metallogels for antimonite and antimonate removal: from experimental to theoretical study, J. Hazard. Mater. 346 (2018) 218–225, https://doi.org/10.1016/j.jhazmat.2017.12.035.
[108] A. Panja, K. Ghosh, Cholesterol-based diazine derivative: Selective sensing of Ag^{+} and Fe^{3+} ions through gelation and the performance of metallogels in dye and picric acid adsorption from water, Mater. Chem. Front. 2 (2018) 2286–2296, https://doi.org/10.1039/c8qm00433a.
[109] S. Sengupta, R. Mondal, A novel gel-based approach to wastewater treatment-unique one-shot solution to potentially toxic metal and dye removal problems, J. Mater. Chem. A 2 (2014) 16373–16377, https://doi.org/10.1039/c4ta03919j.
[110] S. Sengupta, R. Mondal, A novel low molecular weight supergelator showing an excellent gas adsorption, dye adsorption, self-sustaining and chemosensing properties in the gel state, RSC Adv. 6 (2016) 14009–14015, https://doi.org/10.1039/c5ra26713g.
[111] S. Sengupta, A. Goswami, R. Mondal, Silver-promoted gelation studies of an unorthodox chelating tripodal pyridine-pyrazole-based ligand: Templated growth of catalytic silver nanoparticles, gas and dye adsorption, New J. Chem. 38 (2014) 2470–2479, https://doi.org/10.1039/c3nj01334k.
[112] J. Liu, G.F. Gong, Y.J. Li, H. Yao, T.B. Wei, Q. Lin, Novel metallogel-based micro-acanthosphere material constructed from two tripodal gelators for efficient separation of organic dyes, Mater. Lett. 274 (2020), 128015, https://doi.org/10.1016/j.matlet.2020.128015.
[113] G.F. Gong, Y.Y. Chen, Y.M. Zhang, Y.Q. Fan, Q. Zhou, H.L. Yang, Q.P. Zhang, H. Yao, T.B. Wei, Q. Lin, A novel bis-component AIE smart gel with high selectivity and sensitivity to detect CN^{-}, Fe^{3+} and $H_2PO_4^{-}$, Soft Matter. 15 (2019) 6348–6352, https://doi.org/10.1039/c9sm01035a.
[114] H. Wang, B.H. Chen, D.J. Liu, Metal-organic frameworks and metal-organic gels for oxygen electrocatalysis: structural and compositional considerations, Adv. Mater. 33 (2021) 1–41, https://doi.org/10.1002/adma.202008023.
[115] C.K. Karan, M. Bhattacharjee, Self-healing and moldable metallogels as the recyclable materials for selective dye adsorption and separation, ACS Appl. Mater. Interfaces 8 (2016) 5526–5535, https://doi.org/10.1021/acsami.5b09831.
[116] Y. Hong, Z. Gao, M. Chen, J. Hao, S. Dong, Metal-organic gels of catechol-based ligands with Ni(II) acetate for dye adsorption, Langmuir 34 (2018) 9435–9441, https://doi.org/10.1021/acs.langmuir.8b01065.
[117] A. Mallick, E.M. Schön, T. Panda, K. Sreenivas, D.D. Díaz, R. Banerjee, Fine-tuning the balance between crystallization and gelation and enhancement of CO2 uptake on functionalized calcium based MOFs and metallogels, J. Mater. Chem. 22 (2012) 14951–14963, https://doi.org/10.1039/c2jm30866e.
[118] S.C. Zacharias, G. Ramon, S.A. Bourne, Supramolecular metallogels constructed from carboxylate gelators, Soft Matter. 14 (2018) 4505–4519, https://doi.org/10.1039/c8sm00753e.
[119] S.I. Kawano, N. Fujita, S. Shinkai, A coordination gelator that shows a reversible chromatic change and sol-gel phase-transition behavior upon oxidative/reductive stimuli, J. Am. Chem. Soc. 126 (2004) 8592–8593, https://doi.org/10.1021/ja048943+.
[120] S. Bhattacharya, S. Sengupta, S. Bala, A. Goswami, S. Ganguly, R. Mondal, Pyrazole-based metallogels showing an unprecedented colorimetric ammonia gas sensing through gel-to-gel transformation with a rare event of time-dependent morphology transformation, Cryst. Growth Des. 14 (2014) 2366–2374, https://doi.org/10.1021/cg5000827.
[121] T. Tu, W. Assenmacher, H. Peterlik, R. Weisbarth, M. Nieger, K.H. Dötz, An air-stable organometallic low-molecular-mass gelator: Synthesis, aggregation, and catalytic application of a palladium pincer complex, Angew. Chemie Int. Ed. 46 (2007) 6368–6371, https://doi.org/10.1002/anie.200701486.
[122] T. Feldner, M. Häring, S. Saha, J. Esquena, R. Banerjee, D.D. Díaz, Supramolecular metallogel that imparts self-healing properties to other gel networks, Chem. Mater. 28 (2016) 3210–3217, https://doi.org/10.1021/acs.chemmater.6b01144.
[123] M. Xue, Y. Lü, Q. Sun, K. Liu, Z. Liu, P. Sun, Ag(I)-coordinated supramolecular metallogels based on schiff base ligands: structural characterization and reversible thixotropic property, Cryst. Growth Des. 15 (2015) 5360–5367, https://doi.org/10.1021/acs.cgd.5b00952.
[124] J.H. Lee, S. Kang, J.Y. Lee, J.H. Jung, A tetrazole-based metallogel induced with Ag^{+} ion and its silver nanoparticle in catalysis, Soft Matter. 8 (2012) 6557–6563, https://doi.org/10.1039/c2sm25316j.
[125] M. Sharma, P.J. Sarma, M.J. Goswami, K.K. Bania, Metallogel templated synthesis and stabilization of silver-particles and its application in catalytic reduction of nitro-arene, J. Colloid Interface Sci. 490 (2017) 529–541, https://doi.org/10.1016/j.jcis.2016.11.065.
[126] M. Paul, K. Sarkar, P. Dastidar, Metallogels derived from silver coordination polymers of C_3-symmetric tris(pyridylamide) tripodal ligands: synthesis of ag nanoparticles and catalysis, Chem. – A Eur. J. 21 (2015) 255–268, https://doi.org/10.1002/chem.201404959.
[127] S.D. Kurbah, R.A. Lal, Bioinspired catalysis and bromoperoxidase like activity of a multistimuli-responsive supramolecular metallogel: Supramolecular assembly triggered by pi-pi stacking and hydrogen bonding interactions, New J. Chem. 44 (2020) 5410–5418, https://doi.org/10.1039/c9nj05732c.
[128] S. Dhibar, A. Dey, D. Ghosh, S. Majumdar, A. Dey, P.P. Ray, B. Dey, Triethylenetetramine-based semiconducting Fe(III) metallogel: effective catalyst for aryl-S coupling, ACS Omega (2020), https://doi.org/10.1021/acsomega.9b03194.
[129] M. Araújo, B. Escuder, Transient catalytic activity of a triazole-based gelator regulated by molecular gel assembly/disassembly, ChemistrySelect 2 (2017) 854–862, https://doi.org/10.1002/slct.201601816.